Near-Field Cosmology with Extremely Metal-Poor Stars

Anna Frebel[1] and John E. Norris[2]

[1]Department of Physics and Kavli Institute for Astrophysics and Space Research, Massachusetts Institute of Technology, Cambridge, Massachusetts 02139; email: afrebel@mit.edu

[2]Research School of Astronomy & Astrophysics, The Australian National University, Mount Stromlo Observatory, Weston, Australian Capital Territory 2611, Australia; email: jen@mso.anu.edu.au

Abstract

The oldest, most metal-poor stars in the Galactic halo and satellite dwarf galaxies present an opportunity to explore the chemical and physical conditions of the earliest star-forming environments in the Universe. We review the fields of stellar archaeology and dwarf galaxy archaeology by examining the chemical abundance measurements of various elements in extremely metal-poor stars. Focus on the carbon-rich and carbon-normal halo star populations illustrates how these provide insight into the Population III star progenitors responsible for the first metal enrichment events. We extend the discussion to near-field cosmology, which is concerned with the formation of the first stars and galaxies, and how metal-poor stars can be used to constrain these processes. Complementary abundance measurements in high-redshift gas clouds further help establish the early chemical evolution of the Universe. The data appear consistent with the existence of two distinct channels of star formation at the earliest times.

1. INTRODUCTION

1.1. The Stellar Path to the Early Universe

The paradigm that stars in our Galaxy can tell us about conditions that existed during the first few billion years after the Big Bang, as set down by Freeman & Bland-Hawthorn (2002) and described by them as near-field cosmology, is an idea that formed slowly over some decades. During the last century, the study of stars provided a major tool for exploring the nature of the Milky Way Galaxy (the Galaxy), its structure and size, and its origin and history. It also became clear that we live in just one of many galaxies in the Universe (Sandage 1986 and references therein).

In the absence of accurate means of directly determining the ages of all but a few individual oldest stars, it has been assumed that the best available proxy for age, however imperfect, is a star's chemical abundance profile. In particular, the underlying assumption is that the most metal-poor stars (where as usual we refer to all elements heavier than lithium) are most likely to be the oldest stars that exist today. The second premise, based on theoretical arguments (Bromm & Larson 2004), is that stars and galaxies began to form at redshifts $z \sim 20$–30, some 100–200 Myr after the Big Bang. Against this background, the aim of the present review is to use stars and their chemical abundances, in particular stars with [Fe/H] < -3.0, to constrain conditions that existed during the first $\sim$500 Myr.

The secret to the viability of this near-field cosmology lies in the mass-dependent lifetimes of stars. Although high-mass stars soon die as supernovae that can be observed over large distances, their low-mass counterparts (of mass, M) live for $\sim$10 $(M/M_\odot)^{-3}$ Gyr and have witnessed eras long gone. Stellar populations thus contain detailed information about the past of their host systems, connecting the present state of a galaxy to its history of formation and evolution. This fortuitous relationship can be used to study the early Universe and the beginning of star and galaxy formation with long-lived stars. However, the approach requires detailed observations of individual stars, so it is only feasible for unraveling the detailed histories of the Milky Way and its dwarf galaxy satellites.

The key to characterizing individual stars, and indeed entire stellar populations, is their chemical composition, kinematics, and age (where possible). Composition is of particular importance: It yields information concerning a star's formation era because in their atmospheres stars preserve information on the chemical and physical conditions of their birth gas clouds. Overall, the amount of elements heavier than lithium in a star reflects the extent of chemical enrichment within its natal cloud.

During the past four decades, extensive study has been devoted to the search for extremely metal-poor stars within the halo of the Galaxy to piece together early chemical evolution soon after the Big Bang (see Beers & Christlieb 2005). Specifically, these stars provide an exceptionally versatile means for studying a large variety of open questions regarding the nature and evolution of the early Universe. Consequently, this field is often referred to as stellar archaeology because these low-metallicity, low-mass ($M \le 0.8\ M_\odot$) stars reveal unique observational clues about the formation of the very first stars and their supernova explosions, the onset of cosmic chemical evolution, the physics of nucleosynthesis, early metal- and gas-mixing processes, and even early (proto)galaxy formation and the assembly processes of larger galaxies. The latter approach has been termed dwarf galaxy archaeology because entire metal-poor dwarf galaxies are now being used to study star and galaxy formation processes in the early Universe within the actual dwarf galaxy environment, just as individual stars are used for stellar archaeology (Bovill & Ricotti 2009, Frebel & Bromm 2012).

From a more technical point of view, stars are also the easily accessible local equivalent of the high-redshift Universe, offering a complementary approach to the study of photon-starved,

high-redshift observations (far-field cosmology) of, for example, damped Lyα (DLA) and sub-DLA systems (Pettini 2011, Becker et al. 2012). By providing detailed observational data on the era of the first stars and galaxies, stellar and dwarf galaxy archaeology have become increasingly attractive for comparison with theoretical predictions about early Universe physics and galaxy assembly processes (Bromm & Yoshida 2011). In the field of near-field cosmology, the necessary observational and theoretical ingredients are now being effectively combined for comprehensive studies of how metal enrichment drove the evolution of the early Universe and the roles that extremely metal-poor stars and dwarf galaxies played in Galactic halo formation (e.g., Cooke & Madau 2014, Ritter et al. 2015).

1.2. Exploring the Earliest Times

Within the metal-poor star discipline, theoretical and observational works alike have benefited enormously from the discovery, since the turn of the century, of eight individual halo stars in the Galactic halo with abundances in the range [Fe/H] ~ -7.3 to -4.5. All but one of them have a very large overabundance of carbon relative to iron. During the same period, it has become clear that the Milky Way's dwarf galaxy satellites, in particular the ultra-faint systems, contain a surprisingly large fraction of stars with [Fe/H] < -3.0, including carbon-rich (C-rich) stars similar to those found in the Galactic halo.

Spectroscopic abundance measurements of these and other metal-poor halo stars have provided critical missing information in the following areas: the chemical enrichment of the Universe at the earliest times, a more complete characterization of the chemical nature and frequency of carbon enhancement of stars with [Fe/H] < -3.0, the relationship between the Galaxy's halo and its dwarf satellites, the evolution of lithium in the very early Universe, r-process nucleosynthesis, and the various sources of neutron-capture elements. Comparison of observations with the results of cosmological simulations is leading to a more complete characterization of the chemical nature of the first galaxies, with the aim of understanding their relationship to the surviving dwarfs and the building blocks of the Milky Way's halo.

These observational and theoretical endeavors are leading to a deeper understanding of the origin of the elements, the nature of the first stars and galaxies in the Universe, and the chemical enrichment of the Milky Way. The aim of the present review is to examine the progress that has been made in these areas over the past decade.

1.3. Background Material

Interest in the varied results of metal-poor star studies has dramatically increased in recent years owing to their relevance for other subfields of astronomy. These include areas such as galaxy formation, galactic dynamics, supernovae, nucleosynthesis, and nuclear astrophysics. In **Figure 1**, we give a schematic overview of the substantial connections between the different fields of study, and how they connect to near-field cosmology and its main technique, stellar abundance determinations.

Given space constraints, the present review is limited to recent core near-field cosmology results and their implications. To address this restriction, we refer the reader to the following broad range of other relevant works that cover many of the related areas highlighted in **Figure 1**. These references deal with the following topics:

- Bromm & Larson (2004), Bromm & Yoshida (2011), Galli & Palla (2013), and Loeb & Furlanetto (2013) discuss the first stars and galaxies and associated environments for star formation.
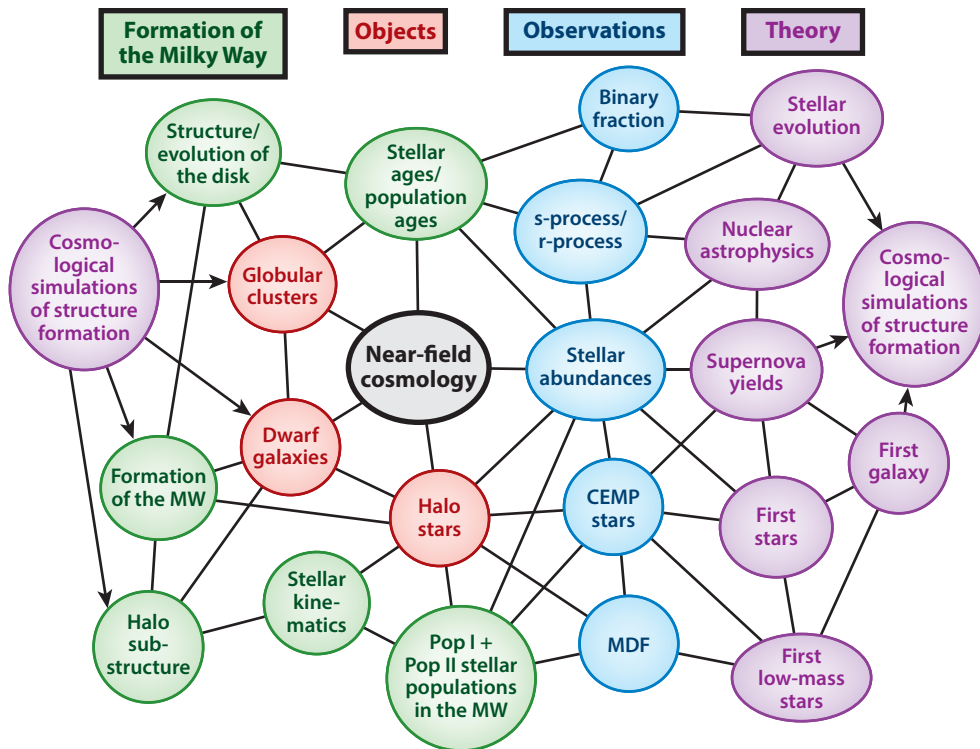
Figure 1

Schematic overview of the many scientific topics related to near-field cosmology. These examples illustrate how closely connected the many different areas are. Abbreviations: CEMP, carbon-enhanced metal-poor; MDF, metallicity distribution function; MW, Milky Way; Pop I and Pop II, Population I and II.

- Pagel (1997), Frebel (2010), Frebel & Norris (2013), and Karlsson et al. (2013) address the context of the early chemical enrichment of the Universe, and how one might use metal-poor stars to explore back in time to the Big Bang.
- Wheeler et al. (1989), Asplund (2005), Gray (2005), Sneden et al. (2008), and Asplund et al. (2009) address the determination of the chemical abundances of stars, the important abundance patterns, and the reliability of the results.
- Beers & Christlieb (2005) describe the search for and discovery of metal-poor stars.
- Sandage (1986), Gilmore et al. (1989), McWilliam (1997), Freeman & Bland-Hawthorn (2002), and Ivezić et al. (2012) discuss the role of abundances in the stellar population paradigm, and the manner in which they inform our understanding of galactic chemical enrichment.
- Woosley & Weaver (1995), Woosley et al. (2002), Kobayashi et al. (2006), Heger & Woosley (2010), and Nomoto et al. (2013) describe the progress in understanding how supernovae produce the chemical elements.
- Mateo (1998), Tolstoy et al. (2009), Willman (2010), and Belokurov (2013) address the discovery, observation, and interpretation of the Milky Way's dwarf galaxy satellites.

These reviews are, of course, not one dimensional, and in many cases, a given review discusses matters in several of the above topics.

1.4. Terms and Assumptions

For the discussion that follows, we begin with definitions of terms, together with their significance in the study of the early Universe using extremely metal-poor stars.

1.4.1. Stellar archaeology, dwarf galaxy archaeology, and near-field cosmology. Throughout this review the term extremely metal-poor star refers to stars having [Fe/H] < −3.0 (Beers & Christlieb 2005).

1.4.1.1. Stellar archaeology. The study of the astrophysical sites, conditions of nucleosynthesis, and the major physical processes that drove early star formation, by using stellar chemical abundance analyses of old stars. This rests on the abundance results of many elements of metal-poor halo stars throughout the periodic table to enable the detailed documentation of the earliest chemical enrichment events and their subsequent interpretation.

1.4.1.2. Dwarf galaxy archaeology. The investigation of galaxy formation on small scales and the associated early metal-mixing processes. By comparing abundances of their metal-poor stars, particularly those in ultra-faint dwarf galaxies, with those of equivalent Galactic halo stars, the (beginning of) cosmic chemical evolution within a galaxy can be tested, providing insight into the relationship between the dwarf galaxies and the building blocks of the Galactic halo, as well as determining whether these systems are the survivors of the first galaxies.

1.4.1.3. Near-field cosmology. The interpretation of the results obtained from stellar and dwarf galaxy archaeology to gain insight into the physical conditions at the earliest times and the assembly history of the Galactic halo. The coupling of low-metallicity stellar abundances with results from cosmological simulations enables studies ranging from the nature of the first stars all the way to the formation mechanism(s) of the metal-poor halo of the Milky Way.

1.4.2. Abundance definitions. We recall the following basic definitions. The abundance of element A, $\epsilon(A)$, is presented logarithmically, relative to that of hydrogen (H), in terms of N_A and N_H, the number of atoms of A and H in Equation 1.

$$\log_{10} \epsilon(A) = \log_{10}(N_A/N_H) + 12. \tag{1}$$

[For lithium, an alternative and more frequently used abundance nomenclature is A(Li), where by definition A(Li) = $\log_{10} \epsilon(Li)$. For hydrogen, by definition, $\log_{10} \epsilon(H) = 12$.]

For stellar abundances in the literature, results are generally presented relative to their values in the Sun, using the so-called bracket notation,

$$[A/H] = \log_{10}(N_A/N_H)_\star - \log_{10}(N_A/N_H)_\odot, \tag{2}$$

and for two elements A and B, one then has

$$[A/B] = \log_{10}(N_A/N_B)_\star - \log_{10}(N_A/N_B)_\odot. \tag{3}$$

In the case of the Fe metallicity, $[Fe/H] = \log_{10}(N_{Fe}/N_H)_\star - \log_{10}(N_{Fe}/N_H)_\odot$. For example, $[Fe/H] = -4.0$ corresponds to an iron abundance 1/10,000 that of the Sun. With this notation, one needs the abundance not only of the star being analyzed, but also of the Sun (see, e.g., Asplund et al. 2009 and Caffau et al. 2011b for details of this aspect of the problem).

In stars, the most commonly measured element is iron, given that it is one of the most abundant and the most readily measurable of the elements in stellar spectra. From a semantic point of view and for the discussion that follows, we note that the term metal-poor is not always synonymous with Fe-poor. For stars with $[Fe/H] > -4.0$, metal-poor in most cases satisfactorily describes the amount of both Fe and metals in the star, but for those with $[Fe/H] < -4.0$, the assumed equality appears to generally break down given the common and huge amounts of carbon and other elements with respect to iron. Needless to say, there are exceptions above and below $[Fe/H] = -4.0$. We refer to stars with $[Fe/H] < -4.5$ as the most Fe-poor stars and use most metal-poor stars when referring generically to stars of the lowest metallicity in the absence of a priori knowledge of the details of their heavy-element abundance distributions.

1.4.3. Model atmosphere assumptions. Most chemical abundance determinations of stars are based on one-dimensional (1D) model stellar atmosphere analyses that assume hydrostatic equilibrium, flux constancy, and local thermodynamic equilibrium (LTE), and these determinations treat convection in terms of a rudimentary mixing-length theory. To first order, the basic atmospheric parameters that define the model are effective temperature (T_{eff}), surface gravity ($\log g$), and chemical composition ([M/H], where M refers to metals). We refer the reader to Gray (2005) and Gustafsson et al. (2008) for the concepts associated with stellar atmosphere modeling. For details of the more realistic and rigorous three-dimensional (3D) model atmosphere and non-LTE (hereafter NLTE) formalisms, rather than the 1D/LTE approximations, see Asplund (2005), and the references therein; examples of recent developments in these areas are found in Lind et al. (2012), Ludwig & Kučinskas (2012), Magic et al. (2013), and Tremblay et al. (2013). We have discussed the corresponding abundance differences that result from these two approaches previously (Frebel & Norris 2013, see their figure 11) to which we refer the reader for details. In brief, differences between LTE and NLTE results, on the one hand, and between 1D and 3D analyses, on the other, are of an order ~0.5 dex for some atomic species. Three-dimensional corrections for the hydrides of C, N, and O are ~0.5–1.0 dex, in the sense that 1D abundances are higher. We note also that LTE/NLTE and 1D/3D differences, determined independently, are not always necessarily in the same direction; and, thus, to some extent, the criticisms that apply to 1D/LTE results remain if only one of the two improvements has been made, as opposed to a complete 3D/NLTE analysis. In general the results of the more rigorous, but very computationally challenging, 3D/NLTE formalism are always to be preferred, if available. In what follows, unless otherwise stated, we present abundances from the more widely used 1D/LTE procedures, which have produced results for a much larger sample of stars. The rationale for this is that it is unwise to mix the results of the 1D/LTE and 3D/NLTE formalisms when investigating abundance trends and objects with apparently anomalous compositions. In contrast, one must bear in mind the problems that could occur if 1D/LTE abundances, rather than the more rigorous 3D/NLTE values, are compared with those of, for example, stellar evolution computations, other theoretical predictions, and nonstellar (e.g., Damped Lyα) systems.

1.5. Overview

We begin in Section 2 with a discussion of the basic properties of the Galaxy, its components, and the different types of stars and objects that are being studied to explore its nature and evolution.

This sets the scene for stellar archaeology in Section 3 and the role of metal-poor stars, which are at the heart of near-field cosmology. There, we trace the search for the most metal-poor stars and the discovery of a small number that have only 10^{-5} to 10^{-7} the amount of iron one finds in the Sun. In stark contrast, the ratio of carbon to iron in these objects is enormous and $\sim 10-10^{+5}$ times the solar ratio. We also discuss the metallicity distribution function for stars with [Fe/H] < -3.0 and the behavior of other elements that place strong constraints of the nature of the first stars. Then, we reach the crux of the matter: Below [Fe/H] ~ -4.0, the chemical abundance patterns are fundamentally different from those of stars above this limit. Section 4 addresses the archaeology of the Milky Way dwarf satellite galaxies and provides a comparison of their properties with those of the Galactic halo population. In Section 5, with the archaeology complete, we move to near-field cosmology. There, we trace the development of the theoretical interpretation of the manner in which the earliest stars and galaxies formed within the framework of the Lambda cold dark matter (ΛCDM) paradigm, and we seek to infer how the first stars and the earliest populations formed in the Universe in light of the chemical abundances of the most metal-poor stars. In Section 6, we compare what we have learned from near-field cosmology with the results of far-field endeavors. Finally, in Section 7, we conclude with expectations for the future.

2. THE MILKY WAY

2.1. Galactic Populations

In a masterful review of the structure and evolution of the Milky Way, Sandage (1986, pg. 421) described the population concept as one of the "grand unifying themes in science." At its center is the idea that stellar populations may be well described in terms of their spatial, kinematic, chemical abundance, and age distributions, which distinguish them one from another and provide the basic information necessary and essential for an understanding of their origin and evolution. In what follows, we mainly concentrate on chemical abundances, given our premise that these are the principal population characteristics that are used in our discussion of near-field cosmology.

2.2. Baryonic Components

2.2.1. Disk, halo, and bulge. The Milky Way consists of several directly observable components—most notably the disk, the halo, and the bulge. The disk can be well described in terms of a thin disk together with a more vertically extended thick disk (Yoshii 1982, Gilmore & Reid 1983) and an even more extended metal-weak thick-disk subcomponent (Morrison et al. 1990, Chiba & Beers 2000, Beers et al. 2014). Young, metal-rich Population I stars similar to the Sun are primarily located in the thin disk, with an average metallicity of [Fe/H] ~ -0.2; for the thick disk, the mean value is [Fe/H] ~ -0.6; and the metal-weak thick disk is even more metal-poor, with $-2.5 \lesssim$ [Fe/H] $\lesssim -1.0$. The stellar halo has a spheroidal distribution that envelops the disk and bulge and reaches out to some 150 kpc. It contains older Population II stars, which are generally more metal-poor: Average halo metallicities for inner and outer halo subcomponents are [Fe/H] ~ -1.6 and -2.2, respectively (Carollo et al. 2007, 2010), with a distribution that stretches down to at least [Fe/H] $= -7.3$ (Keller et al. 2014). Given the extent of the halo, the outer regions beyond a distance of 30 kpc are not well explored in terms of high-resolution spectroscopic abundance analyses, given that the stars are faint, with a magnitude of $V \gtrsim 16$.

Spatial, kinematic, and abundance distributions of halo stars indicate that the Milky Way's halo may not be a single monolithic component but contains substructure resulting from accretion events, superimposed on a dichotomy of inner and outer components (Hartwick 1987; Norris

& Ryan 1989; Carollo et al. 2007, 2010, 2014; de Jong et al. 2010; Deason et al. 2011; Beers et al. 2012 and references therein). We refer the reader to Schönrich et al. (2011, 2014) for an alternative viewpoint on the dual nature of the Galactic halo. The details of the relationships of the substructure to the inner and outer components remain to be clarified. In general, the halo is well described with an inner component that may have formed in situ during the evolution of the Milky Way, together with a more diffuse outer one that originated from past accretion and tidal disruption of dwarf galaxies (Zolotov et al. 2009, 2010; Font et al. 2011; McCarthy et al. 2012; Tissera et al. 2014). The metal-poor component of the Galactic bulge is, observationally, largely unexplored territory. Although its oldest stars formed coevally with the early assembly phases of the Milky Way (e.g., Brook et al. 2007, Tumlinson 2010), several younger populations are also present, making it challenging to efficiently isolate individual members of the first population. Additionally, crowding effects and the large amount of dust extinction toward the bulge complicate this endeavor. Accordingly, only limited progress has been made in identifying its most metal-poor and oldest components. We refer the reader to the works of García Pérez et al. (2013), Ness et al. (2013), and Howes et al. (2014), and references therein, for important recent advances in this area.

Galactic globular clusters have been studied for many decades and were the first probes used to map the structure and extent of the Milky Way (see Shapley 1930). They comprise two subsystems: one associated with the bulge and thick disk, the other with the halo (Zinn 1985). The latter is the more metal-poor group, with mean and minimum [Fe/H] ~ -1.6 and ~ -2.3, respectively. Individual clusters possess extremely complicated chemical abundance patterns, which preclude any clear understanding of their formation and evolution. Poorly understood problems include the following: Some systems have subpopulations with spectacularly large helium abundance, $Y \sim 0.35$ to 0.40 (e.g., King et al. 2012); all display chemical abundance signatures of the lighter elements (correlations and anticorrelations among C, N, O, Na, Mg, and Al) that differ fundamentally from the relationships found among field halo stars (e.g., Gratton et al. 2004); and detailed spectroscopic observations have revealed iron and heavy neutron-capture abundance spreads in an increasing number of clusters (e.g., Yong et al. 2014 and references therein).

2.2.2. Satellite dwarf galaxies. The Milky Way is surrounded by a host of satellite dwarf galaxies that orbit in its outer halo (see Mateo 1998, Tolstoy et al. 2009, Belokurov 2013). The most massive of them are the Large and Small Magellanic Clouds, which are gaseous irregular systems with ongoing star formation. Other less massive dwarf irregular galaxies are complemented by gas-poor dwarf spheroidal (dSph) and ultra-faint dwarf galaxies. In the context of the present review, the dSph and the even less luminous ultra-faint systems are of prime importance because their old stellar populations encode their early histories of star formation and chemical enrichment. Although dSph galaxies have been studied extensively in their own right, it has become clear in recent years that our understanding of the formation of the Milky Way is closely connected to their nature and history as well as the role dwarf galaxies may play as building blocks of larger galaxies.

2.3. The Dark Halo and Putative Population III

Associated with the Galaxy's luminous material is a massive halo of dark matter, extending to ~ 300 kpc from the Galactic center and having a mass in the range 1.0 to 2.4 $\times 10^{12}$ $M_\odot$ (at the 90% confidence level) (Boylan-Kolchin et al. 2013 and references therein). This topic lies outside the present discussion, except insofar as the formation of structure within the Universe was determined by the properties of the dark matter, and its entrainment of baryonic material.

In addition to Population I and II stars, which are traditionally observed to study the nature of the disk and halo of the Milky Way, there is also a putative Population III—a metal-free first

population that lit up the Universe 100–200 Myr after the Big Bang. Early theoretical models of first star formation favored a top-heavy mass function for this population, which renders them unobservable today, given their corresponding short lifetimes of a few tens of millions of years. More recent work, however, suggests this population may have contained stars of significantly lower mass (Stacy & Bromm 2014). If such Population III stars formed, in particular objects having masses less than 1 $M_\odot$, they would have sufficiently long lifetimes to be still observable today. In that case, we would expect them to be eventually found in the Galaxy's halo and/or bulge.

2.4. The Galaxy in the Cosmological Context

Fundamental impetus to an understanding of galaxy formation was provided by White & Rees (1978, pg. 341), who proposed their cold dark matter hierarchical clustering paradigm in which "the entire luminosity content of galaxies. . .results from the cooling and fragmentation of residual gas within the transient potential wells provided by the dark matter." At the same time, the observational community was addressing two essentially different paradigms for the formation of the halo of the Milky Way. On the one hand, the monolithic collapse model of Eggen, Lynden-Bell, and Sandage (hereafter ELS) (Eggen et al. 1962), predicted a very rapid collapse phase (of a few 10^8 years) and a dependence of kinematics on abundance together with a radial abundance gradient for halo material. On the other hand, the fragment accretion model of Searle & Zinn (1978), (hereafter SZ) proposed a longer formation period of a few 10^9 years, no dependence of kinematics on abundance, and no radial abundance gradient. We refer the reader to our previous review of this confrontation (Frebel & Norris 2013). Suffice it here to say, neither fully explains the observations. Rather, as stated there,

> it seems likely the answer will be found within the hierarchical ΛCDM paradigm. . . The work of Zolotov et al. (2009), for example, while supporting the SZ paradigm of halo formation, also produces a dual halo configuration of "*in situ*" and "*accreted*" components, not unlike those envisaged in the ELS and SZ observational paradigms. Remarkably, these paradigms were first established on essentially observational grounds only. They are now being explained in terms of a theoretical framework based on tracing the dark matter evolution from initial density fluctuations early in the Universe. (Frebel & Norris 2013, pg. 52)

The in situ and accreted components can readily be identified with the inner and outer halo components (Carollo et al. 2007, 2010), also supported by simulations such as those of Tissera et al. (2014).

Models of cosmic structure formation and galaxy evolution based on cosmological initial conditions and following the gravitational evolution of collapsing dark matter halos were first undertaken by Moore et al. (1999) and Klypin et al. (1999). These works showed that galaxy evolution is an ongoing assembly process. The emerging central halo (the galaxy) accretes gas from large-scale filaments of the cosmic web as well as smaller halos (dwarf galaxies) that orbit it. In this way, the galaxy grows over billions of years. Recently, hydrodynamic cosmological models have emerged that are capable of modeling the evolution of not only dark matter but also gravitationally entrained baryons as part of the formation of disk galaxies (Agertz et al. 2011, Guedes et al. 2011, Vogelsberger et al. 2014). Indeed, we can see the accretion process in the Milky Way. It is still ongoing, and the many stellar streams and overdensities in the halo are evidence of it (e.g., Pila-Díez et al. 2014). The most prominent example of the phenomenon is the Sagittarius dwarf galaxy (Ibata et al. 1995), which is in the process of being disrupted, leaving a stellar stream wrapped more than once around our Galaxy.
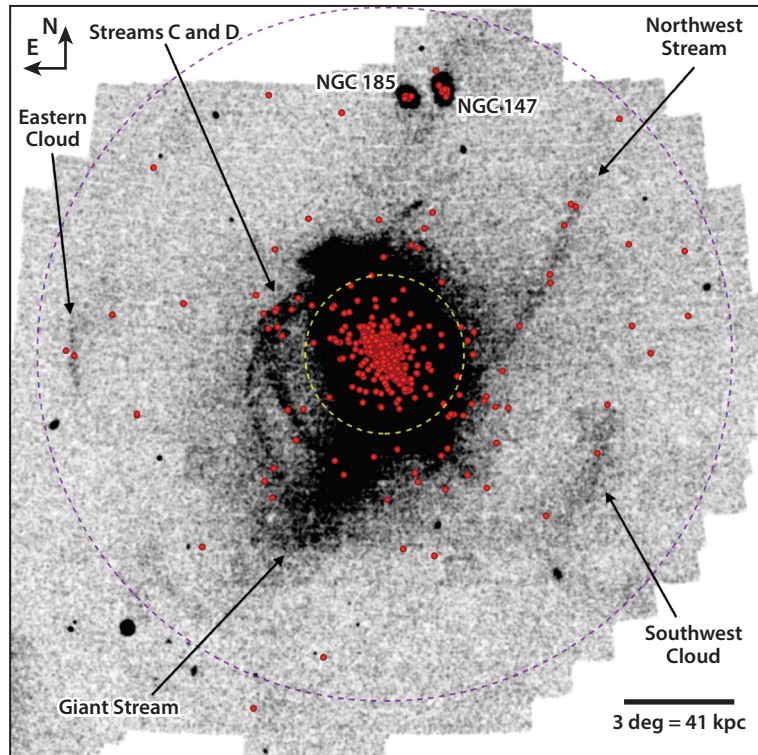
Figure 2

A spatial density map of metal-poor stars ([Fe/H] $\lesssim -1.4$) in the halo of the Andromeda galaxy obtained by the PAndAS team (McConnachie et al. 2009). The red circles represent globular clusters, and their association with stellar streams is clear. The two circles in the figure have radii of 30 and 130 kpc. In this map, the central spiral structure is lost because of the lack of contrast in the exposure. (A.D. Mackey and the PAndAS collaboration, private communication.)

In this context, the oldest stars found in the Galactic halo are the best tracers of the earliest accretion events. They formed as part of the earliest generations of stars in their respective host systems, which means that their current elemental abundances reflect those first local chemical enrichment events. This scenario is broadly supported by stellar age measurements that have shown individual metal-poor halo stars with overabundances of heavy r-process neutron-capture elements to be 13–14 Gyr old (e.g., Hill et al. 2002, Frebel et al. 2007a). Similar ages have been obtained for globular clusters (Marín-Franch et al. 2009) as well as several ultra-faint dwarf galaxies (Brown et al. 2012, 2014). These ages are commensurate with the independently determined age of the Universe of 13.8 Gyr by Ade et al. (2014, the Planck Collaboration).

Being situated inside the Milky Way makes it difficult for us to appreciate these accretion events directly. That said, we are ideally placed to examine the effect in our nearest spiral galaxy neighbor, Andromeda. **Figure 2** shows an extremely deep Pan-Andromeda Archaeological Survey (PAndAS) (McConnachie et al. 2009) spatial density map of metal-poor stars ([Fe/H] $\lesssim -1.4$) in the halo of Andromeda, reaching to a projected galactocentric radius of up to 150 kpc. The remnants of numerous accretion events are clearly seen in Andromeda's halo. Globular clusters are also cataloged and are represented here by superimposed red circles. It is evident that in many cases the clusters are associated with the halo streams and thus accreted with the captured galaxies.

Gilbert et al. (2014) provide new support for such a history and that Andromeda has an inner and outer halo (not unlike that proposed for the Milky Way), and rather similar to at least one of the simulation results of Tissera et al. (2014).

3. STELLAR ARCHAEOLOGY

Stellar archaeology seeks to understand the manner in which stellar populations formed and evolved. The principal parameters available for the endeavor, as noted in Section 2.1, are their spatial distribution, kinematics, chemical abundances, and ages. In the cosmological context, we seek to understand the earliest times and are interested in stars that formed within the first billion years after the Big Bang singularity. Clearly, age is of fundamental importance. The basic problem that confronts us, however, is that we are unable to obtain accurate ages for all but a very small minority of individual stars from this era. We must look for proxies that provide related and complementary information.

3.1. The Role of Chemical Abundances

A basic premise is that some minutes after the singularity, at the era of decoupling of radiation and matter, the only chemical elements in the Universe were hydrogen, helium, and lithium. Within the framework of standard Big Bang nucleosynthesis (SBBN), constrained by the results of the *Wilkinson Microwave Anisotropy Probe* (WMAP), the predicted relative mass densities of these elements are 0.75, 0.25, 2.3 $\times$ 10^{-9}, respectively (Spergel et al. 2007). All other elements (with the exceptions of beryllium and boron) have been produced subsequently in stars and supernova explosions, processes that continue to the present day.

The assumption that follows is that the oldest stars are those that have the lowest total heavy-element abundance. In the absence of an understanding of the nature and evolution of the first stars, however, and in particular because of our lack of insight into their nucleosynthetic yields of individual elements, this is a potentially fraught assumption, to which we return in Sections 3.5 and 5.5. The assumption that we make is that the most Fe-poor stars are the best candidates we have to take us to the earliest stellar generations and closest to the Big Bang. This is the working hypothesis that drives stellar archaeology.

In what follows, we confine our attention to the two most accessible observational areas. The first is the halo of the Milky Way Galaxy, and the second is the Galaxy's dwarf satellite galaxies (its dSph and the relatively recently discovered ultra-faint dwarf galaxies). We limit the present discussion to results of high-resolution, high S/N spectroscopic chemical abundance analyses in these two areas and almost exclusively to objects that have [Fe/H] < −3.0 in an effort to take us closer in time to the Big Bang than would stars of higher Fe abundances. We note that this restriction excludes the Galaxy's globular clusters, and its metal-weak thick-disk and bulge stars, from the discussion. Although the bulge is believed to be the site of some of the very first star formations, its admixture with later stellar generations at the Galaxy's center has to this point precluded discovery of more than a few stars with [Fe/H] < −3.0.

3.2. The Search for Extremely Metal-Poor Stars in the Galactic Halo

In the middle of the twentieth century, the concept of metal-poor stars did not exist. To quote Sandage (1986, pg. 433), "there had grown up a general opinion, shared by nearly all spectroscopists, that there was a single universal curve of all the elements, and that the Sun and all the stars shared...precisely...identical ratios of any element A to hydrogen." Against this

background, Chamberlain & Aller (1951) demonstrated that the A-type subdwarfs HD 19445 and HD 140283 have abundances [Fe/H] ([Ca/H]) $= -0.8 \, (-1.4)$ and $-1.0 \, (-1.6)$, respectively, thereby establishing a profound paradigm shift. This shift opened the way to the discovery of stars having progressively lower and lower chemical abundances, culminating in the recent discovery by Keller et al. (2014) of the halo giant SMSS J031300.36$-$670839.3 (hereafter SM 0313$-$6708), with [Fe/H] < -7.3 and [Ca/H] $= -7.2$, i.e., with Fe undetected at the 10^{-7} level and Ca at some 10^{-7} times those of the Sun.

The decades-long searches have shown that metal-poor stars are rare: In the Solar Neighborhood, below [Fe/H] $= -3.5$, we expect to find only of order one such star among 100,000 field stars. Several techniques (using different criteria) have, therefore, been used to improve the odds of finding these objects in the Galactic halo. We give only a brief description of these efforts here and refer the reader to the comprehensive discussions of Beers & Christlieb (2005), Ivezić et al. (2012), and Frebel & Norris (2013) for more detail. Important contributions that provide candidate metal-poor stars suitable for further observation and analysis are described in the following sections.

3.2.1. Informed serendipity.
Some bright, extremely metal-poor stars have been found by what can best be described as informed serendipity. Perhaps the two best known of these are CD$-38°245$ ([Fe/H] $= -4.0$, $V = 12.8$) (Bessell & Norris 1984) and BD+44°493 ([Fe/H] $= -3.7$, $V = 9.1$ (Ito et al. 2009), which were first recognized following their inclusion in A-star and radial-velocity surveys, respectively.

3.2.2. High proper-motion surveys.
A large fraction of halo stars has high proper motion relative to those of the Galactic disk. The first star with [Fe/H] < -3.0 (G64-12) (Carney & Peterson 1981) was discovered as the result of its high proper motion. The surveys of Ryan & Norris (1991) and Carney et al. (1996) have utilized this technique, and their samples each comprise a few hundred halo main-sequence dwarfs with [Fe/H] < -1.0. Taken together these authors obtained $\sim$10 stars having [Fe/H] < -3.0. It is important to note that this technique produces a sample that does not have any explicit abundance bias. That said, the reader should bear in mind that the sample may be an admixture of subpopulations having different origins. Another example of the role of kinematic selection is provided by the current European Space Agency *Gaia* mission, which will revolutionize our view of the Milky Way (see Perryman et al. 2001).

3.2.3. Schmidt objective-prism surveys.
These permit one to simultaneously obtain large numbers of low-resolution spectra [resolving power $R(= \lambda/\Delta\lambda) \sim 400$] over several square degrees. Examination of the strength of the CaII K line at 3933.6 Å with respect to that of nearby hydrogen lines, or the color of the star, leads to a first estimate of metal weakness. Candidate metal-poor stars are then observed at intermediate resolution ($R \sim 2,000$) to obtain a first estimate of metallicity, again on the basis of the CaII K line. The techniques are described in detail by Beers & Christlieb (2005), who also document important surveys of this type that have obtained these first abundance estimates for some tens of thousands of stars brighter than $B \sim 16.5$ with [Fe/H] < -1.0. The first major surveys of this type for metal-poor stars were those of Bond (1970) and Bidelman & MacConnell (1973). The most comprehensive to date have been the HK survey (Beers et al. 1992) and the Hamburg/ESO (European Southern Observatory) Survey or HES (Christlieb et al. 2008, see also Frebel et al. 2006b and Placco et al. 2011).

Until now, this has been the most efficient way to find metal-poor stars and hence the essential source of objects with [Fe/H] < -3.0 for which high-resolution, high S/N chemical abundance

analyses are currently available. By its nature, the method is strongly biased toward stars of lowest abundance. Current experience suggests that samples are relatively complete for stars with [Fe/H] $\lesssim$ −3.0 (Schörck et al. 2009).

3.2.4. Spectroscopic surveys.
The Sloan Digital Sky Survey (SDSS) and the subsequent Sloan Extension for Galactic Understanding and Exploration (SEGUE) surveys have obtained spectra with resolving power $R \sim 2,000$ and have proved to be a prolific source of metal-poor stars. The Tenth SDSS Data Release may be found at **http://www.sdss3.org/dr10/**. Currently, the Large Sky Area Multi-Object Fiber Spectroscopic Telescope (LAMOST) survey (Deng et al. 2012) is underway to provide metal-poor candidates in the Northern Hemisphere.

3.2.5. Photometric surveys.
Photometric systems have the potential to provide an alternative low-resolution method for discovering metal-poor candidates. In the Johnson *UBV* system, for example, the UV excess δ (*U*−*B*) (driven by the sensitivity of the U magnitude to line blocking by the plethora of metal lines in the *U* bandpass) was useful, in the infancy of this subject, for isolating and obtaining metallicity estimates for metal-poor stars (Roman 1954, Wallerstein & Carlson 1960).

A survey currently underway to discover the most metal-poor stars in the Southern Hemisphere by using a tailor-made intermediate band filter system is the SkyMapper Southern Sky Survey (Keller et al. 2007a,b). The filter set was designed specifically for the determination of the atmospheric parameters of metal-poor stars. During the commissioning period, the most iron-poor star currently known, SM 0313−6708 with [Fe/H] < −7.3, was discovered (Keller et al. 2014).

3.3. High-Resolution, High Signal-to-Noise Follow-Up Spectroscopic Abundance Analyses

After identifying promising candidate metal-poor stars, the next step is to obtain high-resolution ($R \gtrsim 30,000$), high S/N optical spectra to provide the data for the determination of basic stellar information, such as accurate chemical abundances, isotopic ratios (of only very few elements), and in some cases stellar ages. The required high-resolution, high S/N requirements are best achieved with 6–10 m telescope/echelle spectrograph combinations—currently HET/HRS, Keck/HIRES, Magellan/MIKE, Subaru/HDS, and VLT/UVES. In using these facilities, some investigators take short (snapshot) exposures to enable them to choose the most interesting metal-poor stars in their sample before embarking on long exposures (several hours) to obtain the high S/N necessary for a detailed analysis. Two examples of this are Barklem et al. (2005) and Aoki et al. (2013). Most stellar abundances are then determined from equivalent width measurements of spectral absorption lines, which are obtained with an observational uncertainty in equivalent width that varies as $\text{FWHM}^{0.5}/(\text{S/N})$, where FWHM is the full width at half maximum of the line (Cayrel et al. 2004). As the resolving power of the spectrograph and the S/N of the spectrum increase, the line measurement uncertainties decrease, allowing for the detection of weaker features. This is of particular importance when observing the extremely weak-lined most metal-poor stars.

As noted in Section 3.1, we confine our attention in the present work primarily to stars having [Fe/H] < −3.0. The following investigations contain abundances for a significant number of stars ($\gtrsim$15) having [Fe/H] less than this limit: McWilliam et al. (1995), Ryan et al. (1996), Cayrel et al. (2004), Lai et al. (2008), Hollek et al. (2011), Bonifacio et al. (2012b), Cohen et al. (2013), Yong et al. (2013a), and Roederer et al. (2014). For a more comprehensive introduction to the literature for surveys and analyses of metal-poor stars of all abundances, we refer the reader to Roederer et al. (2014, section 1). Two comprehensive and useful compilations of abundances for metal-poor
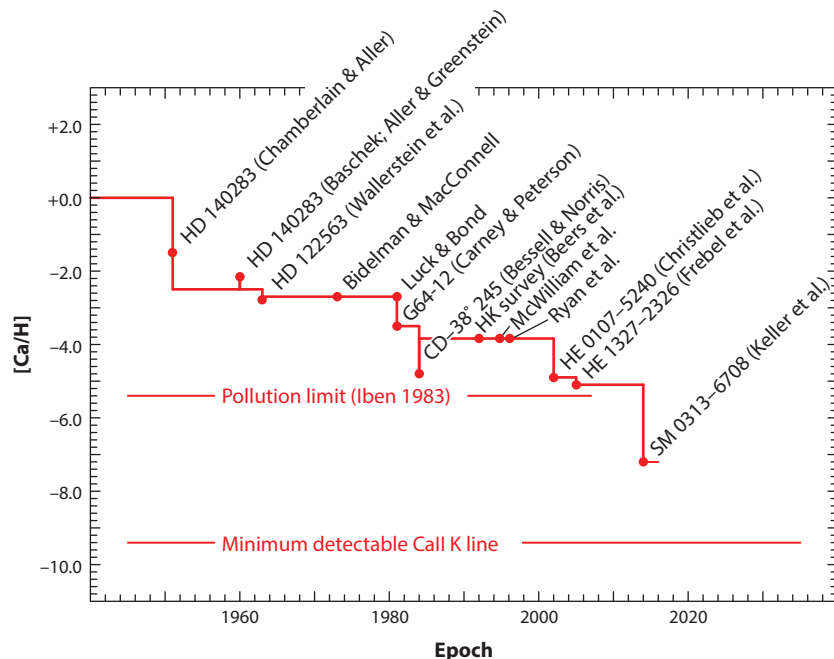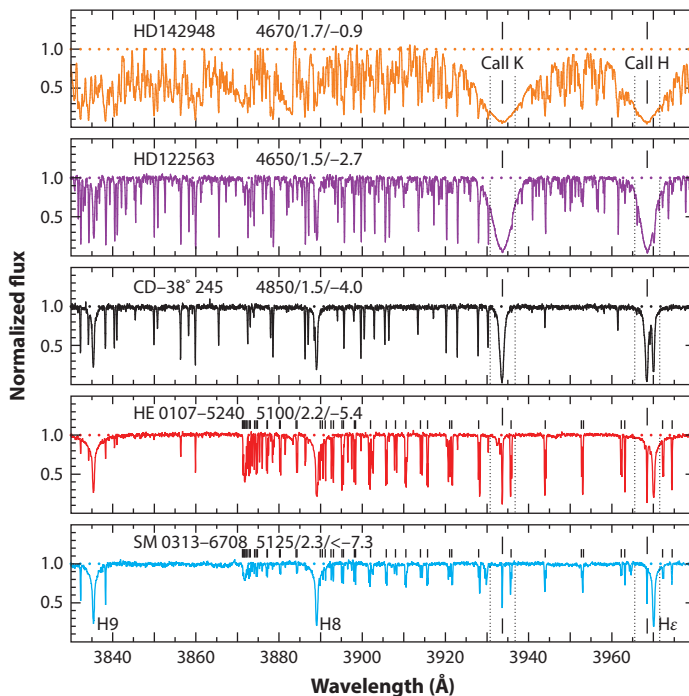
Figure 3

The calcium abundance, [Ca/H], of the most Fe-poor star then known, as a function of epoch of discovery. (We use [Ca/H] because calcium is still observable at lowest metallicities when iron is no longer detectable.) The circles denote the abundance determined by the authors, and the horizontal connecting lines refer, approximately, to currently accepted values. The two lower limiting lines are discussed in the text.

stars, based on high-resolution analyses, are those of Suda et al. (2008) and Frebel (2010). The respective websites are **http://saga.sci.hokudai.ac.jp** and **http://www.metalpoorstars.com**; the latter is used in the next sections.

3.4. The Most Metal-Poor Stars

3.4.1. Metallicity as a function of epoch of discovery. The history of the discovery of the most metal-poor stars in the halo is shown in **Figure 3**, which presents the abundance of calcium, [Ca/H], of the most calcium-poor star then known as a function of the epoch. Discovery references are Chamberlain & Aller (1951), Baschek (1959), Aller & Greenstein (1960), Wallerstein et al. (1963), Bidelman & MacConnell (1973), Carney & Peterson (1981), Luck & Bond (1981), Bessell & Norris (1984), Beers et al. (1992), McWilliam et al. (1995), Ryan et al. (1996), Christlieb et al. (2002), Frebel et al. (2005), and Keller et al. (2014). Also shown, as reality checks, are two estimates of predicted lower limits below which one might not expect to find any star—for physical or technical reasons. The higher of the two limits is the prediction by Iben (1983) of [Fe/H] = −5.7 (assuming [Ca/Fe] = 0.3) as the putative surface value a zero heavy-element abundance star would acquire by accretion of the Galactic interstellar material over the past 10 Gyr, assuming a time-averaged accreted abundance of [Fe/H] = −0.6. Insofar as the Iben calculation is a back-of-the-envelope calculation, one should not be surprised that a star has been observed below this limit. The lower line, in contrast, is the more restrictive limit of Frebel & Norris (2013), which is the calcium abundance one might determine for a very low upper limit of the observed CaII K

Figure 4

High-resolution (R ∼ 40,000), high S/N spectra of metal-poor red giants having similar T_{eff} and $\log g$ in the [Fe/H] range < −7.3 to −0.9 and wavelength range 3830–3980 Å. The numbers in each panel to the right of the star's identification represent the atmospheric parameters $T_{\text{eff}}/\log g/$[Fe/H], with metallicity decreasing from top to bottom. Note that, although the CaII H and K lines become very weak in the two most iron-poor stars, HE 0107−5240 and SM 0313−6708, many more lines have appeared. These are features of CH (the positions of which are indicated immediately above the spectra), resulting from extremely large overabundances of carbon relative to iron in these objects. For convenience, the vertical dotted lines are added to help delineate the positions of the H and K lines in the lower spectra. Alternative representations of the spectra are provided in **Supplemental Figures 1–4**. Follow the **Supplemental Material link** from the Annual Reviews home page at **http://www.annualreviews.org**.

line strength of 20 mÅ in a putative metal-poor red giant having $T_{\text{eff}} = 4,500$ K and $\log g = 0.5$. [The CaII K line is the strongest atomic feature in the spectra of metal-poor stars (see **Figure 4**), and its strength is intrinsically greater in red giants than in near main-sequence dwarfs.] We make two further points about **Figure 3**. First, steady progress has been made over the past six decades to find stars with lower and lower metallicities (notwithstanding the one to two decade periods without progress). Second, we have most likely come to the point where further progress for identifying stars with lower abundances will be very slow. The spectrum of the most metal-poor star currently known, SM 0313−6708 (Keller et al. 2014) has [Ca/H] = −7.2, and no Fe lines have been observed. The only other elements so far detected are H, C, O, Mg, and Si; the strength of the CaII K line is a mere 90 mÅ. For comparison, the strength of this line in CD−38°245 (which has [Fe/H] = −4.0) is 1,485 mÅ.

3.4.2. The eight most iron-poor stars. A very challenging aspect of the study of the most metal-poor stars is their extreme rarity. Below [Fe/H] $\lesssim$ −4.5, only eight of them are known.

Table 1 The eight most Fe-poor stars

Object	RA (2000) Dec	T_{eff}	log g	[Fe/H]	[C/Fe]	V_r (km s^{-1})	References
SM 0313−6708[a]	03 13 00.4 −67 08 39.3	5,125	2.30	<−7.30	>+4.90	ND	Keller et al. (2014)
HE 1327−2326	13 30 06.0 −23 41 49.7	6,180	3.70	−5.66	+4.26	64	Frebel et al. (2005), Aoki et al. (2006)
HE 0107−5240	01 09 29.2 −52 24 34.2	5,100	2.20	−5.39	+3.70	44	Christlieb et al. (2002, 2004)
SD 1035+0641[a]	10 35 56.1 +06 41 44.0	6,262	1.5	<−5.1	>3.5	−70	Bonifacio et al. (2015)
HE 0557−4840	05 58 39.3 −48 39 56.8	4,900	2.20	−4.81	+1.65	212	Norris et al. (2007)
SD 1742+2531[a]	17 42 59.7 +25 31 35.9	6,345	1.5	−4.8	+3.6	−208	Bonifacio et al. (2015)
SD 1029+1729[a]	10 29 15.2 +17 29 28.0	5,811	4.00	−4.73	<+0.93	−34	Caffau et al. (2011a, 2012)
HE 0233−0343	02 36 29.7 −03 30 06.0	6,100	3.40	−4.68	+3.46	64	Hansen et al. (2014)

[a]SM 0313−6708 = SMSS 031300.36−670839.3; SD 1029+1729 = SDSS J102915+172927; SD 1742+2531 = SDSS J174259+253135; SD 1035+0641 = SDSS J103556+064144.

Abbreviations: Dec, declination; ND, no data; RA, right ascension; T_{eff}, effective temperature; V_r, radial velocity.

We present identification details for these in **Table 1**, where the stars are arranged in order of increasing [Fe/H]. Detailed abundances on the basis of model-atmosphere analysis of high-resolution, high-S/N spectra are available for all these stars. For future reference, we draw the reader's attention to the very large overabundances of carbon relative to iron in seven of these eight stars (see **Table 1**, column 6). For the five C-rich stars in which iron is detected, the relative carbon abundances lie in the range [C/Fe] = +1.6 to +4.3. For SM 0313−6708, in which iron is not detected, [C/Fe] > +4.9. The eighth star is SDSS J102915+172927 (hereafter SD 1029+1729) (Caffau et al. 2011a, 2012), where [Fe/H] = −4.8 and [C/Fe] < +0.9. Its comparably low carbon abundance provides a critical challenge for an understanding of the diversity that existed at the earliest times.

For comparison with the number of stars for which high-resolution, high-S/N abundances are currently known at higher metallicity, we estimate roughly that some 200–300 stars have been discovered that have high-resolution estimates of [Fe/H] in the range −4.0 < [Fe/H] < −3.0. Data are available for these, or soon will be, and are suitable for analysis in a homogeneous and self-consistent manner.

The discovery of more stars with [Fe/H] $\lesssim$ −4.5 will prove a challenge. For the stars in **Table 1**, all but one are relatively bright, with V < 15.5. To find more, such as the faintest one (SD 1742+2531) with V = 18.8 (Bonifacio et al. 2015), will require survey observations of greater volumes with telescope time-intensive follow-up high-resolution, high-S/N spectroscopy.

3.4.3. Spectroscopic data. **Figure 4** presents high-resolution, high-S/N spectra of five metal-poor red giants, all having approximately the same effective temperatures and surface gravities, but with very different heavy-element abundances, decreasing as one moves from top to bottom in the figure. (Atmospheric parameters T_{eff}/log g/[Fe/H] are also presented in the figure.) In the top panel, the spectrum of HD 142948, with [Fe/H] = −0.9, is shown as an example of a relatively metal-rich object, whereas each of the other four stars was the most metal-poor object known at its time of discovery (see **Figure 3**). Alternative representations of these spectra, together with their corresponding two-dimensional rainbow-colored spectra [for both metal-poor giants and near main-sequence turnoff (MSTO) stars], are provided in **Supplemental Figures 1–4**.

Supplemental Material

There are two important points to take from **Figure 4**. First, as most clearly seen in the top three panels, the strength of the features in the spectra, in particular the CaII H and K lines, decrease markedly as one moves from the top ([Fe/H] = −0.9) to the middle ([Fe/H] = −4.0) panel. The second point is somewhat more subtle but extremely important for the discussion that follows. As one moves from the middle to the bottom panel of the figure, the CaII H and K lines clearly continue to weaken, and the pattern of the weak lines in the spectra changes in character. This is driven by the fact that, in the bottom two panels, lines of the CH molecule become stronger because of enormous overabundances of carbon not present in the stars in the top three panels. Said differently, HE 0107−5240 and SM 0313−6708, with [Fe/H] = −5.4 and < −7.3, have enormous relative abundances of carbon, with [C/Fe] = 3.7 and >+4.9, respectively. As noted when introducing **Table 1**, large overabundances of C relative to Fe are common features of the most Fe-poor stars. This is a fundamental result, which we discuss at length below.
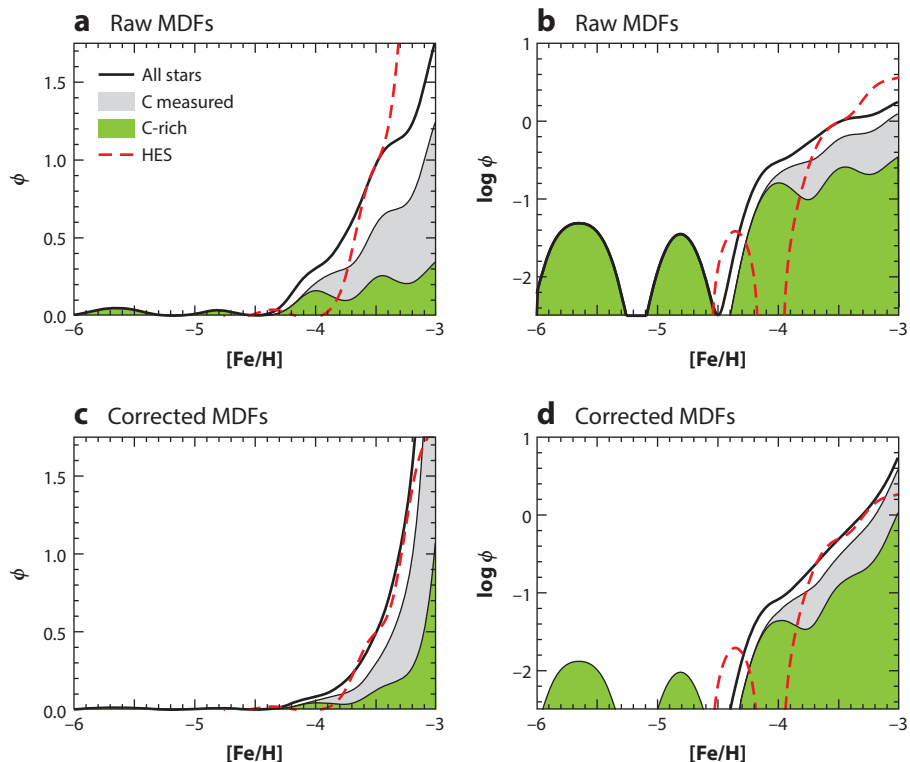
3.5. The Metallicity Distribution Function of the Halo

Metallicity distribution functions (MDFs) provide essential constraints on galactic chemical enrichment models and in the present context on the nucleosynthetic yields of the first stars and the various putative populations that existed at the earliest times. Strictly speaking, MDF refers to the distribution of Z, the fraction of all elements heavier than lithium. In practice, however, a more useful distribution function (both observationally and theoretically) is Z_i, where i refers to the element i. Observationally, in most cases i refers to Fe, given that iron is one of the most abundant and readily measurable elements in stars. It is also observed to be closely related in its abundance proportion to that of Ca, which is of critical importance as one goes to lowest abundance because the CaII K line is intrinsically much stronger than any of the lines of Fe I. Accordingly, the K line may be used more efficiently for discovery purposes and at the lowest metallicities, when Fe is no longer detectable in the spectra of stars, for the determination of their chemical abundances.

In Section 3.4.3, we discussed the increasing disconnect between carbon and iron as one goes to lower and lower abundances. For this reason, the carbon distribution function is also of critical importance. As we see in Section 3.8.1, oxygen is important as well but very difficult to determine in practice. This point highlights the present impracticability of the use of Z as the independent variable for construction of an MDF, given that not all of the major contributing elements are currently measurable. The following discussion thus addresses the distribution functions of only Fe and C.

From a semantic point of view, we recall from Section 1.4.2 that the term metal-poor star is not necessarily synonymous with Fe-poor star. It is also worth noting that when it comes to relating chemical composition to age, it is not obvious which of two stars having the same value of [Fe/H], but one C-rich ([C/Fe] > +0.7) and the other C-normal ([C/Fe] ≤ +0.7), might be older. We return to this point in Section 5.5.

In an earlier review of metal-poor stars (Frebel & Norris 2013), we discussed (Fe) MDFs for the Galactic globular clusters, high-proper-motion samples (Ryan & Norris 1991, Carney et al. 1996), and the medium-resolution abundance samples of the HES (Schörck et al. 2009, Li et al. 2010); we refer the reader to these references for background information. There are two important points that should be emphasized concerning the efficacy of these previously described MDFs in the context of low metallicities. The first is that, of these samples, only the HES reaches well below [Fe/H] < −3.0. The second is that below [Fe/H] ≲ −4.0 at the low spectral resolution of $R \lesssim 2,000$, adopted in these investigations, it is difficult (if not impossible) to determine reliable Fe abundances because of the weakness of the lines, the contamination by CH lines, and occasional interstellar CaII lines in the spectra of these objects. One needs high resolution to meet

Figure 5

The Fe metallicity distribution function based on the high-resolution, high-S/N homogeneous abundance analysis by Yong et al. (2013a). The generalized histograms have been generated using a Gaussian kernel having $\sigma = 0.30$ dex, and these are presented on linear (*left*) and logarithmic (*right*) scales. Green and gray color coding is used to present the contribution of C-rich and C-normal stars, respectively, for which measurement was possible. Panels *a* and *b* refer to the raw data, and panels *c* and *d* show the same data corrected for completeness for the range $-4.0 < [Fe/H] < -3.0$, as described by Yong et al. (2013b). The dashed line shows the metallicity distribution function (MDF), which was based on Hamburg/ESO survey data by Schörck et al. (2009). Reproduced with permission of D. Yong, private communication.

these challenges. For these reasons, we concentrate on recent results of high-resolution, high-S/N analyses that have yielded C and Fe abundances.

Figure 5 shows the (Fe) MDF from the work of Yong et al. (2013b) for a sample of 86 extremely metal-poor stars ([Fe/H] < -3.0), based on their homogeneous chemical abundance analysis of high-resolution, high-S/N data, from both their own observations and from those available in the literature. In this sample, 32 stars have [Fe/H] ≤ -3.5, and there are 9 with [Fe/H] ≤ -4.0. [We note for completeness that three of their stars have [Fe/H] < -4.5, although currently, eight such stars are known (see **Table 1**).]

Figure 5 also shows the relative contributions of C-normal and C-rich stars to the MDF for stars with [Fe/H] < -3.0, where the increasing role of C-rich stars at lowest [Fe/H] is clearly seen. (See Section 3.7 for a discussion of carbon richness.) For three metallicity bins in the range $-4.5 < [Fe/H] < -3.0$ (with medians [Fe/H] ~ -3.1, [Fe/H] ~ -3.4, and [Fe/H] ~ -3.8) containing roughly equal numbers of stars, Yong et al. (2013b, their figure 7) report increasing

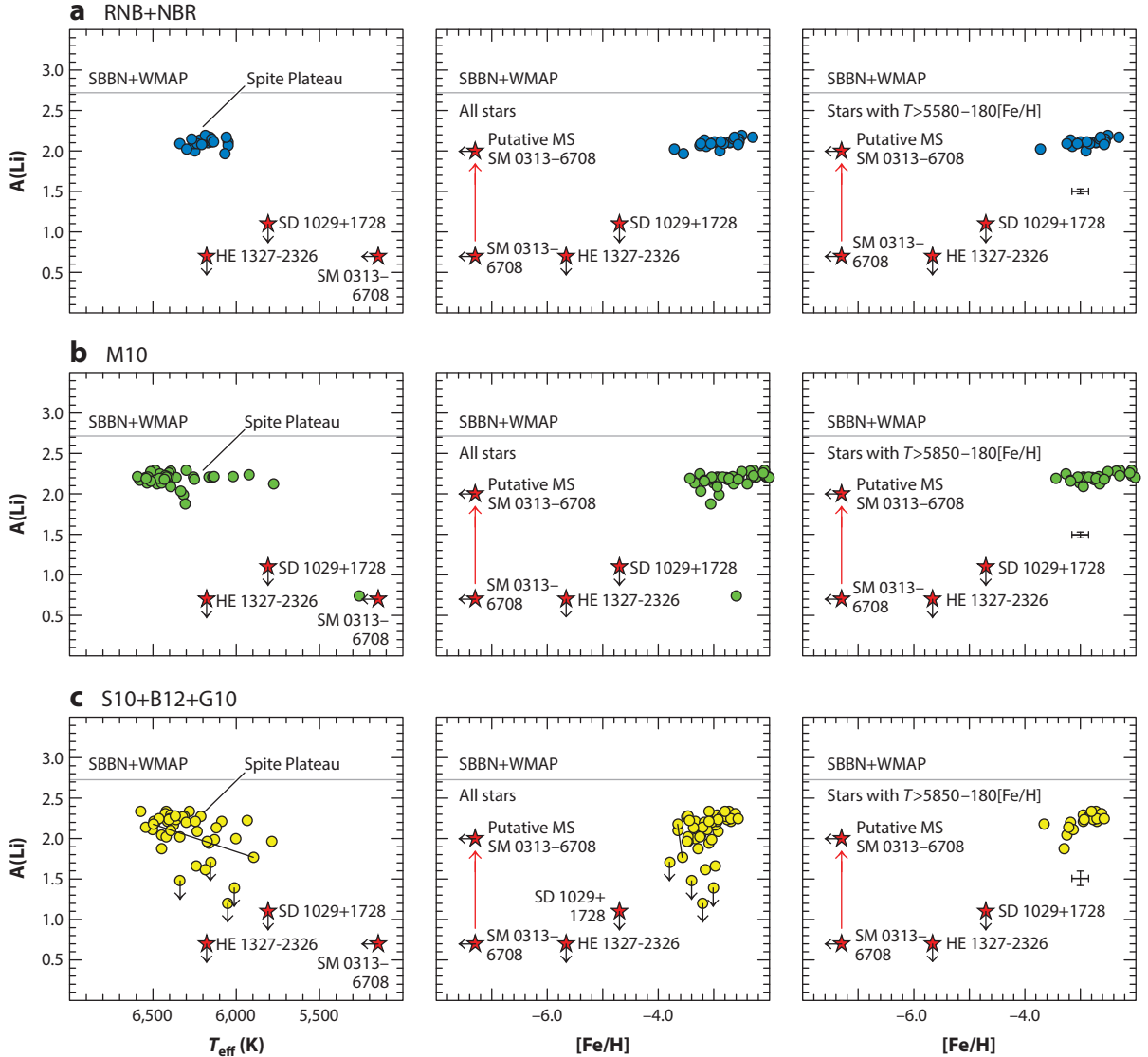C-rich fractions of 0.22, 0.32, and 0.33, as [Fe/H] decreases, and for [Fe/H] < −4.5, the fraction is 1.00. More recently, Placco et al. (2014) have determined the C-rich fractions using all available high-resolution abundances from the literature and taking into account the decrease of the surface carbon abundance for luminous stars on the upper red giant branch (RGB). Understandably, their results yield higher fractions: 0.43, 0.60, 0.70, and 1.00, respectively, for the median [Fe/H] values associated with the Yong et al. (2013b) fractions given above. For additional comparison, the uncorrected Placco et al. (2014) values are 0.32, 0.51, 0.65, and 1.00, respectively, which are also higher than those of Yong et al. This clearly indicates that sample sizes and analysis methods still play a role in establishing these fractions. Homogeneously analyzed data of high-resolution samples, including abundance values of both C and Fe and paired with correction for the surface carbon depletion, are needed to complete the picture. The upcoming and ongoing projects described in Section 3.2 have the potential to supply these data.

We conclude by noting that the theoretical interpretation of the MDFs remains difficult. Simple galactic chemical enrichment models are of only limited usefulness. We would argue that to achieve a meaningful comparison of theory to observation, at the very least, theoretical models should address (*a*) the strong claims that the MDF and C-rich fraction change with Galactocentric distance (Frebel et al. 2006b; Carollo et al. 2010, 2012; An et al. 2013) and (*b*) the need for element yields that recognize that C and Fe are decoupled for abundances below [Fe/H] = −3.0 (most likely because of the existence of two different stellar progenitor populations).

3.6. Lithium and the Fragility of the Spite Plateau for Extremely Metal-Poor Stars

A fundamental prediction of the Big Bang paradigm is the result of Wagoner et al. (1967, pg. 42) that "^{7}Li [is] produced in a universal fireball." SBBN, constrained by the results of WMAP (Spergel et al. 2007), predicts that the primordial lithium abundance is A(Li)$_P$ = $2.72^{+0.05}_{-0.06}$ (Cyburt et al. 2008). Spite & Spite (1982) first demonstrated that when the Li abundance of metal-poor, near-MSTO stars are plotted in the A(^{7}Li), hereafter A(Li), versus T_{eff} plane, the Li abundances appear constant for those stars that lie in the effective temperature range $5,500\,K < T_{eff} < 6,250$ K. They determined that the lithium abundance of these stars is A(Li) = 2.05 ± 0.16.

Since the discovery of the Spite Plateau, there has been an enormous effort, both observationally and theoretically, to refine and understand its implications. We refer the reader to Thorburn (1994), Ryan et al. (1999), Charbonnel & Primas (2005), Asplund et al. (2006), Bonifacio et al. (2007, 2012b), Aoki et al. (2009b), Meléndez et al. (2010), and Sbordone et al. (2010), as well as to the references therein, for details of some of the observational contributions. There are very divergent conclusions among the interpretations of the derived lithium abundances in these studies. In **Figure 6a,b,c,** we present A(Li) for near main-sequence stars (with one exception) as a function of T_{eff} (left column) and [Fe/H] (middle and right columns) to illustrate some of the tensions among these works. The middle column presents all of the results from a given set of authors, and on the right are plotted only those stars that satisfy the Meléndez et al. (2010) criterion $T_{eff} > 5,850\,K − 180 ×$ [Fe/H] to take into account truncation of the cool end of the plateau (by the convective destruction of Li in the stellar outer layers). Although the subject is extensive, we limit this discussion to three main points: First, the most fundamental result to be taken from **Figure 6** is that the Spite Plateau lies well below the primordial Li abundance predicted by SBBN/WMAP by a factor of ~3 (~0.5 dex). Perhaps the most widely held view is that, given the accuracy of the WMAP/SBBN primordial Li abundance, the value obtained from analysis of observed Li line strengths in near-MSTO metal-poor stars is not the primordial value and that an

650 Frebel • Norris

Figure 6

A(Li) versus T_{eff} (*left*) and [Fe/H] (*middle* and *right*) for near main-sequence stars having [Fe/H] < −2.0. The circles represent data from: (*a*) Ryan et al. (1999, abbreviated here as RNB) and Norris et al. (2000, abbreviated as NBR) who both use one-dimensional (1D/LTE) models; (*b*) Meléndez et al. (2010, abbreviated as M10) who use 1D/NLTE models; and (*c*) Sbordone et al. (2010, abbreviated as S10) who use 1D/LTE models and T_{eff} from the Infrared Flux Method, Bonifacio et al. (2012b, abbreviated as B12) using 3D/NLTE, and González Hernández et al. (2008, abbreviated as G10) using 1D/LTE models. (T_{eff}-scale details are given when authors present multiple results.) The Li abundances in the right panels are a subset of those presented in the middle panels, after exclusion of stars that may have experienced Li destruction, following Meléndez et al. (2010). (Here we use slightly different zero points for the Meléndez et al. criterion to allow for differences in T_{eff} scales.) The red star symbols refer to three stars with [Fe/H] < −4.5 and are described in Section 3.6. The most Fe-poor star, SM 0313−6708, with [Fe/H] < −7.3 and A(Li) = +0.7, is connected by a long upward arrow to the Li abundance it may have had when on the main sequence. See Section 3.6 for discussion. The horizontal line in each panel represents the primordial lithium abundance. Abbreviations: LTE, local thermodynamic equilibrium; NLTE, non-LTE.

explanation of the difference will lead to a deeper understanding of the astrophysics of stars. See Asplund et al. (2006) and Frebel & Norris (2013), and references therein, for more detail. Second, further work is urgently needed to thoroughly explore and understand the meltdown of the Spite Plateau reported by Sbordone et al. (2010) and Bonifacio et al. (2012b) (**Figure 6c**). And third, it is critical to limit the putative T_{eff} span of the Spite Plateau to ranges for which the cool end does not include stars that have experienced Li destruction in their convective outer layers.

More relevant to the focus of the present review, we also plot in each of the panels in **Figure 6** the two most Fe-poor near main-sequence stars (HE 1327−2326 with [Fe/H] = −5.7 and SD 1029+1729 with [Fe/H] = −4.7; see **Table 1**). Both stars are extremely Li-poor, falling well below the Spite Plateau. One should thus be alive to the possibility that the Li was already depleted in the material from which these stars formed. That said, there are some restrictions for a scenario in which such a star-forming cloud results from the admixture of the ejecta of a supernova or a rotating massive star into an existing interstellar medium having primordial Li. For example, even if the resulting cloud comprised equal masses of these two components, the first with no Li and the second with the primordial value, the resulting star would have a lithium abundance only 0.3 dex below the primordial value. A more far-reaching global solution that may be relevant here is the suggestion of Piau et al. (2006), in the context of the primordial Li problem, that a significant fraction of the earliest star-forming clouds was processed through Population III stars.

Also important in this context is the Li abundance of the red giant SM 0313−6708, plotted in all panels of **Figure 6**, which has [Fe/H] < −7.3, T_{eff} = 5,125 K, log g = 2.3, and A(Li) = +0.7 (Keller et al. 2014). Given that evolution from main sequence to RGB destroys a considerable amount of lithium in a star's convective envelope during its evolution on the RGB, one might expect that the lithium abundance of SM 0313−6708 would have been much higher when the star was on the main sequence. If, for example, one uses the result of Korn et al. (2007) for the globular cluster NGC 6397 ([Fe/H] = −1.9) as a guide, the Li depletion factor between the MSTO and T_{eff} = 5,100 K on the RGB is ~1.3 dex, which leads to a main sequence abundance for SM 0313−6708 of A(Li)$_{MS}$ ~ 2.0, not unlike the Spite Plateau values, as schematically demonstrated in **Figure 6**. This is a rather significant result, suggesting that the Spite Plateau may have existed at the earliest times for low-mass stars having [Fe/H] ~ −7.0. From stellar isochrones we expect that SM 0313−6708 was at the MSTO relatively recently, ~1 Gyr ago. That is to say, relatively little meltdown appears to have happened at the MSTO, and any putative truncation of the cool edge of the Spite Plateau appears not to have reached the MSTO for stars having [Fe/H] ~ −7.0 or less at the earliest times.

A further basic result of Big Bang nucleosynthesis is that very little ^{6}Li accompanied the production of the initial ^{7}Li (e.g., ^{6}Li/^{7}Li $\gtrsim 10^{-4}$) (Wagoner 1973). Recent predictions by Coc et al. (2012) yield ^{6}Li/^{7}Li = $10^{-4.6}$. For a detailed discussion of the primordial ^{6}Li/^{7}Li ratio and corresponding observations, we refer the reader to the thorough 3D/NLTE analysis of four near-MSTO stars by Lind et al. (2013, see also references therein), who find that none of them has a significant (2 σ) detection of ^{6}Li.

3.7. An Overview of Abundances Relative to Calcium

In this section, we are primarily interested in stars having [Fe/H] < −3.0. To set the scene, we discuss relative abundances, [X/Fe] and [X/Ca], obtained from high-resolution, high-S/N model atmosphere analysis for a representative set of elements in the metallicity range [Fe/H] $\lesssim$ −2.0.

As discussed above, one of the most intriguing, and potentially most important, results concerning the abundance signatures of metal-poor stars is the high incidence of stars with abnormally high relative carbon abundances [C/Fe], a fact that was first appreciated by Beers et al. (1992). Beers & Christlieb (2005), to whom we refer the reader for more details, classified C-rich objects having

[C/Fe] > +1.0 into a number of subclasses of carbon-enhanced metal-poor (CEMP) stars by using the following taxonomy involving the relative abundances of the heavy neutron-capture elements: CEMP-s (s-process element enhancement), CEMP-r (r-process enhancement), CEMP-r/s (both r- and s- enhancements), and CEMP-no (no enhancement of either s- or r-process elements). The CEMP-s subclass represents a large fraction of the C-rich population, the chemical enrichment of which is almost certainly driven by mass transfer across a binary system containing an erstwhile asymptotic giant branch (AGB) star (e.g., Lucatello et al. 2005 and references therein). Such stars are, however, extremely rare below [Fe/H] = −3.0 (Aoki 2010, Norris et al. 2013), and given that this is the abundance range under discussion in the present review, we exclude the CEMP-s subclass by rejecting C-rich stars that have [Ba/Fe] > 0. Stars of the CEMP-r and CEMP-r/s sub-classes, which mainly have [Fe/H] $\gtrsim$ −3.0, were also excluded. We thus expect the C-rich stars in the following figures to belong to the CEMP-no subclass. In the range −4.0 < [Fe/H] < −2.0, the majority of stars have relative abundance ratios that do not differ wildly from the well-defined trends of the bulk of halo stars, which may be regarded as normal. This is, however, not the case for the some 20–30% of stars that are C rich. For [Fe/H] < −4.0, most of the stars are C rich.

Figure 7 presents the dependence of [X/Ca] as a function of [Ca/H] over the range −8.0 < [Ca/H] < −2.0. Normally, the abscissa of choice in this sort of diagram is [Fe/H], and in the sections that follow, we revert to this convention. That said, we choose to use [Ca/H] as abscissa in Figure 7 to highlight the newly discovered star SM 0313−6708 (Keller et al. 2014). With [Ca/H] = −7.2, this star is so metal-poor that only four elements other than hydrogen (Li, C, Mg, and Ca) have currently been observed in its spectrum. Red and black symbols in Figure 7 are used to identify C-rich and C-normal stars, here defined to have carbon abundances larger or smaller than [C/Fe] = +0.7, respectively, following Aoki et al. (2007a). In plotting the diagram, the C-normal stars were set down first, followed by the C-rich objects. From top to bottom, the five rows in the figure contain pairs of elements representative of different nucleosynthesis processes: (*a*) C and O; (*b*) the light odd-elements Na and Al; (*c*) the α-elements Mg and Si; (*d*) the iron-peak Fe and Ni; and (*e*) the heavy neutron-capture elements Sr and Ba. Here are some highlights of these panels.

- In the top-left panel, the upper dotted (red) line delineates the boundary between C-rich and C-normal stars ([C/Fe] = +0.7, and assuming [Ca/Fe] = 0.4). As one proceeds to lower values of [Ca/H] (and [Fe/H]), the fraction of C-rich stars, as well as the enhancement of C relative of the heavier elements Ca and Fe, increases in comparison with the values found in C-normal stars. Below [Ca/H] ~ −4.0, almost all stars are C rich, with enormous relative overabundances Δ[C/Ca] (and Δ[C/Fe]), of order 1 to 4 dex, relative to the values found in C-normal stars.

- For the light elements O to Mg, there are also very large relative overabundances in the C-rich stars for [X/Ca] below [Ca/H] = −4.0, with values up to 1 to 2 dex higher than those found in C-normal stars.

- In contradistinction to what is seen for C to Mg, in the range Si to Ni, there appear to be no major differences between the relative abundances [X/Ca] of C-rich and C-normal stars as a function of [Ca/H].

- There is a large spread in [Sr/Fe] and [Ba/Fe] at all values of [Ca/H], with no obvious dependence on carbon abundance.

We discuss the role of these elements in more detail in Sections 3.8 and 4.2 in our quest to understand what their patterns in the Milky Way's halo and dwarf galaxy satellites have to tell us about conditions and origins at the earliest times.
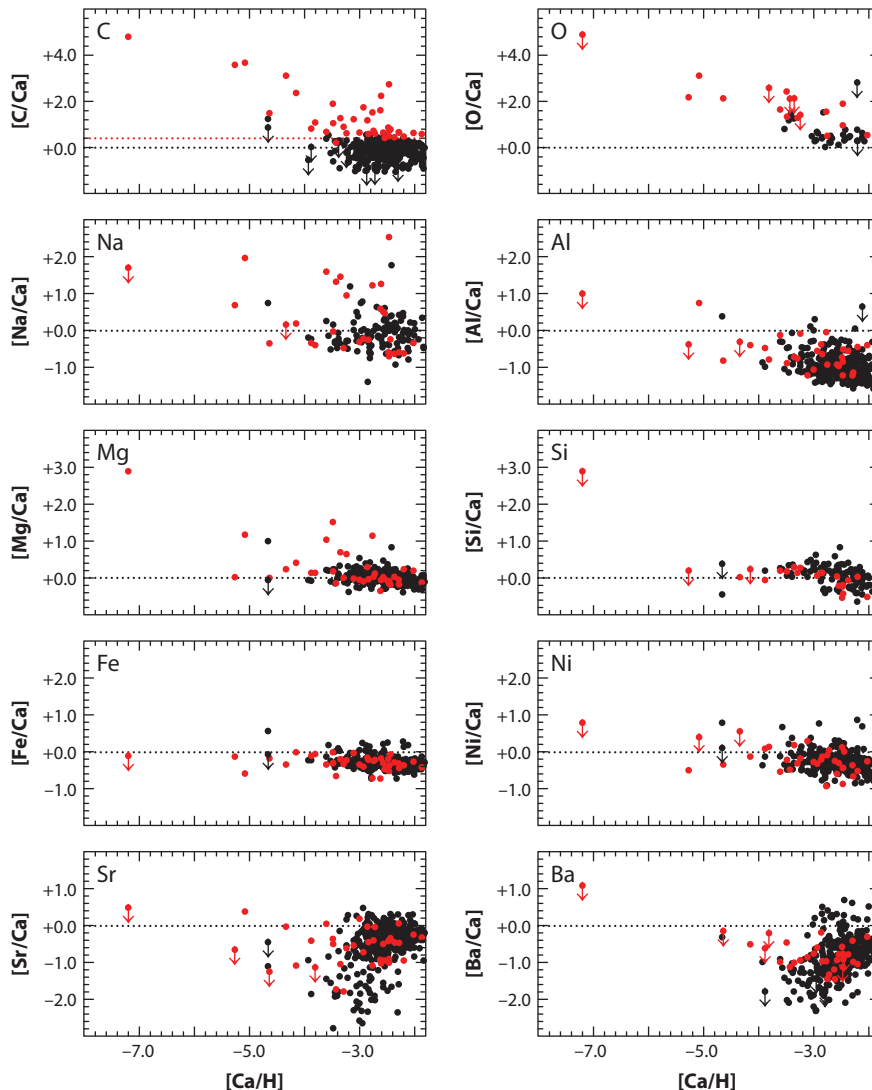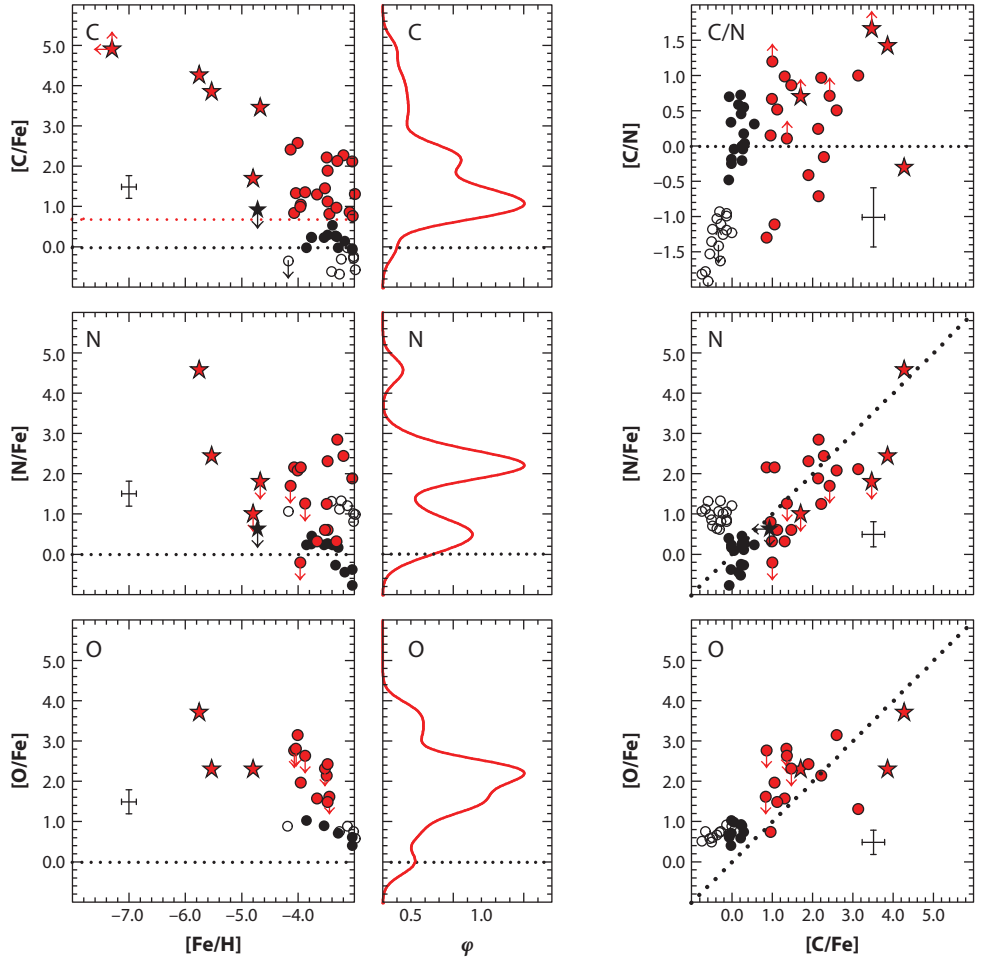
Figure 7

Relative abundances [X/Ca] as a function of [Ca/H] in C-rich stars (*red circles*) and C-normal stars (*black circles*), respectively. The five pairs of panels are representative of (*a*) the CNO elements, (*b*) the light odd elements, (*c*) the α-elements, (*d*) the Fe-peak elements, and (*e*) the heavy neutron-capture elements. In plotting the diagram, the C-normal stars were plotted first, followed by the C-rich objects. (The data for this figure are from Frebel 2010 and references therein, Cohen et al. 2013, Norris et al. 2013, Yong et al. 2013a, Hansen et al. 2014, and Keller et al. 2014.)

3.8. The Carbon-Rich and Carbon-Normal Populations of Extremely Metal-Poor Stars

3.8.1. Carbon, nitrogen, and oxygen. **Figure 8** presents the behavior of C, N, and O, as functions of [Fe/H] and [C/Fe], for stars in the range −8.0 < [Fe/H] < −3.0. We again highlight the differences between the C-rich and C-normal stars. The black symbols represent C-normal

Figure 8

[C/Fe], [N/Fe], and [O/Fe] are shown as a function of [Fe/H] (*left*) and [C/Fe] (*right*). Red and black symbols refer to C-rich (excluding CEMP-s, CEMP-r, and CEMP-r/s subclasses) and C-normal stars, respectively; the circles and star symbols stand for objects with [Fe/H] above and below −4.5, respectively. The middle column contains generalized histograms pertaining to the abundances to the left (Gaussian kernel, with $\sigma = 0.30$). The red dotted line in the upper-left panel is the boundary between C-rich and C-normal stars adopted in the present work. See Section 3.8.1 for discussion. The data are from Cayrel et al. (2004), Spite et al. (2005), Sivarani et al. (2006), Caffau et al. (2012), Cohen et al. (2013), Norris et al. (2013), Yong et al. (2013a), Hansen et al. (2014), and Keller et al. (2014).

stars, and the open and filled circles denote the mixed and unmixed red giant stars, respectively, of Spite et al. (2005). The red symbols stand for C-rich stars (excluding CEMP-s, CEMP-r, and CEMP-r/s subclasses).

The leftmost panels show [C/Fe], [N/Fe], and [O/Fe] as a function of [Fe/H]; the middle panels present the generalized histograms of the abundances of these elements in the C-rich stars. On the right, [C/N], [N/Fe], and [O/Fe] are plotted as a function of [C/Fe].

The important point to take from these data is that for the C-rich stars in which oxygen has been measured this element also shows large overabundances, commensurate with those determined for carbon. (We note for completeness that estimates of the oxygen abundance are not available for several of the stars in **Figure 8**. Although, in part, this may be because of the greater difficulty of measuring the abundance of O in comparison with that of C, it could be due to lower values of [O/Fe] than might be expected from the correlation seen in the figure. Further investigation is necessary to examine this possibility.) For nitrogen, in contrast, there exist both stars with large enhancements and others with only small excesses; its generalized histogram is suggestive of bimodality.

This behavior of the C-rich stars stands in some contrast to the results seen in **Figure 8** for the C-normal red giants (filled and open black circles), where one sees a bimodal behavior of the panels involving C and N, particularly evident in the top right panel. Spite et al. (2005) have convincingly argued that this effect is driven by mixing, on the RGB of material that has been processed by the CN cycle, from interior regions into the outer layers of the observed stars. For the C-rich stars, which comprise not only giants but also dwarfs such as HE 1327−2326 with [Fe/H] = −5.7, [C/Fe] = 4.3, [N/Fe] = 4.6, and [O/Fe] = 3.7; see **Table 1**), the presence of such large overabundances of all of C, N, and O is suggestive of the need of more than just the CN cycle. These results have been discussed in more detail by Norris et al. (2013), to whom we refer the reader. These authors also investigate the behavior of $^{12}C/^{13}C$ in the C-rich stars as a function of [Fe/H], [C/Fe], and [C/N], and note

> one sees perhaps the suggestion of a positive correlation between $^{12}C/^{13}C$ and [C/N], in the sense that would be expected from the processing of hydrogen and carbon in the CN cycle. The large values of [C/Fe] seen in [the ([C/Fe] versus [Fe/H])–plane], however, suggest that, if this were the case, one would require two processes, involving not only the CN cycle, but also helium burning as well.
> —Norris et al. (2013, pg. 6)

3.8.2. The lighter elements—sodium through calcium. The abundances of Na to Ca contain essential information for the understanding of the C-rich stars with [Fe/H] < −3.0. **Figure 9** presents [Na/Fe], [Mg/Fe], [Al/Fe], [Si/Fe], and [Ca/Fe] as a function of [Fe/H] and [C/Fe] for the C-rich and C-normal stars of the Galactic halo, together with generalized histograms for the former. (With the exception of HE 0107−5240, abundance limits are not included.) The data sources are the same as described for **Figure 8**.

There are a number of important points to be taken from **Figure 9**. First, although the data for the C-normal stars show low dispersions for all elements, there are large spreads in Na, Mg, and Al for the C-rich stars of order 1.5–2.5 dex. Second, there seems to be little, in any, spread for Si and Ca. Even though the case for this appears strong for Ca, the abundances for Si depend essentially on only one spectral line, and the result may not be as robust. Comparison of the present result with the apparent range and trend in [Si/Fe] reported by Norris et al. (2013, their figure 4) suggests that the larger data set and improved data quality now available demonstrate that more work on this element is necessary and warranted. Our third and final point is that not all C-rich stars exhibit large overabundances of Na, Mg, and Al. According to Norris and colleagues, only about half show the effect. We conclude the present section by noting that the abundance signatures seen in **Figures 8** and **9** are suggestive of the need of the admixing of material partially processed by nucleosynthetic H burning into regions experiencing He burning in the progenitor star. Taken together, these data led Norris et al. (2013) to suggest that there are two distinct stellar populations below [Fe/H] = −3.0: one C-rich, the other C-normal. We return to this topic in Section 5.5.
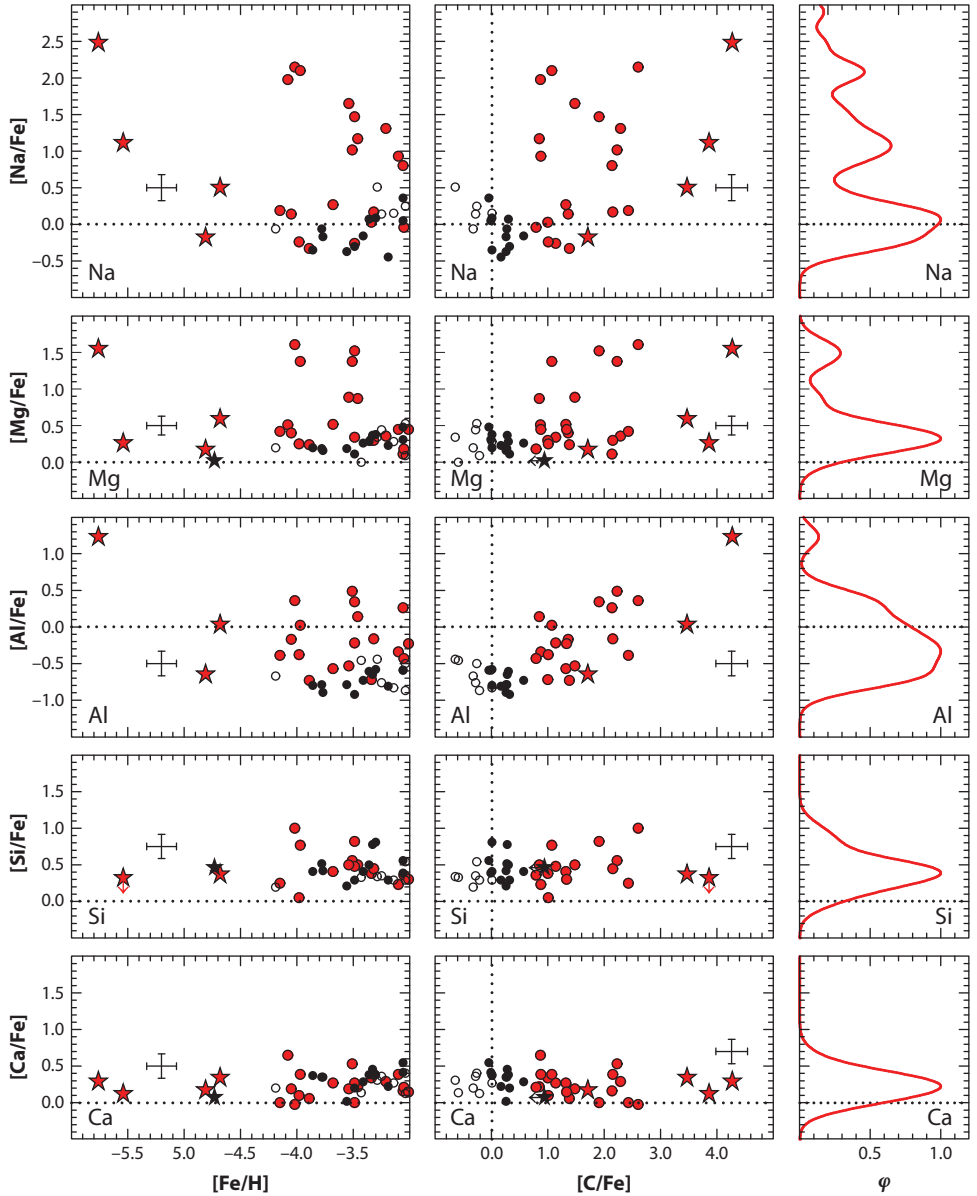
Figure 9

The relative abundances of the light elements Na, Mg, Al, Si, and Ca versus [Fe/H] (*left*) and [C/Fe] (*middle*) for C-rich and C-normal Galactic halo stars. Red and black symbols refer to C-rich (excluding CEMP-s, CEMP-r, and CEMP-r/s subclasses) and C-normal stars, respectively; the circles and star symbols stand for objects with [Fe/H] above and below −4.5, respectively (see leftmost panel). The right column contains generalized histograms pertaining to the abundances of the C-rich stars in the left panels (Gaussian kernel, with $\sigma = 0.15$). See Section 3.8.2 for discussion. The data are from Cayrel et al. (2004), Spite et al. (2005), Sivarani et al. (2006), Caffau et al. (2012), Cohen et al. (2013), Norris et al. (2013), Yong et al. (2013a), Hansen et al. (2014), and Keller et al. (2014). Abbreviations: CEMP, carbon-enhanced metal-poor; CEMP-s, s-process element enhancement; CEMP-r, r-process enhancement; CEMP-r/s, both r- and s-enhancements; C-normal, carbon-normal; C-rich, carbon-rich.

3.9. Unusual Carbon-Normal Extremely Metal-Poor Stars

The diversity of chemical properties for stars with [Fe/H] < −3.0 is not confined to C-rich stars. Rare examples exist of individual (or small numbers of) extremely metal-poor non-CEMP stars that have chemically unusual abundance ratios.

3.9.1. Divergent α-element abundances.

- The Mg-enhanced BS 16934-002, which has [Fe/H] = −2.8, [Si/Fe] = +0.44, and [Ca/Fe] = +0.35, but [Mg/Fe] = +1.23 (Aoki et al. 2007b).
- The α-element-challenged HE 1424−0241, with [Fe/H] = −4.0 and [Mg/Fe] = +0.44, but [Si/Fe] = −1.01 and [Ca/Fe] = −0.44 (Cohen et al. 2007). Recently, Cohen et al. (2013, see their figure 12) identified nine more stars that share this characteristic, albeit at a lower significance level than HE 1424−0241.
- The α-element-ambivalent SDSS J234723.64+010833.4, with [Fe/H] = −3.2 and [Mg/Fe] = −0.10, but [Ca/Fe] = +1.11 (Lai et al. 2009).
- A star likely related to the above three (with only an upper limit of [C/Fe] < +1.7) is HE 2136−6030 with [Fe/H] = −2.9. It has [Mg/Fe] = 0.08, but [Si/Fe] = +1.20 (Yong et al. 2013a).

3.9.2. Iron-rich stars.
Stars with large numbers of elements having [X/Fe] lower by ∼0.3 dex compared with normal halo stars of the same [Fe/H], such as CS 22169-035, with [Fe/H] = −3.0 (Cayrel et al. 2004), and HE 1207−3108, with [Fe/H] = −2.7 (Yong et al. 2013a, see their figure 49).

3.9.3. Outlying abundances.
Yong et al. (2013a) and Cohen et al. (2013) have also examined their databases for individual elements that appear significantly distinct from normal stars of the same [Fe/H]. In the range Na–Ni, Yong et al. (2013a) reported that 21 ± 5% of stars were anomalous with respect to one element and that 4 ± 2% were anomalous with respect to at least two. Cohen and colleagues found a similar result: "Ignoring the C-stars, this leads to approximately 15% of the sample being strong outliers in one or more elements between Mg and Ni." (Cohen et al. 2013, pg. 17; see their table 14.)

Further work is clearly necessary to understand the significance of all of the above results. One might expect that these outliers are most likely indicative of incomplete mixing of the ambient medium from which the stars formed and that they contain clues concerning the nature of the ejecta, perhaps from only a limited part of the initial mass function (IMF) of the previous enriching generation.

3.9.4. Progeny of pair-instability supernovae?
One of the holy grails of metal-poor star research is the discovery of stars showing the signatures of pair-instability supernovae (PISNe) (see Heger & Woosley 2002). Aoki et al. (2014) reported the discovery of SDSS J001820−093939, with [Fe/H] = −2.5, which they suggest is such an object. We defer consideration of this object to Section 5.1.2, following discussion of theoretical modeling of the first stars.

4. DWARF GALAXY ARCHAEOLOGY

Over the past few decades, metal-poor halo stars have successfully been used to study the early Universe. But without a priori knowledge of where these stars actually formed and how they may have entered the Galactic halo through their host system's accretion, detailed information

on their star-forming environments remains elusive. Studying the stellar content of the surviving dwarf galaxies thus offers the opportunity to learn about ancient stellar systems. Moreover, this offers the opportunity to investigate whether there were particular conditions present in both these early systems and the proto–Milky Way that led to the formation of extremely metal-poor stars that are now found in the halo and the dwarf galaxies. In addition, reconstructing the early chemical evolution of these dwarf galaxies sheds light on the star formation and supernova metal enrichment processes within perhaps their first billion years. In this manner, dwarf galaxy archaeology provides missing information complementary to stellar archaeology. The challenge lies in obtaining sufficient observational information of these faint and often sparsely populated systems that are at the technological limits of current telescopes and instrumentation. In this section, we focus on the discussion of the extent to which dwarf galaxy extremely metal-poor stars are now being discovered and how the inferred chemical histories compare with that of the halo. Whether any of the surviving dwarfs are analogs of the so-called Galactic building blocks is addressed in detail in Section 5.6.

## 4.1. The Discovery of Extremely Metal-Poor Stars in the Dwarf Galaxy Satellites

Given that the dwarf galaxies are at distances of ~20 to 200 kpc, their stars are faint (typically $V \gtrsim 17$), and only the red giants can currently be observed with high-resolution spectroscopy. The fact that these systems are relatively compact, however, has meant that large telescopes with multiobject spectrographs have provided a very efficient way of obtaining larger samples of stars at medium resolution to confirm membership and to obtain [Fe/H] estimates, with follow-up at high resolution on somewhat smaller samples of radial-velocity members.

Before the discovery of the ultra-faint dwarf galaxies (roughly $10^3 < L_\odot < 10^5$), the medium-resolution efforts centered on the relatively more luminous classical dSph systems (roughly $10^5 < L_\odot < 10^8$). The CaII infrared triplet was utilized to obtain estimates of [Fe/H], employing a calibration based on globular cluster metallicities. These efforts led to the conclusion that such systems contained no stars with [Fe/H] < −3.0 (Helmi et al. 2006). However, after the first ultra-faint galaxies were discovered (see Belokurov et al. 2007 and references therein), Kirby et al. (2008) developed a method involving the least-squares fitting of medium-resolution spectra (covering the range 6500–9000 Å) against model atmosphere synthetic spectra to obtain abundances that directly measured [Fe/H], and they reported the existence of a total of 15 stars with [Fe/H] < −3.0 in eight ultra-faint systems. In addition, Norris et al. (2008), using blue medium-resolution spectra of stars in the Boötes I ultra-faint dwarf galaxy, reported a star with [Fe/H] = −3.4 based on the CaII K line. These works suggested that the calibration of the CaII triplet in the above-mentioned works on the dSph systems was unsafe for [Fe/H] < −2.5.

Subsequently, the CaII infrared triplet method was revised (Starkenburg et al. 2010). Stars with abundances as low as [Fe/H] ~ −4.0 were soon discovered in the classical dSph galaxies, Sculptor and Fornax (Frebel et al. 2010a, Tafelmeyer et al. 2010), using both medium- and high-resolution techniques. Additional discoveries are forthcoming. Extremely metal-poor stars are now frequently compared with equivalent halo stars to investigate the differences and similarities between the early nucleosynthesis histories of the dwarf galaxies and the halo.

4.2. Early Chemical Evolution in the Dwarf Galaxies

Figure 10 presents the relative abundances [C/Fe], [Na/Fe], [Mg/Fe], [Ca/Fe], [Sr/Fe], and [Ba/Fe] as a function of [Fe/H]. To keep the discussion more focused, we restrict ourselves to dwarf galaxies that contain extremely metal-poor stars ([Fe/H] < −3.0) for which carbon
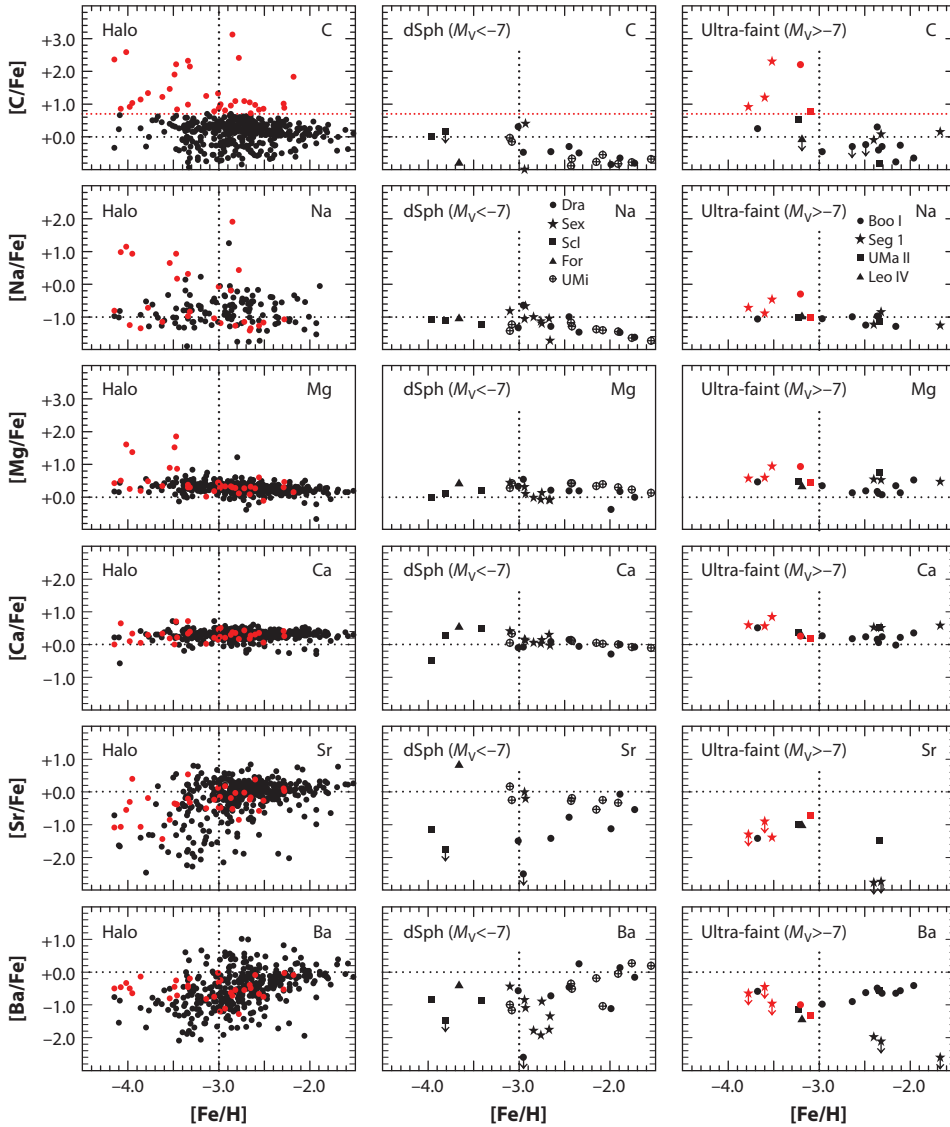
Figure 10

A comparison of the relative [X/Fe] versus [Fe/H] between Galactic halo stars (*left*), dwarf spheroidal (dSph) systems (*middle*), and ultra-faint (*right*) dwarf galaxies. Red and black symbols refer to C-rich and C-normal stars, respectively. The data for the first column are from Frebel (2010 and references therein), Cohen et al. (2013), Norris et al. (2013), Yong et al. (2013a), Hansen et al. (2014), and Keller et al. (2014). The data for the second and third columns are from Fulbright et al. (2004), Norris et al. (2008, 2010a, 2010b), Aoki et al. (2009a), Cohen & Huang (2009, 2010), Frebel et al. (2010a,b, 2014; Simon et al. (2010), Tafelmeyer et al. (2010), Lai et al. (2011), Gilmore et al. (2013), and Ishigaki et al. (2014a).

abundances are available. Hence, only such stars are shown in the figure. We refer the reader to Tolstoy et al. (2009) and Venn et al. (2012) and their extensive references on dwarf galaxy stars having high-resolution abundances for elements other than carbon. We also include data for Galactic halo stars. For ease of comparison, the figure contains three columns, which refer to the halo (left), dSph systems (middle), and ultra-faint dwarf galaxies (right). Although the dwarf galaxy sample meeting the above criteria is still small relative to that available for the halo, we make the following comparisons:

- In large part, there appears to be a general similarity between the lighter element abundance ratios. This implies that the chemical enrichment history of the birth environments from which the extremely metal-poor stars in both the Galactic halo and the various dwarf galaxies formed must have been driven in the main by massive stars (see Frebel et al. 2010b for details).
- The metallicity range covered by the bulk of stars in the halo and in dSph galaxies is similar, reaching from $[Fe/H] \sim -4.0$ to $[Fe/H] \sim 0.0$. The ultra-faint dwarf galaxies, however, seem to lack stars with $[Fe/H] \gtrsim -1.5$ (Kirby et al. 2008), which indicates some level of truncated chemical enrichment and star-formation history.
- Considering the populations of both dSph and ultra-faint dwarf galaxies, it has been shown that as one goes to fainter luminosities in these systems the mean value of $[Fe/H]$ decreases and its dispersion increases (Kirby et al. 2008, 2011; Norris et al. 2010b, Leaman 2012). For additional details on the MDFs of these systems, we refer to the first three references.
- C-rich stars exist in both the halo and the ultra-faint galaxies but not (at least so far) in the dSph galaxies. It is important to note that there are commensurate numbers (albeit small) of extremely metal-poor stars in both the ultra-faint and dSph systems. We discuss this result in Section 5.6.
- For the α-elements, a distinctly different behavior is known to occur in the classical dSph systems at higher values of $[Fe/H]$. There, solar values and even subsolar values of $[\alpha/Fe]$ predominate (see Tolstoy et al. 2009 and references therein). This behavior is readily understood in terms of a slower chemical evolution in the dSph galaxies compared with that found in the halo. As the result of this longer timescale, Type Ia supernovae have enriched the gas with additional iron but at somewhat lower metallicity compared with the halo, resulting in a decrease in the $[\alpha/Fe]$ ratio. We note in passing that low $[\alpha/Fe]$ ratios are occasionally found in the extremely metal-poor regime (see also Section 3.9.1), which can be explained with core-collapse supernova and/or hypernova yields when preferentially sampling the lower mass end of the massive star spectrum (McWilliam et al. 2013, Kobayashi et al. 2014). In contrast, at least up to $[Fe/H] \sim -1.5$, the ultra-faint dwarf galaxy stars show halo-like $[\alpha/Fe]$ ratios. More stars at higher metallicities in the ultra-faint systems would be required to test whether they show the same behavior. Given that these systems seem to contain hardly any such stars, this is a new kind of challenge beyond that of a purely observational/technical one.
- For the neutron-capture elements, generally lower abundance ratios are observed in dwarf galaxy stars than in the halo. We discuss this interesting behavior further in the following section.

4.3. A Unique Dwarf Galaxy Signature: Low Neutron-Capture Element Abundances

Although there are numerous similarities between extremely metal-poor stars in the halo and (in particular) the ultra-faint dwarf galaxies, there also appears one curious difference that is worth examining separately. It pertains to the behavior of heavy neutron-capture element abundance
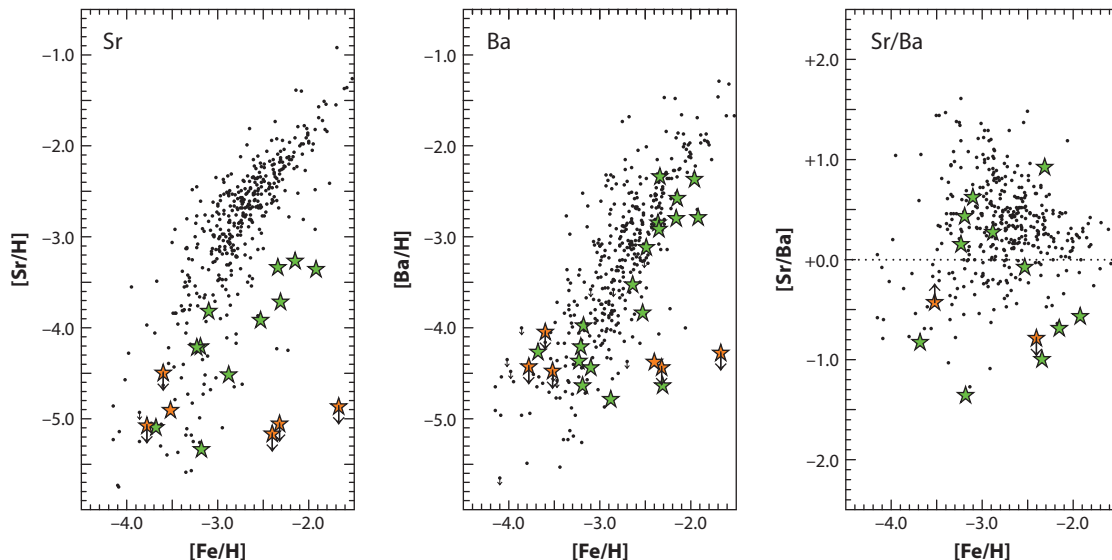
Figure 11

[Sr/H] (*left*), [Ba/H] (*middle*), and [Sr/Ba] (*right*) shown as a function of [Fe/H] for the Galactic halo (*small black circles*) and its ultra-faint dwarf galaxies (*star symbols*, which are *orange* for Segue 1, and *green* for Boötes I, Coma Berenices, Leo IV, and Ursa Major II). The data are from Frebel et al. (2010b, 2014), Simon et al. (2010), Gilmore et al. (2013), and Ishigaki et al. (2014a). See Section 4.3 for discussion.

ratios. **Figure 10** shows [Sr/Fe] and [Ba/Fe] (which can be considered representative neutron-capture elements) as a function of [Fe/H]. A potentially more insightful comparison is that of [Sr/H] and [Ba/H] versus [Fe/H] as shown in **Figure 11** for Galactic halo stars and the red giants of the ultra-faint systems. In this figure, the axes in the panels are nucleosynthetically decoupled. The production of neutron-capture elements is, after all, independent of that of Fe and other lighter elements (Sneden et al. 2008). Moreover, here one can more easily follow the buildup of neutron-capture element material as iron increases.

As can be seen in **Figure 11**, the halo exhibits well-defined [Sr/H] and [Ba/H] trends for [Fe/H] > −3.0. Below this value, the scatter increases, and an overall trend is less well defined and somewhat erratic, especially in the case of Sr. It is important to note that in the range −4.0 < [Fe/H] < −3.0, both elements show variations of more than 3 dex. That said, the ultra-faint dwarf galaxy stars exhibit even lower neutron-capture abundances. That is to say, even though they have values commensurate with the lowest halo stars' abundances, extreme values are found in these systems at (nearly) all values of [Fe/H]. This behavior is more extreme for Sr, where the ultra-faint dwarf galaxy stars appear to form some kind of subpopulation. Their [Sr/Ba] ratios (see **Figure 11**, right panel) also show a curiously distinct pattern with values that are either somewhat offset from the main halo trend (for stars with [Sr/Ba] > 0) or much lower than most halo stars altogether (for [Sr/Ba] < 0).

Subsolar [Sr/Ba] ratios at low metallicity could be understood in terms of a nonstandard s-process operating in rotating massive stars of a previous stellar generation. Frischknecht et al. (2012) found a metallicity dependence of (decreased) Sr and (increased) Ba net production for models of such progenitors: [Sr/Ba] varied between +2.05 and +0.42 for stellar models with $Z = 10^{-5}$, and between +0.02 and −0.54 at $Z = 10^{-7}$. The latter results are qualitatively in agreement with the dwarf galaxy stars having [Sr/Ba] < 0, although most of those observed [Sr/Ba]

values are even lower than ~ -0.5. The stars with [Sr/Ba] > 0 may as well have resulted after $Z = 10^{-5}$ progenitors enriched their birth gas clouds.

Interestingly, in **Figure 10**, the classical dSph galaxies paint a somewhat intermediate picture. They appear to contain stars with halo-like neutron-capture abundances but also show examples of extreme deficiency in these elements, especially in the case of Sr (e.g., a star in Draco, see below). Perhaps this behavior illustrates a transition from the earliest systems to the more evolved ones, such as the most luminous dSph systems Sculptor and Fornax.

Although additional element measurements are needed, the current body of data already indicates that ultra-faint dwarf galaxy stars almost exclusively have distinctly low neutron-capture element abundances and relatively low [Sr/Ba] values, whereas brighter systems and the halo do not. In this context, it becomes interesting to speculate about these observed differences and possible interpretations. Perhaps the most obvious explanation would be that low neutron-capture element abundances (i.e., lower than the typical halo trend) are a signature of the earliest star-forming clouds.

After all, neutron-capture elements are produced independently of the lighter elements (including Fe), and likely occur in a different and more restricted progenitor mass range (8 to 10 $M_\odot$; Wanajo et al. 2006). For stars with [Fe/H] $\lesssim -2.8$, these elements are thought to be produced by the r-process or other neutron-capture processes because below this value, general AGB stellar winds disposing s-process elements are not expected to contribute to chemical evolution. Hence, relatively little or even no neutron-capture element material may have been created by the first stellar generations, especially if most stars were more massive than $\sim$10 $M_\odot$. Observational examples might include the higher metallicity stars in Segue 1 with upper limits of [Sr/H] and Ba/H] of ~ -5.0 and ~ -4.3, respectively (Frebel et al. 2014), or the Draco star D119 with [Fe/H] ~ -3.0 and upper limits of ~ -5.5 for both elements (Fulbright et al. 2004). These upper limits indicate no more than one production event (or even none) in which these heavy elements may have formed (Farouqi et al. 2010). Whether such an event originated in a supernova or neutron-star merger is of ongoing discussion.

Applying this idea to halo star abundances leads to a hypothesis with potentially far-reaching implications. Perhaps the halo stars (and also dSph galaxy stars) with the lowest neutron-capture element abundances (and/or with the lowest [Sr/Ba] value) are those that formed in the earliest gas clouds, similar to those that resulted in extremely metal-poor stars present in the ultra-faint dwarfs. Later gas clouds might have had additional neutron-capture element enrichment but not necessarily increased Fe enrichment (or vice versa), owing to different mass functions of the enriching progenitors or other factors. Such a scenario might explain the increased halo star scatter in Sr and Ba abundances at [Fe/H] < -3.0. As a consequence, neutron-capture element abundances might be suitable for discriminating halo stars that originated in systems similar to the surviving faintest dwarf galaxies and thus even be able to separate out the oldest stars formed in the earliest star-forming regions for a given [Fe/H] value. We note that in Section 5.6, we more broadly discuss the role of neutron-capture elements as part of the question of whether any of the surviving ultra-faint dwarfs could be a surviving first galaxy.

It would be interesting to obtain abundances of additional neutron-capture elements in any of the dwarf galaxy stars to further test this idea. However, given their low abundances to begin with, and often only moderate data quality because of the faintness of these stars, this is a challenging task. Sr and Ba can be measured because they exhibit relatively strong lines in the spectra, whereas the other neutron-capture elements exhibit much weaker features. Even in the cases of Sr and Ba, limited spectral coverage has resulted in only a few Sr measurements (the two lines are located in the harder to access blue spectral regions at 4077 Å and 4215 Å). Fortunately, several Ba lines further in the red region (reaching up to $\sim$6500 Å) have led to Ba abundances in most dwarf galaxy stars.

5. NEAR-FIELD COSMOLOGY

Observations of metal-poor stars in the Galactic halo and the dwarf galaxies provide a wealth of information about the local chemical abundance ratios at the time of star formation in the early Universe. These local conditions are driven by cumulative effects, such as those arising from the mass distribution of Population III stars, the subsequent star-formation rate, supernova yields, infall, outflows, etc. In this way, the assembly of the chemical elements can be reconstructed for a given host system. Established chemical evolution trends as well as any outliers, however, need to be understood and interpreted on the basis of the physical principles of (supernova) nucleosynthesis and the host galaxy's environment in which the enrichment events occurred. After all, the key to deciphering stellar abundance signatures lies in unraveling how these nuclei were formed, how they were expelled and mixed in the stellar birth gas cloud, how they were incorporated into a star in its natal galaxy, and how that star then ended up in the Galactic halo where we observe it today.

5.1. Properties of the First Stars and the Nature of the First Chemical Enrichment Events

Based on the current state of observational searches for the most metal-poor stars, no truly metal-free first star has yet been discovered. Although a few stars with exceptionally low Fe abundances ($[Fe/H] < -5.0$) have been found, their accompanying large carbon abundances strongly suggest that they are some of the first Population II stars to have formed in the Universe (e.g., Umeda & Nomoto 2003, Keller et al. 2014), rather than being true Population III first stars.

These searches have shown that the most metal-poor stars are extremely rare. Is the apparent absence of Population III stars the result of observational difficulties or is there a physical reason for their absence? Over the past decade, the nature and properties of the first stars have been much debated as simulations of these objects have become more and more detailed (Abel et al. 2002; Bromm et al. 2002; Yoshida et al. 2004, 2008; Turk et al. 2009; Stacy et al. 2010; Clark et al. 2011; Greif et al. 2011; Hosokawa et al. 2011; Turk et al. 2012; Susa 2013; Stacy & Bromm 2014). The subject has been extensively reviewed by Bromm & Larson (2004) and Bromm (2013), to whom we refer the reader for a more in-depth discussion. Here, we summarize the latest findings of the field and highlight results relevant to an understanding of the beginning of chemical enrichment and how metal-poor stars provide constraints on the existence of Population III stars.

5.1.1. The mass range of the first stars.
Consensus exists that owing to the lack of cooling agents in primordial gas (i.e., metals or dust), significant fragmentation of the available gas was largely suppressed so that these first objects must have been very massive. Since the beginning of this field about 15 years ago, however, there has been a slow but steady paradigm shift concerning the typical mass scale of a Population III star. Although early works suggested single stars had masses of order 100 $M_\odot$, the more recent simulations, which follow the formation of the protostar for a much longer time to the important accretion phase, paint a more complex and varied picture.

Recent detailed modeling of the formation process of Population III stars (e.g., Hosokawa et al. 2011, who follow the formation of an eventual 43 $M_\odot$ star until the beginning of nuclear fusion) has generally not yielded stars with masses above 100 $M_\odot$. Instead, following the accretion process, which appears to be the main determinant of the final mass of the Population III star, eventual fragmentation of the accretion disk because of gravitational instabilities can lead to the formation of small multiples (e.g., Turk et al. 2009, Stacy et al. 2010, Clark et al. 2011) in most simulated halos. As a result, secondary stars with lower masses, of order 1 $M_\odot$, can form. The primary star, however, remains massive (at least a few tens of solar masses). For example, Susa (2013) obtained masses of 4.4 $M_\odot$ and 60 $M_\odot$ in their simulation. Stacy & Bromm (2014) even found a system with

just two Population III stars of mass $<1\ M_{\odot}$ and $\sim 5\ M_{\odot}$, although in a very unusual environment with very high angular-momentum content. The protostellar disk in this system is thus unusually extended, with reduced fragmentation and small protostellar accretion rates.

Although the early results for exclusively very massive Population III stars implied extremely short lifetimes (a few million years), and hence, no chance of their ever being observed, the prospect of Population III stars with $M < 1\ M_{\odot}$ and correspondingly long lifetimes (>13 Gyr) has reopened this possibility. It thus remains to be seen whether a true low-mass Population III star will be discovered. Efficient large-scale surveys, such as that carried out with the SkyMapper telescope, will play a vital role in answering this important question from an observational point of view, and simulations will deliver more refined estimates concerning the possible formation channel of these stars.

Knowledge about the lower mass end of Population III stellar masses is going to be as important as establishing what the overall mass function of the first stars may have been. This IMF—the number of stars per mass bin—is the most important characteristic of this population and a vital ingredient for essentially any interpretation or simulation associated with Population III stars, early star and galaxy formation, chemical enrichment, and evolution. Knowledge of the IMF is particularly important for stellar archaeology because stellar mass determines a star's fate. This immediately implies that the IMF determines the overall chemical output of this population and thus how the chemical enrichment of the Universe began.

In summary, contrary to the present-day mass function, which is dominated by low-mass stars, the Population III IMF was likely top-heavy and dominated by massive stars. However, owing to various modeling difficulties and global challenges such as cosmic variance, it remains poorly determined. That said, first attempts are now being made to quantify the IMF by using large suites of simulations. Susa et al. (2014) find a top-heavy IMF that peaks at several tens of solar masses, and with stars in the range of $10\ M_{\odot}$ to $100\ M_{\odot}$. Similarly, Hirano et al. (2014) find a reasonably flat distribution over the range of $10\ M_{\odot}$ to $1{,}000\ M_{\odot}$, on the basis of 100 first stars' simulations. Only more detailed and dedicated modeling will result in a reliable IMF determination; in the meantime, explorations on the low- and high-mass ends will advance our understanding of the full range of Population III stellar masses and of the corresponding implications.

For completeness, we note that stars having masses of thousands of solar masses are being predicted within the cosmological framework. This follows earlier work on stars with hundreds of solar masses (e.g., Fryer et al. 2001). Hosokawa et al. (2013) simulated Population III stars with masses of $10^{4-5}\ M_{\odot}$, which are expected to collapse directly into a supermassive black hole. Although not contributing to chemical enrichment, these monstrous objects might be luminous enough to be observable with the *James Webb Space Telescope* (JWST) and, moreover, be the seeds of future galaxies' supermassive black holes. In the same context, calculations have been made of the luminosity of the first massive Population III star cluster and its observability with JWST (Johnson 2010). These massive objects might offer the only chance of ever directly observing Population III stars in the high-redshift Universe—if such a suitable cluster, or massive star, ever existed. Johnson et al. (2013) then modeled a $55{,}000\ M_{\odot}$ star that completely disrupts in a gigantic supernova with an explosion energy of up to 10^{55} erg instead of collapsing to a black hole. This would presumably leave behind enormous instantaneous metal enrichment that would trigger the formation of metal-rich low-mass second-generation stars. These, however, would likely be too metal rich to be found in surveys for metal-poor stars. Uncovering observational evidence of these behemoths will thus be rather difficult.

5.1.2. First star nucleosynthesis. Stars with masses of $8\ M_{\odot}$ or more will, in the main, end their lives as supernovae. Depending on the stellar mass and rotation state, however, the stellar

remnants may be vastly different. Some explosions will lead to chemical enrichment, and others will not contribute elements at all. We refer the reader to Heger & Woosley (2002) for an overview of the likely outcomes for nonrotating stars that initially had heavy-element abundance $Z = 0$. As with the analysis of stellar atmospheres, the large majority of modeling of the evolution of stars is undertaken within the framework of 1D analyses, which in this case is based on the assumption of spherical symmetry. We caution also that the modeling of final explosive events, of necessity, makes fundamental and ad hoc assumptions about, in particular, the energy of the explosion and the mass cut above which material is potentially ejected (e.g., Nomoto et al. 2013). In the present context, stars that die as element-contributing PISNe and core-collapse supernovae are of prime interest for stellar archaeology and dwarf galaxy archaeology. Hence, we do not discuss the neutron stars and black holes that are also end products of stellar evolution.

Detailed calculations of the yields of $Z = 0$, nonrotating core-collapse supernovae in the mass range 10 to 40 $M_\odot$ have been presented, for example, by Woosley & Weaver (1995) and Kobayashi et al. (2006). Galactic chemical enrichment models using the above yields, together with additional ones covering $0 < Z < Z_\odot$, have been used by these authors and others for comparison with observations of Galactic metal-poor stars.

Although the role of core-collapse supernovae in producing the observed chemical abundance signatures in metal-poor stars is clear, the same may not be said concerning PISNe, predicted to be the end product of $Z = 0$, nonrotating, high-mass Population III stars with $M \sim 140$ to 260 $M_\odot$. Calculations of the chemical yields of these objects predict a very strong so-called odd-even effect in their abundance patterns (large differences between elements with neighboring atomic numbers), together with enhancements of calcium (and Mg and Si) relative to iron (see Heger & Woosley 2002, their figure 5). Certainly, until very recently, no stars had been discovered with PISNe abundance signatures. Karlsson et al. (2008) have argued that observational selection effects, inherent in the use of the CaII K line in the discovery of metal-poor stars, have militated against detection of metal-poor stars (with [Fe/H] $\lesssim -2.5$) and PISNe abundance characteristics. We note that systematic efforts are now underway by Ren et al. (2012) to search for this type of signature. This fundamental question has remained unanswered for some time.

As we noted in Section 3.9.4, Aoki et al. (2014) reported the discovery of an object, SDSS J001820−093939, with [Fe/H] $= -2.5$ and unusually low, subsolar C, Mg, and Co together with some of the PISNe odd-even pattern. The critic would note that, even though the odd-even effect is clear for values of Sc/Ti and Co/Ni in this star, which is in reasonable agreement with their PISNe model calculations, this is not the case for Na/Mg, Al/Si, V/Cr, and Mn/Fe. Indeed, an alternative model presented by Aoki et al. (2014, their figure 2), which includes chemical enhancement by both type II (core-collapse) and Type Ia supernovae ejecta, seems to provide a better fit to the observations. [We also note that their dismissal of their model including Type Ia enrichment seems open to question in light of the Type Ia-like signatures that have been noted by Yong et al. 2013a for stars with [Fe/H] ~ -2.5 (CS 22169-035 and HE 1207−3108).]

Finally, in the past 10 to 15 years, driven in large part by observed chemical abundance signatures of the kind discussed above in Section 3, theoretical attention has increasingly focused at $Z = 0$, and in the mass range 25 to 60 $M_\odot$, on the effects of (*a*) stellar rotation on nucleosynthesis (e.g., Fryer et al. 2001; Meynet et al. 2006, 2010), and (*b*) mixing and fallback of the material above the mass cut of the supernova explosion and the resulting (noncanonical) ejecta (see Nomoto et al. 2013). That said, many details regarding, for example, the masses and explosion energies involved are still being debated. We return to the interpretation of the observed abundances of the most metal-poor stars in Section 5.4.

5.2. The First Galaxies and the Formation of the First Low-Mass Stars

Early structure formation led to the existence of so-called minihalos with masses of $\sim 10^6$ M$_\odot$ dark matter, which collapsed at high redshifts of $z \sim 20$–30 (Tegmark et al. 1997) entraining baryonic matter with it, about 100 to 200 million years after the Big Bang (e.g., Greif et al. 2011). Each minihalo hosted one first star (or a small number of them), which evolved and provided chemical enrichment to the minihalo (depending on the star's mass-dependent element yields, and other relevant parameters, as outlined above).

Throughout their brief life, massive stars provided vast amounts of ionizing radiation that changed the conditions of the surrounding primordial gas, including that in neighboring minihalos, and thus the details of subsequent star formation. In particular, whereas cooling in the first phase of star formation was provided by H$_2$, in this second phase, cooling was driven by the molecule HD, leading to lower gas temperatures and smaller stellar masses (e.g., Greif & Bromm 2006, Johnson & Bromm 2006). In this context, it is interesting to note that in minihalos that had experienced no metal enrichment there could have formed a generation of metal-free stars, some having typical masses of order ~ 10 M$_\odot$.

As structure formation and Population III stellar evolution proceeded, of order 10 such minihalos merged to form so-called atomic cooling halos (Greif et al. 2008, Wise & Abel 2008) with dark matter masses of $\sim 10^8$ M$_\odot$ at redshifts of $z \sim 10$ to 15. Although molecular hydrogen was the primary coolant in minihalos, now atomic hydrogen took over owing to a larger virial temperature of the gas ($\sim 10^4$ K, as opposed to $\sim 1{,}000$ K in minihalos). Metals were immediately present in these systems, brought in from the merging minihalos that hosted core-collapse Population III supernovae or stars that were about to explode. Atomic cooling halos can be considered as first galaxies because they were massive and metal rich enough to host Population II star formation—including the formation of the first low-mass metal-poor stars—and able to withstand supernova explosions of Population III and massive Population II stars as well as other feedback effects without immediately disrupting. We refer the interested reader to the review of Bromm & Yoshida (2011) for additional details on the first galaxies. Alternatively, it may have been possible that at least some of the first low-mass stars were already formed in minihalos. Depending on the strength of the explosion and mass (<40 M$_\odot$) of the Population III star in such a minihalo, the recovery time of the system may have been rather short (~ 10 Myr), leading to prompt Population II star formation (Cooke & Madau 2014, Jeon et al. 2014).

Simulations of first galaxies that model metal enrichment by Population III stars and take into account subsequent metal mixing have found these systems to become significantly enriched to average metallicities of $Z > 10^{-3}$ Z$_\odot$ (Greif et al. 2010, Safranek-Shrader et al. 2014b). Metal mixing, however, occurs in a rather inhomogeneous fashion resulting in large abundance spreads of several dex across the system (Greif et al. 2010, Wise et al. 2012). In this context, it is not unlikely that some of the first galaxies received external metal enrichment from neighboring halos. In the process of undergoing massive supernova explosions that evacuate their own minihalos, metal enrichment may occur over large length scales that affect neighboring minihalos regardless of whether or not they host their own Population III stars.

These recent works have thus all shown that the first galaxies were enriched in metals, possibly provided via different avenues and most certainly in an inhomogeneous fashion. This naturally set the scene for the formation of Population II stars since the first galaxies provided the first star-forming environments, which were ready for the formation of metal-poor, low-mass stars with $M < 1$ M$_\odot$. Metal cooling became possible because of the metallicity floor set by the Population III stars during or shortly after the formation of the atomic cooling halo (or even in a minihalo). With the availability of metals, dust formation (and in turn, subsequent dust cooling)

became possible (e.g., in supernova ejecta) (Todini & Ferrara 2001; Nozawa et al. 2003; Schneider et al. 2004, 2012a; Omukai et al. 2005; Cherchneff & Dwek 2010; Klessen et al. 2012).

Although the formation mode of the first low-mass stars remains an ongoing debate, the details largely revolve around the concept of a critical metallicity. Above the critical metallicity, vigorous fragmentation of the gas occurs. In such environments, it could be possible to form long-lived low-mass stars as a result of the N-body dynamical ejection of accreting protostars before these objects had the chance to accumulate their thermal Jeans mass. If indeed formed, they would be able to survive to the present day and would be observable in the Milky Way or dwarf galaxies. In turn, below such a critical metallicity, only massive, short-lived stars would be able to form. Two different pathways for low-mass star formation have thus been suggested: The first is based on atomic fine structure line cooling, and the second on dust thermal cooling, which results in a drop in the Jeans mass to <1 $M_\odot$. The critical metallicities are $Z_{crit} \sim 10^{-3.5}$ $Z_\odot$ for the line cooling (Bromm & Loeb 2003) and $Z_{crit} \sim 10^{-5}$ $Z_\odot$ for dust cooling (Schneider et al. 2003, 2012a; Omukai et al. 2005). In both cases, sufficient fragmentation is assumed to follow, and with it, low-mass star formation.

Given the already complex nature and interplay of the metal content of supposedly simple systems, such as the first galaxies, many details of the cooling-induced fragmentation process or processes remain unsettled. However, one way forward to test whether the mechanisms might be feasible in facilitating Population II star formation is to compare relevant predictions with observational chemical abundance results of the most iron-poor stars. After all, these are the stars that can be assumed to have formed in the first, or at least earliest, galaxies out of sparsely enriched gas and could thus provide information about their formation mechanism.

Frebel et al. (2007b) developed an observer-friendly formulation of early CII and OI metal line cooling (Bromm & Loeb 2003). They predicted that all metal-poor stars that formed through this mechanism should have carbon and/or oxygen abundances in excess of the line cooling critical metallicity. To date, all stars with [Fe/H] < -3.0 indeed show sufficiently enhanced levels of carbon and oxygen, with only one exception, SD 1029+1729 (see **Table 1** and Section 3.4). Instead, the existence of this star has been successfully explained in terms of a dust-cooling mechanism (Klessen et al. 2012, Schneider et al. 2012b, Ji et al. 2014). A more recent study has suggested that, even though both mechanisms may be important for forming the first low-mass stars, they may occur as part of separate formation pathways and/or environments (Ji et al. 2014). Detailed numerical simulations of star formation in atomic cooling halos have already suggested where these pathways may occur, although details so far remain unclear (Wise & Abel 2007, Greif et al. 2008, Ritter et al. 2012).

With additional metal-poor star observations becoming available, the details of the cooling and star-formation processes can be tested further. It will be particularly interesting to investigate the specific physical reasons as to why the two cooling mechanisms would be mutually exclusive (Ji et al. 2014). Understanding the underlying physics of early star formation will then provide a much improved framework for understanding the nature and origin of the most iron-poor stars as well as for future modeling of star and galaxy formation within large-scale simulations of galaxy growth and evolution.

In the meantime, it is important to further explore the implications of the findings that all but one of the eight most iron-poor stars (with [Fe/H] < -4.5) are C-rich (see **Table 1**) and that some 20% to 30% (or 40% to 70%, following Placco et al. 2014) of the metal-poor stars in the range of $-4.5 <$ [Fe/H] < -3.0 are also C rich. Is this really a signature of a specific gas-cooling process or could there be another explanation? Said differently, were there specific supernova yields or other processes that led to the population of C- and O-rich metal-poor stars?

5.3. Origins of the Chemical Composition of Carbon-Rich Extremely Metal-Poor Stars with [Fe/H] < −3.0

No universally accepted hypothesis currently exists to explain the origins of the C-rich stars with [Fe/H] < −3.0 (which are almost exclusively CEMP-no stars). Given that all but one of the eight most iron-poor stars ([Fe/H] < −4.5) are C rich, any acceptable scenario should explain the fundamental aspects of the first chemical enrichment events in the Universe. This topic has been considered by many authors in recent literature, and we refer the reader to Fujimoto et al. (2000), Suda et al. (2004), Beers & Christlieb (2005), Meynet et al. (2006, 2010), Nomoto et al. (2006, 2013), Frebel et al. (2007c), Norris et al. (2007, 2013), Cohen et al. (2008), Lai et al. (2008), Heger & Woosley (2010), Joggerst et al. (2010), Masseron et al. (2010), Frebel & Norris (2013), and Tominaga et al. (2014) for previous discussions. The next sections are scenarios (following Norris et al. 2013) that have been suggested to have played a role in the production of stars having abnormally large carbon enhancements from material initially having zero or very low heavy-element content.

Detailed comparisons of the stellar abundances with these diverse approaches to the calculations of yields can help constrain Population III star properties. Investigating the results within different environments will hopefully reveal the underlying processes that drove star formation in the earliest galaxies.

5.3.1. Fine-structure line transitions of CII and OI as a major cooling agent in the early universe.
C- and/or O-rich gas forms stars, through fragmentation, on shorter timescales than in regions where these elements are of lower abundances, leading to the formation of long-lived, low-mass C- and/or O-rich stars still observable today (Bromm & Loeb 2003, Frebel et al. 2007b).

5.3.2. Supermassive rapidly rotating stars.
In high-mass stars (100 to 300 $M_\odot$, rapid rotation leads to mixing, by meridional circulation, of C and O from the He-burning core into the H-burning shell. This results in extra N production, and then enhanced N as well as C and O surface abundances and subsequent yields (Fryer et al. 2001).

5.3.3. Multiple type II supernovae involving fallback.
The ejecta from a normal supernova in the mass range 10 to 40 $M_\odot$ is combined with that from one of low energy in which the outer layers (rich in light elements) are expelled, whereas much of the inner layers (rich in the heavier elements) fall back onto the central remnant (Limongi et al. 2003).

5.3.4. Mixing and fallback type II supernovae.
Low-energy supernovae in the mass range 10 to 40 $M_\odot$ eject material preferentially from their outer regions, which are enhanced in light elements, with the expulsion of only relatively small amounts of the heavier elements formed deeper in the star. During the explosion, internal mixing occurs in an annulus outside the mass cut at which the expansion is initiated. A small amount of mixed material is eventually expelled from the star, with most of it falling back into the central regions. (Umeda & Nomoto 2003, Iwamoto et al. 2005; see Tominaga et al. 2014 for a recent profiling of extremely metal-poor stars.)

5.3.5. Type II supernovae with relativistic jets.
A relativistic jet-induced black-hole-forming explosion of a 40 $M_\odot$ supernova leads to infall of inner material that "decreases the [ejected] amount of inner core material (Fe) relative to that of outer material (C)" (Tominaga et al. 2007a).

5.3.6. Zero-metallicity rotating, massive intermediate-mass stars. Rotationally driven meridional circulation in ~60 and ~7 $M_\odot$ stars leads to CNO enhancements and large excesses of ^{13}C (and hence low ^{12}C/^{13}C values), Na, Mg, and Al in material expelled in stellar winds. The essential role of rotation is to admix and further process the products of H and He burning (Meynet et al. 2006, 2010; Hirschi 2007).

5.3.7. A combination of rotation, mixing, and fallback. For investigations of the combined effects of mixing, fallback, and rotation in massive stars over wide parameter ranges, we refer the reader to Heger & Woosley (2010) and Joggerst et al. (2010).

5.3.8. Nucleosynthesis and mixing within low-mass, low-metallicity stars. Driven by a helium flash, carbon is mixed into the outer layers of low-mass, extremely metal-poor giant stars, whereas protons are transported into the hot convective core. Enhancements of Na, Mg, Al, and heavy neutron-capture elements are also predicted (Fujimoto et al. 2000, Campbell et al. 2010).

5.3.9. Population III binary evolution with mass transfer, and subsequent accretion from the interstellar medium. The primary of a zero-heavy-element binary system is postulated to transfer C- and N-rich material, during its AGB phase, onto the currently observed secondary, which later accretes Fe from the interstellar medium (ISM) to become a CEMP star (Suda et al. 2004, Campbell et al. 2010). Currently, radial velocity monitoring of C-rich (CEMP-no) stars with [Fe/H] $\lesssim$ −3.0 does not support universal binarity among this group of stars (Norris et al. 2013, Starkenburg et al. 2014). Rather, the reported binary fraction is roughly similar to the value found for C-normal Galactic halo stars.

5.3.10. Separation of gas and dust beyond the stellar surface during stellar evolution, followed by the accretion of the resulting dust-depleted gas. Peculiar abundance patterns result from fractionation of the elements onto grains, as determined by their condensation temperatures, during stellar evolution, rather than being the result of natal variations (Venn & Lambert 2008, Venn et al. 2014). Subsequent examination of the critical elements sulfur and zinc in the Fe-poor, C-rich stars CS 22949-037 ([Fe/H] = −4.0) and HE 1327−2326 ([Fe/H] = −5.8) by Spite et al. (2011) and Bonifacio et al. (2012a), respectively, shows that these elements are not detected in either object, in contrast to what might be expected in this model. A search for mid-infrared excesses in these objects has been relatively unsuccessful, with five out of their six C-rich stars showing no mid-IR excesses, whereas a small mid-IR excess near 10 μm was detected at the 2 σ level in the exception (HE 0107−5240) (Venn et al. 2014).

5.4. Interpreting the Abundance Signatures of Extremely Metal-Poor Stars

The most metal-poor stars very likely reflect the earliest enrichment events by just one or a few prior Population III supernovae. This concept can be understood by considering the following simple example. Assume an average iron yield of a core-collapse supernova to be 0.1 $M_\odot$ (e.g., Heger & Woosley 2010) that is homogeneously and instantaneously mixed into a typical pristine star-forming cloud of mass of 10^5 $M_\odot$. The resulting metallicity of the gas, and hence the star formed in this cloud, is [Fe/H] = −3.2. This implies that stars with [Fe/H] $\lesssim$ −3.0 can, in principle, be second-generation stars whose heavy elements were provided by just one supernova. Various effects, such as mixing mass and mixing efficiency of the supernovae ejecta into the ambient gaseous medium, as well as different supernova yields, would of course alter this threshold value. The most metal-poor stars are thus the most important and readily available diagnostic tool for learning about Population III supernovae. In turn, this provides information about the nature and properties of the progenitor first stars.

5.4.1. Limitations. The critical challenge when working with the most metal-poor stars lies in correctly and sufficiently interpreting the stellar chemical abundance patterns with the help of Population III nucleosynthesis model calculations. Unfortunately, there are many issues that arise on several fronts:

1. Observational: A good match between observed abundances and model predictions depends crucially on having available as many elements measured in the star as possible. With the most iron-poor stars, this can become the limiting factor, as the recent example of SM 0313−6708, with [Fe/H] < −7.3, shows. For this star, abundances could be determined for only four elements (together with several upper limits) because of its overall low abundance, resulting in poorly constrained progenitor star properties (Ishigaki et al. 2014b, Keller et al. 2014). Complicating things further are systematic abundance uncertainties arising from the use of 1D/LTE model atmospheres to obtain the abundances rather than 3D/NLTE modeling. As highlighted in Section 1.4.3, for example, corrections for C, N, and O can exceed 0.5 dex, which can change the results of the matching of the observed abundances with theoretical yields significantly. All of these issues can thus lead to different conclusions about the progenitor properties: For example, Ishigaki et al. (2014b) infer solutions for 25 $M_\odot$ and 40 $M_\odot$ progenitors, whereas Keller et al. (2014) find a best fit using a 60 $M_\odot$ model.

2. Theoretical: Current nucleosynthesis model calculations are plagued by many free parameters and gross uncertainties (Umeda & Nomoto 2005, Heger & Woosley 2010). Essential details, such as the explosion mechanism (e.g., 1D versus 3D models, energy injection through a piston approach), explosion energy, mass cut, stellar rotation, existence/nonexistence/extent of nucleosynthesis reactions and processes, etc., are often poorly constrained. Moreover, treatment of the explosion has been largely limited to spherical symmetry, which simplifies current procedures but also introduces further systematic uncertainties. All of these caveats prevent actual ab initio nucleosynthesis predictions. Rather, in most cases so far, only postdictions have been feasible by searching for the best match of theory with observations.

3. Others: (*a*) Heterogeneous gas mixing processes in the star-forming cloud could lead to different amounts of local dilution and hence different abundance patterns across one stellar generation (Greif et al. 2010, Ritter et al. 2015). (*b*) Accretion of interstellar matter during the lifetime of a star could change its surface abundance pattern (Suda et al. 2004, Hattori et al. 2014), as would any surface pollution by a binary star companion.

5.4.2. Sensitive and robust abundance probes. In the absence of more refined knowledge or more exact solutions to many or even all of these issues, the focus has been on reproducing certain abundance ratios that appear to be particularly sensitive to overall progenitor properties and nucleosynthesis calculations (but which are robust to different overall modeling assumptions). Some of these are listed in **Table 2**, where we present abundance ratios [X/Fe], how large (or small) the observed abundance ratio in question needs to be to effectively constrain the scenario, what property they constrain, and the references to which we refer the reader for additional details on the role of these abundance ratios. Regarding their interpretation, the individual abundance patterns of the most iron-poor stars with [Fe/H] < −4.5 were described extensively in Sections 3.4 and 3.8. What remains to be discussed are the extent to which their elemental patterns have been reproduced by supernova nucleosynthesis calculations and what has been concluded thus far about the properties of the first star progenitors. We summarize the most important findings below.

Table 2 Key abundance ratios that constrain Population III star properties and supernova nucleosynthesis

| Ratio	Level (dex)	Population III properties	References
[C/Fe]	>1.0	Mixing and fallback, $Z = 0$, supernovae[a]	Umeda & Nomoto (2003)
		Rotating, $Z \sim 0$, massive stars	Meynet et al. (2006)
[C/N]	<0.0	Rotating, $Z \sim 0$, massive stars	Meynet et al. (2006)
[Na, Mg, Al/Fe]	>1.0	Mixing and fallback, $Z = 0$, supernovae[a]	Umeda & Nomoto (2003)
		Rotating, $Z \sim 0$, massive stars	Meynet et al. (2006)
[α/Fe]	~0.4	Supernovae[a]	Woosley & Weaver (1995)
[Ca/Fe]	>1.0	PISNe signature	Heger & Woosley (2002)
[Zn/Fe]	>0.5	High explosion energy supernovae[a]	Umeda & Nomoto (2002)

[a]Core-collapse.
Abbreviations: PISNe, pair-instability supernovae.

5.4.3. Fitting with mixing and fallback models. Low Fe abundances coupled with a high [C/Fe] value are a striking feature of seven of the eight most iron-poor stars, which we discussed in great detail in Section 5.3. Many interpretations are listed that are all potentially applicable to the [Fe/H] $\lesssim -4.5$ stars. Perhaps the most promising, or at least the most extensively studied scenario, is the mixing and fallback model. There, owing to a relatively low explosion energy ($\lesssim 10^{51}$ erg) (Umeda & Nomoto 2003), only the outer layers of the exploding star containing principally lighter elements, made in the earlier phases of stellar evolution, are ultimately ejected. The innermost layers containing iron-peak elements, and especially iron from the last burning stage, remain close to the core and fall back onto the newly created black hole. Only a small fraction (arbitrarily chosen during modeling) is then ejected, resulting in little or even no enrichment in these elements. The origin of the elements in the seven C-rich stars in **Table 1** (all with [Fe/H] < -4.5) for which adequate abundance data are available may all be explained in this manner.

Comparison of the abundance patterns of stars with [Fe/H] < -3.0 with theoretical predictions by Tominaga et al. (2007b, 2014) and Ishigaki et al. (2014b) demonstrate that generally good fits can be obtained with the yields of mixing and fallback core-collapse supernovae. The modeling involves some five free parameters: (a) the explosion energy, E_{51} (in units of 10^{51} ergs); (b) the mass of the inner boundary of the mixing region M_{cut}; (c) the mass of the outer boundary of the mixing region M_{mix}; (d) the ejection factor f_{ej} (the fraction of the mass M_{mix}–M_{cut} that is ejected from the star; and (e) a low-density factor f_{ρ}, defined by Tominaga et al. (2014). We refer the reader to these works for details and in particular to Tominaga et al. (2014, their figure 3) for the range of fitting parameters adopted in their investigation of 48 stars with [Fe/H] < -3.5.

Figure 12, adapted from the work of Ishigaki et al. (2014b), presents the abundances, [X/Ca], (filled black circles) as a function of atomic number for five of the most iron-poor stars currently known (four are C rich, and one has [C/Fe] $< +0.9$). Comparisons of the observed abundances shows the interesting and obvious stark contrast between the overall abundance patterns of C through Al in the C-rich stars in the top four panels and the C-normal star, SD 1029 + 1729 (also known as J102915+172927), in the bottom panel. Although the C-rich stars have large overabundances of C through Al (ranging over several dex), such a spread does not exist in SD 1029 + 1729. (Note also that the y-axis abundance scale in the bottom panel is only half that of the top four panels).

Each observed abundance pattern is overplotted with the mixing and fallback nucleosynthesis calculations of Ishigaki et al. (2014b) for two different explosion energies (red squares and green
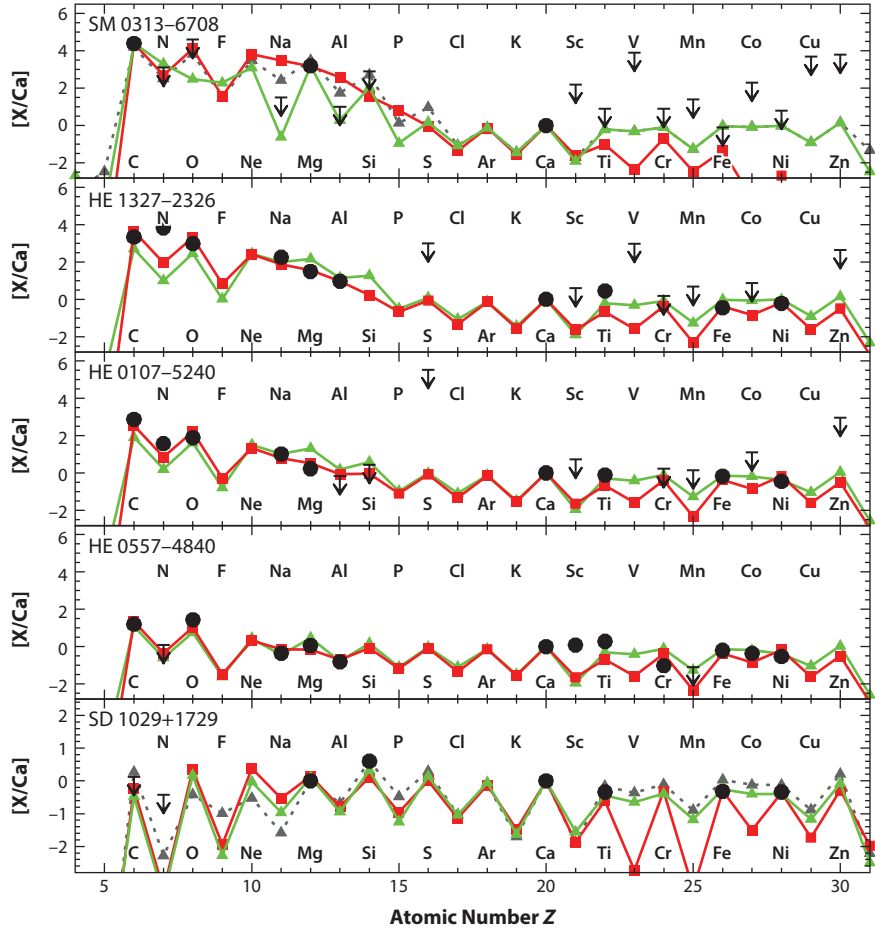
Figure 12

Examples of the abundance-fitting procedure for five of the most iron-poor stars with [Fe/H] < −4.5 (*black circles*) to infer properties of the Population III stars that enriched their respective birth gas clouds (data taken from Ishigaki et al. 2014b). From top to bottom, the observed stellar iron abundances are [Fe/H] < −7.3, −5.7, −5.4, −4.8, and −4.7. Red squares and green triangles show 25 $M_{\odot}$ model results for supernovae with E_{51} = 1 (in units of 10^{51} erg) and E_{51} = 10, respectively, for the carbon-enhanced stars in the top four panels. The bottom panel shows a noncarbon-enhanced star fit with a 40 $M_{\odot}$ model having energies of E_{51} = 1 and 30 (*red squares* and *green triangles*, respectively). Note the factor of two change on the [X/Ca] axis for this panel. The *gray triangles* with the dotted line indicate a higher-energy model having an alternative set of parameters. Reproduced with permission of M. Ishigaki.

triangles). For the C-rich stars, in the top four panels, 25 $M_{\odot}$ models with E_{51} = 1 and 10 are used. For the C-normal star, SD 1029 +1729, in the bottom panel, 40 $M_{\odot}$ models with energies of E_{51} = 1 and 30 are presented. Although the authors were unable to determine one best-fitting energy for SM 0313−6708 because of the small number of elements observed, they do report best fits of E_{51} = 1 for the three other C-rich stars, and E_{51} = 30 for the C-normal star.

5.4.4. The case for rotation. An important exception to the good fits in **Figure 12** is nitrogen in the warm C-rich subgiant HE 1327−2326 (T_{eff} = 6190 K, log g = 3.7, [Fe/H] = −5.7,

[C/Fe] = +4.3, [N/Fe] = +4.6, and [O/Fe] = +3.7) (Aoki et al. 2006, Frebel et al. 2006a), which is severely underproduced in the model compared with the observed value. Nitrogen thus defies explanation in terms of mixing and fallback. Its overabundance, however, is readily explained in terms of the zero-metallicity, rapidly rotating massive (~60 $M_\odot$) stars of Meynet et al. (2006, 2010) in which rotationally driven meridional circulation leads to large amounts of surface enhancements in C, N, O, Na, Mg, and Al in material that will subsequently be expelled in stellar winds prior to the star exploding.

The essential role of rotation is to spatially admix and further process the products of H and He burning. In Section 3.8.2, we reported large variations of Na, Mg, and Al that correlate with carbon in some 50% of the C-rich stars. As also demonstrated by Meynet and coworkers (Maynet et al. 2006, 2010), one naturally expects enhancements of Na, Mg, and Al as the result of the further nuclear processing of the admixture of the products of H and He burning, via (p, γ) reactions. In mixing and fallback models, in contrast, this could result from the admixing of different radial zones, their subsequent nuclear burning, and the expulsion of material that contains different relative amounts of synthesized Na, Mg, and Al. The prospect of observing nucleosynthetic signatures of rotation-related element patterns is further supported by recent simulations of Population III stars, showing that they may have been rapidly rotating (e.g., Stacy et al. 2013).

5.4.5. A test between mixing, and fallback and rotation. There is a basic difference between the rotating star models, on the one hand, and those that experience mixing and fallback on the other. In principle at least, the two cases sample different regions of the progenitor stars that produce the enrichment. In the rotating models, the regions providing the enrichment are the outer layers that mix via meridional circulation, and much of the ejecta are expelled in stellar winds before exhaustion of the nuclear fuel in the central regions leads to a potential explosion. In the other class of model, the entire enrichment patterns are determined in the supernova phase, during which there is mixing and expulsion, potentially at least, of material from all parts of the star outside the core. Insofar as Si and Ca are produced deeper in a star than are the lighter elements, they present the opportunity to test the predictions of the different models more closely. In particular, more accurate abundances for Si in a larger sample of C-rich stars are needed for comparison with more detailed predictions of the two classes of models. In **Figure 9**, we see no evidence for enhancement of Si and Ca, as might be expected, in the rapidly rotating scenario. It would, however, be interesting to have the detailed abundance predictions of the mixing and fallback models. This could be a very useful future avenue of investigation.

5.4.6. Open questions. We comment, finally, on two signatures that are absent from the abundance patterns of the most iron-poor stars presented in **Table 1**. First, no star exhibits a pronounced odd-even effect or a significantly high [Ca/Fe] ratio, which was a prediction of PISNe enrichment (see Section 5.1.2). As we noted in our discussion of PISNe (above), the most iron-poor stars in **Table 1** appear not to have been enriched by ejecta from these extremely massive explosions.

Second, no zinc measurement is available in any of the stars with [Fe/H] < −4.5 because the only two available Zn lines are too weak at these metallicities. Zn, however, is an indicator of the explosion energy (Umeda & Nomoto 2002). Higher [Zn/Fe] (and also [Co/Fe]) abundances can be explained with explosions of higher energy, (E_{51} > 10). Perhaps future Zn measurements in these stars could provide an independent estimate of the explosion energy, in addition to the more indirect method of inferring the energy based on the combination of low [Fe/H] and high [C/Fe] ratios discussed here.

5.4.7. Summary. Significant progress in this area will likely depend on a more refined understanding of supernova nucleosynthesis and the availability of additional metal-poor stars for a broad mapping of the observed abundance parameter space. One promising possibility for progress in this respect would be a more comprehensive treatment of multiple mechanisms involving the mixing and fallback of rapidly rotating stars.

5.5. The Relationship Between the Carbon-Rich and Carbon-Normal Populations

What is the basic difference between the origins of the C-rich and C-normal populations with [Fe/H] < −3.0? As discussed in Section 5.2, an attractive possibility is that there were two distinct cooling processes—CII and OI metal line cooling, on the one hand, and dust thermal cooling, on the other—that operated at the earliest times after the first Population III stars exploded and enriched the material from which Population II stars formed. What was not clear is why the two processes should operate to different extents, with the C and O cooling apparently being predominant.

Norris et al. (2013) advocated a simple scenario whereby the first Population II star-forming clouds, which fragmented to produce low-mass stars that still exist today, contained large amounts of carbon and oxygen relative to their heavier element content. The enriching Population III stars may have been partly or completely described by the stellar evolutionary models in Section 5.3, i.e., the rotating 250–300 $M_\odot$ models of Fryer et al. (2001); the mixing and fallback models of Umeda & Nomoto (2003) and Iwamoto et al. (2005); the relativistic jet-induced explosions of Tominaga et al. (2007a); and the rapidly rotating stars of Meynet et al. (2006, 2010). Following Frebel et al. (2007b), it was also suggested that during the subsequent star formation within the second generation (the first Population II generation), the material with large enhancements of carbon and oxygen fragmented to form the low-mass, long-lived stars that are still observable today. They identified the C-rich population as having been formed from carbon-enriched material. In contrast, to explain the C-normal star SD 1029+1729, with [Fe/H] = −4.7 and [C/Fe] < +0.9 (Caffau et al. 2011a, 2012), it was suggested that some fraction of the Population III stars did not produce large [C/Fe] ratios (as the result perhaps of canonical supernovae explosions without fallback or with slower rotation) but instead produced ejecta with chemical abundance patterns that were rather more solar-like in nature. The gas enriched by this material then experienced dust-induced star formation and fragmentation once the dust's critical metallicity was exceeded (e.g., de Bennassuti et al. 2014).

Cooke & Madau (2014) considered the formation of C-rich stars using cosmological simulations of chemical enrichment within minihalos. Adopting the supernova model yields of Heger & Woosley (2010), they found that low-energy, mixing and fallback supernovae, which produced material with a high value of [C/Fe], were not powerful enough to evacuate the gas from their host minihalos. In their simulations, Cooke & Madau (2014, pg. 11) assumed "that each minihalo that is able to retain its gas will form a second generation of stars." This subsequent Population II star formation then resulted in a population of C-rich stars. At the other extreme of the energy scale, the authors reported that high-energy PISNe would have sufficient energy to remove all gas from the minihalo (see also Greif et al. 2007). This would preclude subsequent star formation that would carry the characteristic PISNe signature of the odd-even effect and the large [Ca/Fe] values discussed above in Section 5.1.2. In the general case, the assumed supernova energy and IMF, together with their yields, thus determine the enrichment patterns in the minihalos. Within this framework the simulations were able to explain (*a*) the essential features of the distribution of CEMP-no stars with [Fe/H] < −3.0 in the ([C/Fe], [Fe/H]) plane and (*b*) the

increasing fraction of C-rich stars with decreasing iron abundance. We refer the reader to Cooke & Madau (2014) for more details of this work.

A semantic question that remains unanswered in the discussions of both Norris et al. (2013) and Cooke & Madau (2014) is which of the C-rich and the C-normal stars formed first. Hopefully, insight into this question will be provided by future simulations that model the timescales associated with CII and OI metal line cooling, on the one hand, and with dust cooling, on the other.

5.6. The Ultra-Faint Dwarfs: Survivors of the First Galaxies?

The metallicity-luminosity relation for dwarf galaxies (Kirby et al. 2008) clearly shows that the faintest galaxies have average metallicities of [Fe/H] ~ -2.5 with underlying [Fe/H] spreads of up to ~ 2.5 dex. In addition, these systems are lacking stars with [Fe/H] > -1.0, which is perhaps the main reason why they contain, relatively speaking, such a large fraction of metal-poor stars. Having galaxies now available with average metallicities close to the extremely metal-poor regime provides an exciting new prospect for the study of early star-forming environments and associated conditions. In fact, instead of just using individual metal-poor stars, as in previous stellar archaeology investigations, now entire galaxies have become the fossil records that can be studied together with their stellar content. Thus, dwarf galaxy archaeology has become the latest tool in the field of near-field cosmology. Topically, it elegantly bridges the gap between observational stellar archaeology and the theoretical simulation studies of the first stars and first galaxies. After all, with the discovery of ultra-faint dwarf galaxies with as few as $\sim 1{,}000$ stars the question that has arisen is whether any of these faintest systems could be related to Galactic building blocks and/or the earliest galaxies to have formed in the Universe. The answer is of great importance to observers and theorists alike.

All of the Milky Way's dSph galaxies, and now also the ultra-faint dwarfs, have been subject to intensive studies with two common goals: What can these systems tell us about galaxy formation and chemical evolution on small scales? And what is their relationship with the building blocks of the Milky Way? With their large relative fraction of extremely metal-poor stars, the metal-deficient ultra-faint dwarfs likely formed at the earliest times and are thus ideal test objects for answering these questions (Bovill & Ricotti 2009).

Let us first briefly recall that the first galaxies must have harbored the first long-lived low-mass metal-deficient Population II stars. Learning about the environment in which these stars formed would help to understand the origin of the most metal-poor stars found in the halo. On the basis of the first galaxy simulation results, Frebel & Bromm (2012) explored what the chemical tell-tale signatures of a first galaxy might be, assuming it survived until the present day. The basic idea rests upon the assumption that a first galaxy would have only experienced a Population III star generation plus one additional first generation of Population II stars (formed from somewhat metal-enriched gas) before losing its gas and the possibility of subsequent star formation (through a possible blowout of gas by the more massive Population II stars, or reionization). The Population II star generation would contain the first long-lived low-mass stars. The corresponding chemical makeup of such a galaxy with this heavily truncated star-formation history, which underwent only chemical enrichment and no chemical evolution, can be straightforwardly predicted. In brief, for a system observed today, we list the criteria required for it to qualify as a candidate surviving first galaxy.

- A large [Fe/H] spread with low average metallicity and the existence of stars with [Fe/H] < -3.0, which can be explained with inhomogeneous mixing in the early gas cloud

- Generally, a halo-like chemical abundance pattern that signals core-collapse supernova enrichment
- No signs of AGB star-driven enrichment of heavy neutron-capture elements, such as Sr and Ba, because no additional long-lived stars should have formed from material enriched by the ejecta of the AGB stars of the first Population II stars
- No downturn in [α/Fe] at any higher metallicity (e.g., [Fe/H] > -2.0) owing to the onset of iron-producing supernovae Type Ia because no additional long-lived stars would have formed after the Type Ia explosions

We note that, as research continues into the nature and evolution of the first galaxies, these criteria may need to be refined or even extended in the future, but overall these basics should remain valid. Comparison of these criteria with abundances of stars in the ultra-faint dwarf galaxies should thus shed light on the question of whether any of today's least luminous dwarfs are perhaps surviving first galaxies. In turn, this would provide hints as to whether it might be possible for any of the first galaxies to have survived until the present day—an exciting prospect for near-field cosmology.

The issue can be approached by using the Segue 1 system as the most relevant example. With $L \sim 1,000$ L$_\odot$, Segue 1 is the faintest galaxy yet discovered (Belokurov et al. 2007). It was found because it is only 23 kpc away in the halo. Its average metallicity is [Fe/H] ~ -2.5, which is, however, difficult to accurately determine given its fairly flat and sparsely populated distribution of [Fe/H] (e.g., Simon et al. 2011). Some controversy about the nature of Segue 1 occurred soon after its discovery. Although Niederste-Ostholt et al. (2009) advocated categorizing it as a star cluster, additional studies have shown that it is a highly dark matter–dominated galaxy (Geha et al. 2009, Simon et al. 2011). This result is supported by the (*a*) large [Fe/H] and [C/Fe] spreads (Δ[Fe/H] $= 2.4$ and Δ[C/Fe] $= 2.4$), (*b*) existence of stars with [Fe/H] < -3.0, (*c*) halo-like chemical abundances of light elements, and (*d*) consistently low neutron-capture element abundances of all its stars studied with high-resolution spectroscopy (Frebel et al. 2014). Without a doubt, these are all signatures associated with galactic chemical enrichment rather than with any star cluster that does not show signs of chemical evolution. It was thus concluded that Segue 1 is most likely the most primitive galaxy known.

The detailed chemical abundances of eight stars in Segue 1 were thus compared with the above criteria (Frebel et al. 2014). All of them were met, making Segue 1 the first viable surviving first galaxy candidate. In contrast, inspection of the limited abundance data available for stars in the somewhat more luminous ultra-faint dwarf galaxies indicates that systems with $L \gtrsim 10^{4.5}$ L$_\odot$ already show signs of chemical evolution (in particular, some lower, solar-like α-element abundances) and thus do not fulfill all of the criteria. This suggests that these systems already had multiple generations of stars and that some chemical evolution had occurred, albeit still very little in comparison with the luminous dSph galaxies, which clearly show extended star formation and chemical evolution. This luminosity limit is not unlike that suggested by Bovill & Ricotti (2011) of $L < 10^6$ L$_\odot$ (based on simulation work) as a limit for the fossil nature of the ultra-faint systems.

Surviving dwarf galaxies like Segue 1 thus give unique clues as to what the conditions of early galaxies may have been. At the same time, Segue 1 should be considered a building block–type galaxy that survived the Milky Way's assembly process. Whether it survived for a particular reason remains unanswered for now (although structure formation simulations may shed light on this more general issue of the survival rate and preference of building blocks during the evolution of large galaxies).

That said, accepting Segue 1 as an analog of the accreted building blocks offers tantalizing insights. Considering its stellar content, it appears plausible that Segue 1-like objects may have populated the low-metallicity tail of the halo metallicity distribution function. Given its low mass and the current incomplete knowledge of the metal-poor end of the halo metallicity distribution

function, it remains unclear how many such systems would be required to populate the entire tail. It thus seems likely that the bulk of the halo stars must have come from more massive systems. This is supported by the excellent agreement between the abundance signatures of the most metal-poor Segue 1 stars and those of the metal-poor halo stars that have similar values of [Fe/H]. This means that we can use Segue 1-type systems to learn about the origin of the most metal-poor halo stars. It closes an important loop because otherwise we can only speculate that halo stars must have formed in some kind of early systems.

The example of Segue 1 illustrates that studying the surviving dwarf galaxies is helping to fill in the missing information that the most metal-poor halo stars by themselves cannot offer us: Where they formed and how they made their way into the halo of the Milky Way. See also Revaz & Jablonka (2012). More generally, the ultra-faint dwarf galaxies with their limited star-formation histories might be the best test objects for chemical tagging in dwarf galaxies because all their stars likely formed in chemically homogenous star clusters (Bland-Hawthorn et al. 2010). As more sophisticated simulations become available, dwarf archaeology can be established as a major empirical constraint on the formation process of the first galaxies and the first long-lived low-mass stars.

Finally, we note that, after having found one candidate first galaxy in the Northern Hemisphere, further progress on the observational side will depend on finding more of these faintest Segue 1–type dwarf galaxies in the south, for example, in the data obtained by the Dark Energy Survey (DES), the SkyMapper Telescope and the Large Synoptic Survey Telescope (LSST) (see Section 7.2), and also with search techniques involving stellar proper-motion measurements (Fabrizio et al. 2014). The availability of new systems is important because all dwarf galaxy stars are extremely faint. Often only 1–3 stars per galaxy can be observed with high-resolution spectroscopy, and by now, essentially all of the accessible stars in the currently known ultra-faint dwarf systems have been observed. More new dwarfs, such as the recent DES discoveries (DES Collab., Bechtol et al. 2015; Koposov et al. 2015) are needed to provide a fresh supply of sufficiently bright stars for high-resolution spectroscopy with current facilities for the detailed abundance work that may lead to the discovery of additional first-galaxy candidates.

6. NEAR-FIELD MEETS FAR-FIELD COSMOLOGY

The study of the most metal-poor stars provides information about the early Universe and the conditions at the time and place of their birth. Near-field results, however, rest on the implicit assumption that the most metal-poor stars did indeed form from low-metallicity gas within the first billion years or so after the Big Bang. Although this conclusion is clearly supported by the age dating of the rare group of r-process enhanced stars, which have ages of 13 to 14 Gyr and [Fe/H] ~ -3.0 (e.g., Hill et al. 2002, Frebel et al. 2007a, Sneden et al. 2008), it is of critical importance to verify this by investigating high-redshift early gaseous systems and their metal content via direct observations.

Metallicity measurements have been obtained for some 200 high-redshift Damped Lyman-α (DLA) systems with $z \sim 2$ to 5 (e.g., Jorgenson et al. 2013, Rafelski et al. 2014 and references therein), observed along the sightline to a given quasar (where it remains unknown whether the nucleus or the diffuse outer halo is being probed). The data of Rafelski et al. (2014), on average, reveal a slow but steady decrease in metallicity with increasing redshift, and by $z \sim 4.7$ the mean metallicity is [M/H] ~ -2.2. Although the distribution of abundances has a floor at [M/H] ~ -2.5, there are important exceptions. Cooke et al. (2011) have reported a small number of objects in the extremely metal-poor regime, with [Fe/H] < -3, at $z = 2.3$ to 3.7. This is indicative that at least some of these early gas clouds could have hosted the formation of the first/early low-mass Population II stars, which we observe as the most metal-poor halo stars today.

We have, moreover, reached an interesting point in the field of metal abundance determinations pertaining to both stellar archaeology and high-redshift DLA systems as well as to other gas clouds of the Lyman-α forest. Objects in both disciplines are now being discovered that have such low abundances that only the upper limits can be determined. The stellar archaeology example is SM 0313−6708, with [Fe/H] < -7.3, which was discussed in Sections 3 and 5 (see also **Table 1**, and **Figure 4**). We now address the far-field low-abundance limits.

6.1. The Most Metal-Poor High-Redshift Gaseous Systems

Fumagalli et al. (2011) have reported Lyman limit systems along two quasar sightlines having redshifts $z \sim 3.4$ and $z \sim 3.1$ with metallicity upper limits of $Z < 10^{-4.2}$ $Z_\odot$ and $Z < 10^{-3.8}$ $Z_\odot$ (i.e., [M/H] $= -4.2$ and -3.8), respectively. These redshifts imply an epoch about 2 Gyr after the Big Bang. It seems reasonable, therefore, to suggest that systems like these could be representative of the initial clouds in the early Universe, which hosted some of the first Population II stars. However, this is not that early in the evolution of the Universe (compared with the epochs earlier than 500 Myr of interest in the present discussion) and possibly implies that low-metallicity gas, or even metal-free clouds, may have survived for this long. It is unclear, of course, whether these particular Lyman limit systems have actually formed metal-poor stars.

An even more extreme case, reported by Simcoe et al. (2012), is a gaseous cloud with $z \sim 7$, observed along the sightline to the quasar ULAS J1120+0641. This redshift corresponds to an age of the Universe of only $\sim$800 Myr. No metal absorption is found in the spectrum of the cloud, leading to metallicity limits of $Z < 10^{-3.0}$ $Z_\odot$, if the gas is simply diffuse and unbound, or of $Z < 10^{-4.0}$ $Z_\odot$, if it is a gravitationally bound protogalaxy (i.e., [M/H] $= -3.0$ and -4.0, respectively).

6.2. Chemical Abundances Within the High-Redshift Gas Clouds

A critical point of comparison between near-field and far-field endeavors lies in their detailed relative abundances. In the following sections, we restrict our attention to quasar absorption line systems having redshifts $z > 2$, in particular the metal-poor DLA systems at lower redshifts $2 < z \lesssim 4$ (e.g., Cooke et al. 2011, and references therein) and the so-called sub-DLAs over the range $4 \lesssim z < 6$ (e.g., Becker et al. 2012 and references therein). In the DLA systems below redshifts of $z \sim 4$, the amounts of hydrogen and several elements, X, can be determined along the sightline to the background quasar, and both [X/H] and [X/Fe] can be obtained. For the sub-DLAs, however, in the range $4 \lesssim z < 6$, the amount of hydrogen is not well measured, and relative abundances of only the other elements (e.g., [X/Fe]) are available.

In the lower redshift regime, Cooke et al. (2011) report column densities for some 11 elements. In a sample of 21 objects with [Fe/H] $\lesssim -2.0$, the three most metal-poor systems have [Fe/H] in the range of -3.5 to -3.0. They also report that the ratios of C/O and O/Fe are consistent with values determined for stars in the Galactic halo. Of particular interest, in the present context, is the result that one (J0035–0918) of the ten systems having both C and Fe abundances has the composition similar to that of a CEMP-no star, [Fe/H] $= -3.0$ and [C/Fe] $= +0.6$ [initially reported to have [C/Fe] $= +1.5$; see Cooke et al. 2015 for details on the carbon measurement, which now follows predictions in Becker et al. 2012 (their section 4), and Carswell et al. 2012]. Cooke et al. (2012) then report a second, very similar carbon-enhanced object (J1358+6522), with [Fe/H] $= -2.8$ and [C/Fe] $= +0.6$.

The results of Becker et al. (2012) for the sub-DLAs extend the data set to redshift $z = 6.3$ and provide abundance information for C, O, Si, and Fe. These authors supplement their results with

those of others at lower redshifts to provide a sample of 20 objects over the redshift range $z = 2$ to 6. In their figure 11, Becker et al. (2012) plot [C/O], [Si/O], [C/Si], [C/Fe], [O/Fe], and [Si/Fe] as functions of redshift. In this diagram, there is no evidence for a large variation in any of the relative abundances. In particular, for their four systems having C and O abundances in the redshift range $4.7 < z < 6.3$, they report mean values $\langle[\text{C/Fe}]\rangle = +0.17 \pm 0.07$ and $\langle[\text{O/Fe}]\rangle = +0.50 \pm 0.05$, respectively. That is to say, the C and O abundances of sub-DLA systems at the highest redshifts currently observed are the same as those of normal noncarbon-enhanced Galactic halo stars. Concerning the comparison with the abundances of carbon in the most Fe-poor stars in the Milky Way, Becker et al. (2012, pg. 11) suggest: "If carbon-enhanced stars fairly reflect their native ISM abundances, then these abundances are no longer common by redshift of $z \sim 6$. This raises the intriguing possibility that most carbon-enhanced stars were formed at even earlier times."

We have come to the crux of the matter. If one includes the two carbon-enhanced extremely metal-poor systems of Cooke et al. (2012, 2015) with those of Becker et al. (2012, their figure 11), and assuming [C/Fe] $= +0.6$ is sufficient for classifying them as carbon-rich systems, one finds (*a*) that in the range $2 < z < 6.3$, the fraction of C-rich DLAs is $\sim$0.15 (2 out of 13) compared with the value of $\sim$0.40 (Placco et al. 2014; see Section 3.5) for C-rich metal-poor stars at [Fe/H] < -3.0 and (*b*) that the carbon abundance of the two DLA systems ([C/Fe] $= +0.6$) is smaller in comparison with the values one finds for the Galactic C-rich stars discussed in Section 3, which span the range in [C/Fe] from $\sim +0.7$ to >4.9. The number of DLA systems involved here is clearly too small to permit any meaningful conclusion, especially because we do not know which region of the DLA is being studied with the observed sightline. That said, the tension needs to be resolved in the future. More DLA abundance measurements of iron and carbon should be obtained to ensure that the current result is not caused by the use of small-number statistics. Given that the redshifts of the DLAs discussed here are associated with epochs more than 800 Myr after the Big Bang, an intriguing alternative is that the DLA and sub-DLA abundances reflect the average abundances of the medium at that time, depending on the level and length scales of mixing in these early clouds. Potentially, the stellar abundances could reflect more detailed local conditions at earlier times. In this case, the abundance patterns of both the most metal-poor halo stars and the high-redshift DLAs could be understood in terms of chemical enrichment by the ejecta of massive stars exploding as core-collapse supernovae, albeit with the stars and DLA systems being at different phases in their evolution.

7. THE BRIGHT FUTURE OF NEAR-FIELD COSMOLOGY

The past decade has seen a steep increase in activities related to stellar archaeology and near-field cosmology. A number of exciting discoveries have been made, such as the stars with [Fe/H] < -5.0 and the ultra-faint dwarf galaxy population. This opened up entirely new lines of research and drew attention to near-field cosmology as an important area of study that connects stellar astrophysics with galaxy formation and evolution.

Several observational large-scale efforts to characterize the Milky Way, its stellar content, satellite population, and formation history have contributed enormously to near-field cosmology, ushering in a new era of exploration. Most notably among them is SDSS (primarily its extensions focused on Galactic science), but there have also been the numerous individual studies that have collectively led to the detailed analysis of more than 1,000 stars with [Fe/H] < -2.0. This number is now expected to rapidly increase; we list major near-term surveys for more metal-poor stars in Section 7.2.

In addition to these and other observational advances that have brought much attention to the topics of galactic astrophysics, stellar populations, chemical evolution, and galaxy formation,

crucial progress has been made in the area of first-star and first-galaxy simulations. These works directly relate to metal-poor stars and their formation as well as to the nature and history of dwarf galaxies. We are thus at an interesting crossover point right now where simulations of early star-forming environments can finally be compared, rudimentarily, with observational near-field cosmology results and where stellar archaeology and, in particular, dwarf galaxy archaeology inspire and constrain these simulations. This close connection promises to be vital for future progress in both areas, especially once the detailed evolution of metals can be traced more generically in simulations. Efforts toward this goal are well underway (e.g., Greif et al. 2010; Wise et al. 2012; Jeon et al. 2014; Safranek-Shrader et al. 2014a,b). In this manner, interpretation of the stellar abundance patterns will soon be undertaken in the context of detailed simulation results.

7.1. Open Questions in Near-Field Cosmology

Despite the enormous progress both observationally and theoretically, important questions remain to be answered. Many of these have only arisen as the result of recent advances, which illustrate that near-field cosmology is a vibrant field that is rapidly moving forward. Below we list a number of open key questions that describe the state of the field while simultaneously providing hints as to what may be coming in the next decade.

What are the lowest stellar iron and carbon abundances? Could there be stars with arbitrarily low Fe abundances? What is the fraction of C-rich stars at the lowest metallicities? What is the spatial distribution of the most metal-poor stars and do they reflect an accreted halo component as opposed to an in situ component?

Are there any surviving low-mass Population III stars? Can Population II stars form in minihalos? To what extent are stellar abundance patterns altered by accretion of ISM material or nearby supernova explosions? What are the nucleosynthesis yields of the earliest supernova? How does metal dispersal operate in early star-forming environments? What are the details of the manner in which the Milky Way's halo was assembled?

How many ultra-faint dwarf galaxies are out there? Faint systems, such as Segue 1, can currently only be identified out to $\sim$30 kpc. How many are yet to be found in the unexplored Southern Hemisphere? Are systems like Segue 1 really undisturbed first/early galaxies that have survived until today? How many of them could be orbiting the Milky Way? Have the classical dSph galaxies already been assembled from smaller (gaseous) fragments?

Answers to some questions can already be estimated by pushing toward the technical limit of observations or simulations. One example is that of the lowest iron and carbon abundances in halo stars. The current technical limit for an abundance measurement by just detecting the strongest iron line is [Fe/H] < -7.2 (Frebel et al. 2009). Using SM 0313$-$6708 as an example, a carbon abundance of down to [C/H] $\sim$ -4.0 would be measurable based on the detection of the G-band of the CH molecule at 4313 Å and assuming the availability of a high S/N ($\sim$100) spectrum. If SM 0313$-$6708 was cooler (it has $T_{\rm eff}$ = 5,125 K), for example, with $T_{\rm eff}$ = 4,500 K, a carbon abundance of [C/H] $\sim$ -4.2 would still be measurable.

A cool giant star's hypothetical spectrum with no metal absorption lines (just hydrogen lines) would thus yield abundance limits of [Fe/H] < -7.2, [Ca/H] < -9.4, [Mg/H] < -6.0, and [C/H] < -4.0 (Frebel et al. 2009, Frebel & Norris 2013). This highlights an important point regarding the nature and origin of C-rich metal-poor stars. The current detection limit essentially prevents us from measuring accurate carbon abundances that are very low, with underabundances similar to those of iron. However, it might just be enough to at least discriminate formation scenarios for these low-mass stars. The $D_{\rm trans}$ criterion of Frebel et al. (2007b) is $D_{\rm trans} = \log(10^{[{\rm C/H}]} + 0.3 \times 10^{[{\rm O/H}]}) > -3.5$ and is based on a combined abundance of carbon

and oxygen. A value of [C/H] ~ -4.0, especially if additionally down corrected by appropriate 3D abundance corrections, might already indicate that dust cooling and not fine-structure line cooling would have led to the formation of the object. However, because much lower carbon values cannot be determined, a direct confirmation of a dust-cooling scenario may not be possible for these stars.

7.2. Near-Term Searches for Metal-Poor Stars and Dwarf Galaxies

Looking back some 40 years, one sees that the search for metal-poor stars has transitioned from relatively small-scale projects into an enormous enterprise. Several surveys operating around the globe have dedicated programs for metal-poor stars and galactic exploration, whereas others are more generally usable for the characterization of the Milky Way's structure, stellar populations, and history. We briefly list the main near-term projects below.

The Apache Point Observatory Galactic Evolution Experiment (APOGEE) (Majewski et al. 2010) is part of the third extension of the SDSS (**http://www.sdss.org**). Since 2011, it has been mapping the Galaxy (bulge, disk, and even parts of the halo) with high-resolution, near-infrared spectroscopy to establish the Milky Way's chemical and kinematical evolution.

The LAMOST survey (Deng et al. 2012) has a dedicated Galactic program called the LAMOST Experiment for Galactic Understanding and Exploration (LEGUE), which provides low-resolution ($R \sim 1,500$) spectroscopy of up to 4,000 stars per pointing (facilitated by 16 linked spectrographs, each with 250 fibers) in the Northern Hemisphere. Metal-poor candidates are already being selected from these data (Data Release 1; **http://dr1.lamost.org**).

The SkyMapper Telescope (Keller et al. 2007b) is now efficiently selecting metal-poor candidates based on its combination of broad- and narrow-band filters designed to straightforwardly characterize stellar properties. Its photometric Southern Sky Survey will also provide deep images in the future to search for southern ultra-faint dwarf galaxies and stellar streams.

The Anglo-Australian Telescope's high-resolution multiobject spectrograph HERMES (Heijmans et al. 2012) is being used to observe $\sim$1 million stars (400 at a time) to characterize the history of star formation in the Galaxy through detailed chemical abundance measurements as part of the GALAH survey.

The satellite all-sky mission *Gaia* (e.g., Cacciari 2009) will produce astrometry and photometry for some 1 billion stars down to magnitude $V = 20$ (about 3.5×10^5 sources to $V = 10$, 2.6×10^7 to $V = 15$, and 2.5×10^8 to $V = 18$). Additional spectroscopy ($R \sim 10,000$; over 8450 to 8720 Å, the region of the CaII triplet) will enable stellar parameter determinations of perhaps six million objects from which metal-poor candidates can be selected. We refer the reader to Gilmore et al. (2012) for a description of the synergy between *Gaia* and ground-based facilities that will together provide basic detailed chemical abundances for an unprecedented sample of the Galaxy's metal-poor stars.

The LSST (Ivezić et al. 2008, version 4) will carry out a deep southern sky photometric survey using broadband filters in the early 2020s. These data will allow a detailed assessment of Galactic structure and facilitate the search for southern ultra-faint dwarf galaxies and stellar streams.

7.3. Next-Generation Telescopes

Near-field cosmology will greatly benefit from the construction of the three next-generation extremely large telescopes currently planned to be operational from $\sim$2020. In particular, the Giant Magellan Telescope (GMT) promises great advances in stellar and dwarf galaxy archaeology because it selected the high-resolution optical spectrograph G-CLEF (Szentgyorgyi et al. 2012) as one of its first light instruments. This fiber-fed spectrograph will enable detailed studies of metal-poor stars at resolving powers of $R \sim 20,000$, $40,000$, and $100,000$ in the outskirts of the

Milky Way and in dwarf galaxies. The GMT will also have a low-resolution optical spectrograph, GMACS, suitable for observation of the fainter stars in the dwarf galaxies and deep low-resolution stellar spectroscopy within the Galaxy.

The European Extremely Large Telescope (E-ELT) and the Thirty Meter Telescope (TMT) will not initially be equipped with optical high-resolution spectrographs but instead with optical and near-infrared imagers and low-resolution spectrographs. These instruments will enable unprecedented observations of high-redshift galaxies, which will deliver complementary information to that provided by near-field cosmology concerning the earliest epochs of star and galaxy formation. In the same vein, the JWST will allow the highest-redshift spectroscopic observations of the earliest galaxies, perhaps even the first massive star clusters to have formed in the Universe.

7.4. Theoretical Insight: The Journey from First Stars to the Milky Way

Observations of metal-poor stars located in the Milky Way permit powerful insight into the earliest epochs of star and galaxy formation. However, they cannot provide direct information on where exactly these stars formed and how their respective host systems were accreted by the Galaxy. Cosmological simulations of early star-forming processes and structure formation in the Universe are necessary to reveal this type of global information. With the emergence of powerful supercomputers, tremendous progress has been made in this area. Within the next decade, near-field cosmology, paired with far-field cosmology and supported by large-scale simulations of galaxy assembly, will provide a comprehensive picture of how the Milky Way assembled and how to interpret the nature and history of its stellar content.

DISCLOSURE STATEMENT

The authors are not aware of any affiliations, memberships, funding, or financial holdings that might be perceived as affecting the objectivity of this review.

LITERATURE CITED

Abel T, Bryan GL, Norman ML. 2002. *Science* 295:93–98
Ade PAR, Aghanim N, Armitage-Caplan C, et al. 2014. *Astron. Astrophys.* 571:16–82
Agertz O, Teyssier R, Moore B. 2011. *MNRAS* 410:1391–408
Aller LH, Greenstein JL. 1960. *Ap. J. Suppl.* 5:139–86
An D, Beers TC, Johnson JA, et al. 2013. *Ap. J.* 763:65

Aoki W. 2010. In *Chemical Abundances in the Universe: Connecting First Stars to Planets. IAU Symp. 265*, ed. K Cunha, M Spite, B Barbuy, pp. 111–16. Cambridge, UK: Cambridge Univ. Press

Aoki W, Arimoto N, Sadakane K, et al. 2009a. *Astron. Astrophys.* 502:569–78

Aoki W, Barklem PS, Beers TC, et al. 2009b. *Ap. J.* 698:1803–12

Aoki W, Beers TC, Christlieb N, et al. 2007a. *Ap. J.* 655:492–521

Aoki W, Beers TC, Lee YS, et al. 2013. *Astron. J.* 145:13

Aoki W, Frebel A, Christlieb N, et al. 2006. *Ap. J.* 639:897–917

Aoki W, Honda S, Beers TC, et al. 2007b. *Ap. J.* 660:747–61

Aoki W, Tominaga N, Beers TC, Honda S, Lee YS. 2014. *Science* 345:912–15

Asplund M. 2005. *Annu. Rev. Astron. Astrophys.* 43:481–530

Asplund M, Grevesse N, Sauval AJ, Scott P. 2009. *Annu. Rev. Astron. Astrophys.* 47:481–522

Asplund M, Lambert DL, Nissen PE, Primas F, Smith VV. 2006. *Ap. J.* 644:229–59

Barklem PS, Christlieb N, Beers TC, et al. 2005. *Astron. Astrophys.* 439:129–51

Baschek B. 1959. *Z. Astrophys.* 48:95–139

Becker GD, Sargent WLW, Rauch M, Carswell RF. 2012. *Ap. J.* 744:91

Beers TC, Carollo D, Ivezić Ž, et al. 2012. *Ap. J.* 746:34

Beers TC, Christlieb N. 2005. *Annu. Rev. Astron. Astrophys.* 43:531–80

Beers TC, Norris JE, Placco VM, et al. 2014. *Ap. J.* 794:58

Beers TC, Preston GW, Shectman SA. 1992. *Astron. J.* 103:1987–2034

Belokurov V. 2013. *New Astron. Rev.* 57:100–21

Belokurov V, Zucker DB, Evans NW, et al. 2007. *Ap. J.* 654:897–906

Bessell MS, Norris J. 1984. *Ap. J.* 285:622–36

Bidelman WP, MacConnell DJ. 1973. *Astron. J.* 78:687–733

Bland-Hawthorn J, Karlsson T, Sharma S, Krumholz M, Silk J. 2010. *Ap. J.* 721:582–96

Bond HE. 1970. *Ap. J. Suppl.* 22:117–56

Bonifacio P, Caffau E, Spite M, et al. 2015. *Astron. Astrophys.* 579:A28

Bonifacio P, Caffau E, Venn KA, Lambert DL. 2012a. *Astron. Astrophys.* 544:A102

Bonifacio P, Molaro P, Sivarani T, et al. 2007. *Astron. Astrophys.* 462:851–64

Bonifacio P, Sbordone L, Caffau E, et al. 2012b. *Astron. Astrophys.* 542:A87

Bovill MS, Ricotti M. 2009. *Ap. J.* 693:1859–70

Bovill MS, Ricotti M. 2011. *Ap. J.* 741:17

Boylan-Kolchin M, Bullock JS, Sohn ST, Besla G, van der Marel RP. 2013. *Ap. J.* 768:140

Bromm V. 2013. *Rep. Prog. Phys.* 76:112901

Bromm V, Coppi PS, Larson RB. 2002. *Ap. J.* 564:23–51

Bromm V, Larson RB. 2004. *Annu. Rev. Astron. Astrophys.* 42:79–118

Bromm V, Loeb A. 2003. *Nature* 425:812–14

Bromm V, Yoshida N. 2011. *Annu. Rev. Astron. Astrophys.* 49:373–407

Brook CB, Kawata D, Scannapieco E, Martel H, Gibson BK. 2007. *Ap. J.* 661:10–18

Brown TM, Tumlinson J, Geha M, et al. 2014. *Ap. J.* 796:213–32

Brown TM, Tumlinson J, Geha M, et al. 2012. *Ap. J. Lett.* 753:L21

Cacciari C. 2009. *Mem. Soc. Astron. Ital.* 80:97–102

Caffau E, Bonifacio P, Francois P, et al. 2011a. *Nature* 477:67–69

Caffau E, Bonifacio P, Francois P, et al. 2012. *Astron. Astrophys.* 542:A51

Caffau E, Ludwig HG, Steffen M, Freytag B, Bonifacio P. 2011b. *Solar Phys.* 268:255–69

Campbell SW, Lugaro M, Karakas AI. 2010. *Astron. Astrophys.* 522:L6

Carney BW, Laird JB, Latham DW, Aguilar LA. 1996. *Astron. J.* 112:668–92

Carney BW, Peterson RC. 1981. *Ap. J.* 245:238–46

Carollo D, Beers TC, Bovy J, et al. 2012. *Ap. J.* 744:195

Carollo D, Beers TC, Chiba M, et al. 2010. *Ap. J.* 712:692–727

Carollo D, Beers TC, Lee YS, et al. 2007. *Nature* 450:1020–25

Carollo D, Freeman K, Beers TC, et al. 2014. *Ap. J.* 788:180

Carswell RF, Becker GD, Jorgenson RA, Murphy MT, Wolfe AM. 2012. *MNRAS* 422:1700–8

Cayrel R, Depagne E, Spite M, et al. 2004. *Astron. Astrophys.* 416:1117–38

Chamberlain JW, Aller LH. 1951. *Ap. J.* 114:52–72

Charbonnel C, Primas F. 2005. *Astron. Astrophys.* 442:961–92

Cherchneff I, Dwek E. 2010. *Ap. J.* 713:1–24

Chiba M, Beers TC. 2000. *Astron. J.* 119:2843–65

Christlieb N, Bessell MS, Beers TC, et al. 2002. *Nature* 419:904–6

Christlieb N, Gustafsson B, Korn AJ, et al. 2004. *Ap. J.* 603:708–28

Christlieb N, Schörck T, Frebel A, et al. 2008. *Astron. Astrophys.* 484:721–32

Clark PC, Glover SCO, Smith RJ, et al. 2011. *Science* 331:1040–42

Coc A, Goriely S, Xu Y, Saimpert M, Vangioni E. 2012. *Ap. J.* 744:158

Cohen JG, Christlieb N, McWilliam A, et al. 2008. *Ap. J.* 672:320–41

Cohen JG, Christlieb N, Thompson I, et al. 2013. *Ap. J.* 778:56

Cohen JG, Huang W. 2009. *Ap. J.* 701:1053–75

Cohen JG, Huang W. 2010. *Ap. J.* 719:931–49

Cohen JG, McWilliam A, Christlieb N, et al. 2007. *Ap. J. Lett.* 659:L161–64

Cooke R, Pettini M, Jorgenson RA. 2015. *Ap. J.* 800:12–31

Cooke R, Pettini M, Murphy MT. 2012. *MNRAS* 425:347–54

Cooke R, Pettini M, Steidel CC, Rudie GC, Nissen PE. 2011. *MNRAS* 417:1534–58

Cooke RJ, Madau P. 2014. *Ap. J.* 791:116

Cyburt RH, Fields BD, Olive KA. 2008. *J. Cosmol. Astropart. Phys.* 11:12

Deason AJ, Belokurov V, Evans NW. 2011. *MNRAS* 416:2903–15

de Bennassuti M, Schneider R, Valiante R, Salvadori S. 2014. *MNRAS* 445:3039–54

de Jong JTA, Yanny B, Rix HW, et al. 2010. *Ap. J.* 714:663–74

Deng LC, Newberg HJ, Liu C, et al. 2012. *Res. Astron. Astrophys.* 12:735–54

DES Collab., Bechtol K, Drlica-Wagner A, Balbinot E, et al. 2015. *Ap. J.* 807:50

Eggen OJ, Lynden-Bell D, Sandage AR. 1962. *Ap. J.* 136:748–66

Fabrizio M, Raimondo G, Brocato E, et al. 2014. *Astron. Astrophys.* 570:A61

Farouqi K, Kratz KL, Pfeiffer B, et al. 2010. *Ap. J.* 712:1359–77

Font AS, McCarthy IG, Crain RA, et al. 2011. *MNRAS* 416:2802–20

Frebel A. 2010. *Astron. Nachr.* 331:474–88

Frebel A, Aoki W, Christlieb N. 2005. *Nature* 434:871–73

Frebel A, Bromm V. 2012. *Ap. J.* 759:115

Frebel A, Christlieb N, Norris JE, Aoki W, Asplund M. 2006a. *Ap. J. Lett.* 638:L17–20

Frebel A, Christlieb N, Norris JE, et al. 2006b. *Ap. J.* 652:1585–603

Frebel A, Christlieb N, Norris JE, et al. 2007a. *Ap. J. Lett.* 660:L117–20

Frebel A, Johnson JL, Bromm V. 2007b. *MNRAS* 380:L40–44

Frebel A, Johnson JL, Bromm V. 2009. *MNRAS* 392:L50–54

Frebel A, Kirby EN, Simon JD. 2010a. *Nature* 464:72–75

Frebel A, Norris JE. 2013. In *Metal-Poor Stars and the Chemical Enrichment of the Universe in Planets, Stars and Stellar Systems. Volume 5: Galactic Structure and Stellar Populations*, ed. TD Oswalt, G Gilmore, pp. 55–114. Dordrecht, Neth.: Springer Science+Bus. Media

Frebel A, Norris JE, Aoki W, et al. 2007c. *Ap. J.* 658:534–52

Frebel A, Simon JD, Geha M, Willman B. 2010b. *Ap. J.* 708:560–83

Frebel A, Simon JD, Kirby EN. 2014. *Ap. J.* 786:74

Freeman K, Bland-Hawthorn J. 2002. *Annu. Rev. Astron. Astrophys.* 40:487–537

Frischknecht U, Hirschi R, Thielemann FK. 2012. *Astron. Astrophys.* 538:L2

Fryer CL, Woosley SE, Heger A. 2001. *Ap. J.* 550:372–82

Fujimoto MY, Ikeda Y, Iben I Jr. 2000. *Ap. J. Lett.* 529:L25–28

Fulbright JP, Rich RM, Castro S. 2004. *Ap. J.* 612:447–53

Fumagalli M, O'Meara JM, Prochaska JX. 2011. *Science* 334:1245–49

Galli D, Palla F. 2013. *Annu. Rev. Astron. Astrophys.* 51:163–206

García Pérez AE, Cunha K, Shetrone M, et al. 2013. *Ap. J. Lett.* 767:L9

Geha M, Willman B, Simon JD, et al. 2009. *Ap. J.* 692:1464–75

Gilbert KM, Kalirai JS, Guhathakurta P, et al. 2014. *Ap. J.* 796:76–96

Gilmore G, Norris JE, Monaco L, Yong D, Wyse RFG, Geisler D. 2013. *Ap. J.* 763:61

Gilmore G, Randich S, Asplund M, et al. 2012. *Messenger* 147:25–31

Gilmore G, Reid N. 1983. *MNRAS* 202:1025–47

Gilmore G, Wyse RFG, Kuijken K. 1989. *Annu. Rev. Astron. Astrophys.* 27:555–627

González Hernández JI, Bonifacio P, Ludwig HG, et al. 2008. *Astron. Astrophys.* 480:233–46

Gratton R, Sneden C, Carretta E. 2004. *Annu. Rev. Astron. Astrophys.* 42:385–440

Gray DF. 2005. *The Observation and Analysis of Stellar Photospheres.* Cambridge, UK: Cambridge Univ. Press. 3rd ed.

Greif TH, Bromm V. 2006. *MNRAS* 373:128–38

Greif TH, Glover SCO, Bromm V, Klessen RS. 2010. *Ap. J.* 716:510–20

Greif TH, Johnson JL, Bromm V, Klessen RS. 2007. *Ap. J.* 670:1–14

Greif TH, Johnson JL, Klessen RS, Bromm V. 2008. *MNRAS* 387:1021–36

Greif TH, Springel V, White SDM, et al. 2011. *Ap. J.* 737:75

Guedes J, Callegari S, Madau P, Mayer L. 2011. *Ap. J.* 742:76

Gustafsson B, Edvardsson B, Eriksson K, et al. 2008. *Astron. Astrophys.* 486:951–70

Hansen T, Hansen CJ, Christlieb N, et al. 2014. *Ap. J.* 787:162

Hartwick FDA. 1987. In *NATO ASIC Proc. 207: The Galaxy*, ed. G Gilmore, B Carswell, pp. 281–90. Dordrecht, Neth.: Reidel

Hattori K, Yoshii Y, Beers TC, Carollo D, Lee YS. 2014. *Ap. J.* 784:153

Heger A, Woosley SE. 2002. *Ap. J.* 567:532–43

Heger A, Woosley SE. 2010. *Ap. J.* 724:341–73

Heijmans J, Asplund M, Barden S, et al. 2012. In *Proc. SPIE Conf. Ser.* 8446:0W

Helmi A, Irwin MJ, Tolstoy E, et al. 2006. *Ap. J. Lett.* 651:L121–24

Hill V, Plez B, Cayrel R, et al. 2002. *Astron. Astrophys.* 387:560–79

Hirano S, Hosokawa T, Yoshida N, et al. 2014. *Astrophys. J.* 781:60

Hirschi R. 2007. *Astron. Astrophys.* 461:571–83

Hollek JK, Frebel A, Roederer IU, et al. 2011. *Ap. J.* 742:54

Hosokawa T, Omukai K, Yoshida N, Yorke HW. 2011. *Science* 334:1250–53

Hosokawa T, Yorke HW, Inayoshi K, Omukai K, Yoshida N. 2013. *Ap. J.* 778:178

Howes L, Asplund M, Casey AR, et al. 2014. *MNRAS* 445:4241–46

Ibata RA, Gilmore G, Irwin MJ. 1995. *MNRAS* 277:781–800

Iben I Jr. 1983. *Mem. Soc. Astron. Ital.* 54:321–30

Ishigaki MN, Aoki W, Arimoto N, Okamoto S. 2014a. *Astron. Astrophys.* 562:A146

Ishigaki MN, Tominaga N, Kobayashi C, Nomoto K. 2014b. *Ap. J. Lett.* 792:L32–36

Ito H, Aoki W, Honda S, Beers TC. 2009. *Ap. J. Lett.* 698:L37–41

Ivezić Z, Beers TC, Jurić M. 2012. *Annu. Rev. Astron. Astrophys.* 50:251–304

Ivezić Z, Tyson JA, Abel B, et al. 2008. arXiv:0805.2366

Iwamoto N, Umeda H, Tominaga N, Nomoto K, Maeda K. 2005. *Science* 309:451–53

Jeon M, Pawlik AH, Bromm V, Milosavljevic M. 2014. *MNRAS* 444:3288–300

Ji AP, Frebel A, Bromm V. 2014. *Ap. J.* 782:95

Joggerst CC, Almgren A, Bell J, et al. 2010. *Ap. J.* 709:11–26

Johnson JL. 2010. *MNRAS* 404:1425–36

Johnson JL, Bromm V. 2006. *MNRAS* 366:247–56

Johnson JL, Whalen DJ, Even W, et al. 2013. *Ap. J.* 775:107

Jorgenson RA, Murphy MT, Thompson R. 2013. *MNRAS* 435:482–501

Karlsson T, Bromm V, Bland-Hawthorn J. 2013. *Rev. Mod. Phys.* 85:809–48

Karlsson T, Johnson JL, Bromm V. 2008. *Ap. J.* 679:6–16

Keller S, Bessell M, Schmidt B, Francis P. 2007a. In *The Future of Photometric, Spectrophotometric and Polarimetric Standardization. ASP Conf. Ser., Vol. 364*, ed. C Sterken, pp. 177–85. San Francisco: ASP

Keller SC, Bessell MS, Frebel A, et al. 2014. *Nature* 506:463–66

Keller SC, Schmidt BP, Bessell MS, et al. 2007b. *Publ. Astron. Soc. Aust.* 24:1–12

King IR, Bedin LR, Cassisi S, et al. 2012. *Astron. J.* 144:5

Kirby EN, Lanfranchi GA, Simon JD, Cohen JG, Guhathakurta P. 2011. *Ap. J.* 727:78

Kirby EN, Simon JD, Geha M, Guhathakurta P, Frebel A. 2008. *Ap. J. Lett.* 685:L43–46

Klessen RS, Glover SCO, Clark PC. 2012. *MNRAS* 421:3217–21

Klypin A, Kravtsov AV, Valenzuela O, Prada F. 1999. *Ap. J.* 522:82–92

Kobayashi C, Ishigaki MN, Tominaga N, Nomoto K. 2014. *Ap. J. Lett.* 785:L5

Kobayashi C, Umeda H, Nomoto K, Tominaga N, Ohkubo T. 2006. *Ap. J.* 653:1145–71

Koposov SE, Belokurov V, Torrealba G, Wyn Evans N. 2015. *Ap. J.* 805:130

Korn AJ, Grundahl F, Richard O, et al. 2007. *Ap. J.* 671:402–19

Lai DK, Bolte M, Johnson JA, et al. 2008. *Ap. J.* 681:1524–56

Lai DK, Lee YS, Bolte M, et al. 2011. *Ap. J.* 738:51

Lai DK, Rockosi CM, Bolte M, et al. 2009. *Ap. J. Lett.* 697:L63–67

Leaman R. 2012. *Astron. J.* 144:183

Li HN, Christlieb N, Schörck T, et al. 2010. *Astron. Astrophys.* 521:A10

Limongi M, Chieffi A, Bonifacio P. 2003. *Ap. J. Lett.* 594:L123–26

Lind K, Bergemann M, Collet R, Asplund M, Magic Z. 2012. In *Galactic Archaeology: Near-Field Cosmology and the Formation of the Milky Way. ASP Conf. Proc. 458*, ed. W Aoki, M Ishigaki, T Suda, T Tsujimoto, N Arimoto, pg. 109. San Francisco: ASP

Lind K, Melendez J, Asplund M, Collet R, Magic Z. 2013. *Astron. Astrophys.* 554:A96

Loeb A, Furlanetto SR. 2013. *The First Galaxies in the Universe*. Princeton, NJ: Princeton Univ. Press

Lucatello S, Tsangarides S, Beers TC, et al. 2005. *Ap. J.* 625:825–32

Luck RE, Bond HE. 1981. *Ap. J.* 244:919–37

Ludwig HG, Kučinskas A. 2012. *Astron. Astrophys.* 547:A118

Magic Z, Collet R, Asplund M, et al. 2013. *Astron. Astrophys.* 557:A26

Majewski SR, Wilson JC, Hearty F, Schiavon RR, Skrutskie MF. 2010. In *Chemical Abundances in the Universe: Connecting First Stars to Planets. IAU Symp. 265*, ed. K Cunha, M Spite, B Barbuy, pp. 480–81. Cambridge, UK: Cambridge Univ. Press

Marín-Franch A, Aparicio A, Piotto G, et al. 2009. *Ap. J.* 694:1498–516

Masseron T, Johnson JA, Plez B, et al. 2010. *Astron. Astrophys.* 509:A93

Mateo ML. 1998. *Annu. Rev. Astron. Astrophys.* 36:435–506

McCarthy IG, Font AS, Crain RA, et al. 2012. *MNRAS* 420:2245–62

McConnachie AW, Irwin MJ, Ibata RA, et al. 2009. *Nature* 461:66–69

McWilliam A. 1997. *Annu. Rev. Astron. Astrophys.* 35:503–56

McWilliam A, Preston GW, Sneden C, Searle L. 1995. *Astron. J.* 109:2757–99

McWilliam A, Wallerstein G, Mottini M. 2013. *Ap. J.* 778:149

Meléndez J, Casagrande L, Ramírez I, Asplund M, Schuster WJ. 2010. *Astron. Astrophys.* 515:L3

Meynet G, Ekström S, Maeder A. 2006. *Astron. Astrophys.* 447:623–39

Meynet G, Hirschi R, Ekstrom S, et al. 2010. *Astron. Astrophys.* 521:A30

Moore B, Ghigna S, Governato F, et al. 1999. *Ap. J. Lett.* 524:L19–22

Morrison HL, Flynn C, Freeman KC. 1990. *Astron. J.* 100:1191–222

Ness M, Freeman K, Athanassoula E, et al. 2013. *MNRAS* 430:836–57

Niederste-Ostholt M, Belokurov V, Evans NW, et al. 2009. *MNRAS* 398:1771–81

Nomoto K, Kobayashi C, Tominaga N. 2013. *Annu. Rev. Astron. Astrophys.* 51:457–509

Nomoto K, Tominaga N, Umeda H, Kobayashi C, Maeda K. 2006. *Nucl. Phys. A* 777:424–58

Norris JE, Beers TC, Ryan SG. 2000. *Ap. J.* 540:456–67

Norris JE, Christlieb N, Korn AJ, et al. 2007. *Ap. J.* 670:774–88

Norris JE, Gilmore G, Wyse RFG, et al. 2008. *Ap. J. Lett.* 689:L113–16

Norris JE, Gilmore G, Wyse RFG, Yong D, Frebel A. 2010a. *Ap. J. Lett.* 722:L104–9

Norris JE, Ryan SG. 1989. *Ap. J. Lett.* 336:L17–19

Norris JE, Wyse RFG, Gilmore G, et al. 2010b. *Ap. J.* 723:1632–50

Norris JE, Yong D, Bessell MS, et al. 2013. *Ap. J.* 762:28

Nozawa T, Kozasa T, Umeda H, Maeda K, Nomoto K. 2003. *Ap. J.* 598:785–803

Omukai K, Tsuribe T, Schneider R, Ferrara A. 2005. *Ap. J.* 626:627–43

Pagel BEJ. 1997. *Nucleosynthesis and Chemical Evolution of Galaxies*. Cambridge, UK: Cambridge Univ. Press

Perryman MAC, de Boer KS, Gilmore G, et al. 2001. *Astron. Astrophys.* 369:339–63

Pettini M. 2011. *R. Soc. Lond. Proc. Ser. A* 467:2735–51

Piau L, Beers TC, Balsara DS, et al. 2006. *Ap. J.* 653:300–15

Pila-Díez B, Kuijken K, de Jong JTA, Hoekstra H, van der Burg RFJ. 2014. *Astron. Astrophys.* 564:A18

Placco VM, Frebel A, Beers TC, Stancliffe RJ. 2014. *Ap. J.* 797:21–40

Placco VM, Kennedy CR, Beers TC, et al. 2011. *Astron. J.* 142:188

Rafelski M, Neeleman M, Fumagalli M, Wolfe AM, Prochaska JX. 2014. *Ap. J. Lett.* 782:L29

Ren J, Christlieb N, Zhao G. 2012. *Res. Astron. Astrophys.* 12:1637–48

Revaz Y, Jablonka P. 2012. *Astron. Astrophys.* 538:A82

Ritter JS, Safranek-Shrader C, Gnat O, Milosavljević M, Bromm V. 2012. *Ap. J.* 761:56

Ritter JS, Sluder A, Safranek-Shrader C, Milosavljević M, Bromm V. 2015. *MNRAS.* 451:1190–98

Roederer IU, Preston GW, Thompson IB, et al. 2014. *Astron. J.* 147:136

Roman NG. 1954. *Astron. J.* 59:307–12

Ryan SG, Norris JE. 1991. *Astron. J.* 101:1835–64

Ryan SG, Norris JE, Beers TC. 1996. *Ap. J.* 471:254–78

Ryan SG, Norris JE, Beers TC. 1999. *Ap. J.* 523:654–77

Safranek-Shrader C, Milosavljević M, Bromm V. 2014a. *MNRAS* 440:L76–80

Safranek-Shrader C, Milosavljević M, Bromm V. 2014b. *MNRAS* 438:1669–85

Sandage A. 1986. *Annu. Rev. Astron. Astrophys.* 24:421–58

Sbordone L, Bonifacio P, Caffau E, et al. 2010. *Astron. Astrophys.* 522:A26

Schneider R, Ferrara A, Salvaterra R. 2004. *MNRAS* 351:1379–86

Schneider R, Ferrara A, Salvaterra R, Omukai K, Bromm V. 2003. *Nature* 422:869–71

Schneider R, Omukai K, Bianchi S, Valiante R. 2012a. *MNRAS* 419:1566–75

Schneider R, Omukai K, Limongi M, et al. 2012b. *MNRAS* 423:L60–64

Schönrich R, Asplund M, Casagrande L. 2011. *MNRAS* 415:3807–23

Schönrich R, Asplund M, Casagrande L. 2014. *Ap. J.* 786:7

Schörck T, Christlieb N, Cohen JG, et al. 2009. *Astron. Astrophys.* 507:817–32

Searle L, Zinn R. 1978. *Ap. J.* 225:357–79

Shapley H. 1930. *Star Clusters*. Harvard Obs. Monogr. 2. New York: McGraw-Hill

Simcoe RA, Sullivan PW, Cooksey KL, et al. 2012. *Nature* 492:79–82

Simon JD, Frebel A, McWilliam A, Kirby EN, Thompson IB. 2010. *Ap. J.* 716:446–52

Simon JD, Geha M, Minor QE, et al. 2011. *Ap. J.* 733:46

Sivarani T, Beers TC, Bonifacio P, et al. 2006. *Astron. Astrophys.* 459:125–35

Sneden C, Cowan JJ, Gallino R. 2008. *Annu. Rev. Astron. Astrophys.* 46:241–88

Spergel DN, Bean R, Doré O, et al. 2007. *Ap. J. Suppl.* 170:377–408

Spite F, Spite M. 1982. *Astron. Astrophys.* 115:357–66

Spite M, Caffau E, Andrievsky SM, et al. 2011. *Astron. Astrophys.* 528:A9

Spite M, Cayrel R, Plez B, et al. 2005. *Astron. Astrophys.* 430:655–68

Stacy A, Bromm V. 2014. *Ap. J.* 785:73

Stacy A, Greif TH, Bromm V. 2010. *MNRAS* 403:45–60

Stacy A, Greif TH, Klessen RS, Bromm V, Loeb A. 2013. *MNRAS* 431:1470–86

Starkenburg E, Hill V, Tolstoy E, et al. 2010. *Astron. Astrophys.* 513:A34

Starkenburg E, Shetrone MD, McConnachie AW, Venn KA. 2014. *MNRAS* 441:1217–29

Suda T, Aikawa M, Machida M, Fujimoto M, Iben I. 2004. *Ap. J.* 611:476–93

Suda T, Katsuta Y, Yamada S, et al. 2008. *Publ. Astron. Soc. Jpn.* 60:1159–71

Susa H. 2013. *Ap. J.* 773:185

Susa H, Hasegawa K, Tominaga N. 2014. *Ap. J.* 792:32

Szentgyorgyi A, Frebel A, Furesz G, et al. 2012. In *Proc. SPIE Conf. Ser.* 8446:1H

Tafelmeyer M, Jablonka P, Hill V, et al. 2010. *Astron. Astrophys.* 524:A58

Tegmark M, Silk J, Rees MJ, et al. 1997. *Ap. J.* 474:1–12

Thorburn JA. 1994. *Ap. J.* 421:318–43

Tissera PB, Beers TC, Carollo D, Scannapieco C. 2014. *MNRAS* 439:3128–38

Todini P, Ferrara A. 2001. *MNRAS* 325:726–36

Tolstoy E, Hill V, Tosi M. 2009. *Annu. Rev. Astron. Astrophys.* 47:371–425

Tominaga N, Iwamoto N, Nomoto K. 2014. *Ap. J.* 785:98
Tominaga N, Maeda K, Umeda H, et al. 2007a. *Ap. J. Lett.* 657:L77–80
Tominaga N, Umeda H, Nomoto K. 2007b. *Ap. J.* 660:516–40
Tremblay P-E, Ludwig H-G, Freytag B, Steffen M, Caffau E. 2013. *Astron. Astrophys.* 557:A7
Tumlinson J. 2010. *Ap. J.* 708:1398–418
Turk MJ, Abel T, O'Shea B. 2009. *Science* 325:601–5
Turk MJ, Oishi JS, Abel T, Bryan GL. 2012. *Ap. J.* 745:154
Umeda H, Nomoto K. 2002. *Ap. J.* 565:385–404
Umeda H, Nomoto K. 2003. *Nature* 422:871–73
Umeda H, Nomoto K. 2005. *Ap. J.* 619:427–45
Venn KA, Lambert DL. 2008. *Ap. J.* 677:572–80
Venn KA, Puzia TH, Divell M, et al. 2014. *Ap. J.* 791:98
Venn KA, Shetrone MD, Irwin MJ, et al. 2012. *Ap. J.* 751:102
Vogelsberger M, Genel S, Springel V, et al. 2014. *Nature* 509:177–82
Wagoner RV. 1973. *Ap. J.* 179:343–60
Wagoner RV, Fowler WA, Hoyle F. 1967. *Ap. J.* 148:3–49
Wallerstein G, Carlson M. 1960. *Ap. J.* 132:276–77
Wallerstein G, Greenstein JL, Parker R, et al. 1963. *Ap. J.* 137:280–300
Wanajo S, Nomoto K, Iwamoto N, Ishimaru Y, Beers TC. 2006. *Ap. J.* 636:842–47
Wheeler JC, Sneden C, Truran JW Jr. 1989. *Annu. Rev. Astron. Ap.* 27:279–349
White SDM, Rees MJ. 1978. *MNRAS* 183:341–58
Willman B. 2010. *Adv. Astron.* 2010:285454
Wise JH, Abel T. 2007. *Ap. J.* 665:899–910
Wise JH, Abel T. 2008. *Ap. J.* 685:40–56
Wise JH, Turk MJ, Norman ML, Abel T. 2012. *Ap. J.* 745:50
Woosley SE, Heger A, Weaver TA. 2002. *Rev. Mod. Phys.* 74:1015–71
Woosley SE, Weaver TA. 1995. *Ap. J. Suppl.* 101:181–235
Yong D, Norris JE, Bessell MS, et al. 2013a. *Ap. J.* 762:26
Yong D, Norris JE, Bessell MS, et al. 2013b. *Ap. J.* 762:27
Yong D, Roederer IU, Grundahl F, et al. 2014. *MNRAS* 441:3396–416
Yoshida N, Bromm V, Hernquist L. 2004. *Ap. J.* 605:579–90
Yoshida N, Omukai K, Hernquist L. 2008. *Science* 321:669–71
Yoshii Y. 1982. *Publ. Astron. Soc. Jpn.* 34:365–79
Zinn R. 1985. *Ap. J.* 293:424–44
Zolotov A, Willman B, Brooks AM, et al. 2009. *Ap. J.* 702:1058–67
Zolotov A, Willman B, Brooks AM, et al. 2010. *Ap. J.* 721:738–43